



779
2023

Berichte

zur Polar- und Meeresforschung

Reports on Polar and Marine Research

**The Expedition PS135/1 and PS135/2
of the Research Vessel POLARSTERN
to the Atlantic Ocean in 2023**

Edited by

Yvonne Schulze Tenberge and Björn Fiedler

with contributions of the participants

Die Berichte zur Polar- und Meeresforschung werden vom Alfred-Wegener-Institut, Helmholtz-Zentrum für Polar- und Meeresforschung (AWI) in Bremerhaven, Deutschland, in Fortsetzung der vormaligen Berichte zur Polarforschung herausgegeben. Sie erscheinen in unregelmäßiger Abfolge.

Die Berichte zur Polar- und Meeresforschung enthalten Darstellungen und Ergebnisse der vom AWI selbst oder mit seiner Unterstützung durchgeführten Forschungsarbeiten in den Polargebieten und in den Meeren.

Die Publikationen umfassen Expeditionsberichte der vom AWI betriebenen Schiffe, Flugzeuge und Stationen, Forschungsergebnisse (inkl. Dissertationen) des Instituts und des Archivs für deutsche Polarforschung, sowie Abstracts und Proceedings von nationalen und internationalen Tagungen und Workshops des AWI.

Die Beiträge geben nicht notwendigerweise die Auffassung des AWI wider.

Herausgeber

Dr. Horst Bornemann

Redaktionelle Bearbeitung und Layout

Susan Amir Sawadkuhi

Alfred-Wegener-Institut
Helmholtz-Zentrum für Polar- und Meeresforschung
Am Handelshafen 12
27570 Bremerhaven
Germany

www.awi.de

www.awi.de/reports

Der Erstautor bzw. herausgebende Autor eines Bandes der Berichte zur Polar- und Meeresforschung versichert, dass er über alle Rechte am Werk verfügt und überträgt sämtliche Rechte auch im Namen seiner Koautoren an das AWI. Ein einfaches Nutzungsrecht verbleibt, wenn nicht anders angegeben, beim Autor (bei den Autoren). Das AWI beansprucht die Publikation der eingereichten Manuskripte über sein Repository ePIC (electronic Publication Information Center, s. Innenseite am Rückdeckel) mit optionalem print-on-demand.

The Reports on Polar and Marine Research are issued by the Alfred Wegener Institute, Helmholtz Centre for Polar and Marine Research (AWI) in Bremerhaven, Germany, succeeding the former Reports on Polar Research. They are published at irregular intervals.

The Reports on Polar and Marine Research contain presentations and results of research activities in polar regions and in the seas either carried out by the AWI or with its support.

Publications comprise expedition reports of the ships, aircrafts, and stations operated by the AWI, research results (incl. dissertations) of the Institute and the Archiv für deutsche Polarforschung, as well as abstracts and proceedings of national and international conferences and workshops of the AWI.

The papers contained in the Reports do not necessarily reflect the opinion of the AWI.

Editor

Dr. Horst Bornemann

Editorial editing and layout

Susan Amir Sawadkuhi

Alfred-Wegener-Institut
Helmholtz-Zentrum für Polar- und Meeresforschung
Am Handelshafen 12
27570 Bremerhaven
Germany

www.awi.de

www.awi.de/en/reports

The first or editing author of an issue of Reports on Polar and Marine Research ensures that he possesses all rights of the opus, and transfers all rights to the AWI, including those associated with the co-authors. The non-exclusive right of use (einfaches Nutzungsrecht) remains with the author unless stated otherwise. The AWI reserves the right to publish the submitted articles in its repository ePIC (electronic Publication Information Center, see inside page of verso) with the option to "print-on-demand".

*Titel: Studierende der dritten Kohorte des WASCAL Studienganges "Climate Change and Marine Sciences" erwarten voller Vorfreude die Ankunft des Forschungseisbrechers Polarstern in Mindelo, Cabo Verde
(Foto: Björn Fiedler, GEOMAR)*

*Students of the third cohort of the WASCAL study programme "Climate Change and Marine Sciences" eagerly await the arrival of the research icebreaker Polarstern in Mindelo, Cabo Verde
(Photo: Björn Fiedler, GEOMAR)*

The Expedition PS135/1 and PS135/2 of the Research Vessel POLARSTERN to the Atlantic Ocean in 2023

Edited by

Yvonne Schulze Tenberge and Björn Fiedler

with contributions of the participants

Please cite or link this publication using the identifiers

<https://hdl.handle.net/10013/epic.7f5e917e-4035-4947-9fdf-13d26fe7ff69>

https://doi.org/10.57738/BzPM_0779_2023

ISSN 1866-3192

**PS135/1
PS135/2**

9 March 2023 – 11 April 2023

Punta Arenas – Mindelo – Bremerhaven

Chief scientists

**Yvonne Schulze Tenberge
(PS135/1 Punta Arenas – Mindelo)**

**Björn Fiedler
(PS135/2 Mindelo – Bremerhaven)**

**Coordinator
Ingo Schewe**

Contents

1.	Überblick und Expeditionsverlauf	2
	Summary and Itinerary	4
	Weather conditions during PS135/1 and PS135/2	7
2.	Bathymetric Underway Measurements	8
3.	Atmospheric and Oceanic Transport of Emerging Organic Contaminants in the Atlantic Ocean	13
4.	Athmospheric Measurements	18
5.	WASCAL Floating University	52
	APPENDIX	70
A.1	Teilnehmende Institute / Participating Institutes	71
A.2	Fahrtteilnehmer:innen / Cruise Participants	72
A.3	Schiffsbesatzung / Ship's Crew 135/1	74
	Schiffsbesatzung / Ship's Crew PS135/2	76
A.4	Stationsliste / Station List PS135/1	78
	Stationsliste / Station List PS135/2	83

1. ÜBERBLICK UND EXPEDITIONSVERLAUF

Björn Fiedler¹, Yvonne Schulze Tenberge²

¹DE.GEOMAR

²DE.AWI

Der Fahrtabschnitt PS135 der *Polarstern* war der letzte Abschnitt der antarktischen Forschungssaison 2022/23 und diente der Überführung des Schiffes in seinen Heimathafen Bremerhaven. Die Expedition PS135 startete in Punta Arenas am 9. März 2023 und endete am 11. April 2023 in Bremerhaven. Am 28. März 2023 wurde ein planmäßiger Zwischenstopp in Mindelo durchgeführt, der die Fahrt in die Abschnitte PS135/1 und PS135/2 gliederte. Auf dem ersten Abschnitt lag der Fokus auf *en route* Messungen, welche ebenfalls auf dem zweiten Abschnitt fortgeführt wurden. Ab Mindelo lag der Schwerpunkt auf einer akademischen Ausbildungsfahrt („Floating University“) für westafrikanische M.Sc. Studierende, bei welcher zusätzliche Stationsarbeiten entlang der Route nach Bremerhaven durchgeführt wurden. Die Ausbildung auf diesem Abschnitt fand im Rahmen des vom Bundesministerium für Bildung und Forschung (BMBF) finanzierten WASCAL Programms statt (West African Science Service Centre on Climate Change and Adapted Land-Use).

Auf der gesamten Reise (Abschnitte 1 und 2) wurden folgende *en route* Messungen und Tätigkeiten durchgeführt:

- Mit den schiffsinternen hydroakustischen Systemen wurden auf der gesamten Strecke ein Streifen Meeresbodentopographie bathymetrisch vermessen.
- Es wurden Wasser- und Luftproben zur Bestimmung von persistenten organischen Schadstoffen (POPs) sowie von neuartigen, noch nicht regulierten organischen Kontaminanten genommen.
- Atmosphärische Messungen von Aerosolen, Wasserdampf und Wolken wurden mittels eines Sonnenphotometers und einer Wolkenkamera durchgeführt.
- Biogeochemische Messungen im Oberflächenozean wurden mittels im Durchfluss betriebener Sensorik (u.a. CO₂ Partialdruck, gelöster Sauerstoff etc.) durchgeführt.

In Mindelo sind dann 11 Studierende des WASCAL Programms, 9 Wissenschaftler verschiedener Institute sowie eine Technikerin des Alfred-Wegener-Instituts (AWI) hinzugestiegen und die Fahrtleitung des zweiten Fahrtabschnitts wurde vom GEOMAR Helmholtz Zentrum für Ozeanforschung Kiel übernommen. Tägliche Stationsarbeiten mit dem bordeigenen CTD Kranzwasserschöpfer sowie einem Multischließnetz wurden ab Mindelo täglich durchgeführt. Dabei wurden die beiden Zeitserienstationen CVOO nördlich von Cabo Verde („Cabo Verde Ocean Observatory“) sowie ESTOC nördlich von Gran Canaria („European Station of Time-Series in the Ocean of the Canary Islands“) beprobt, um Langzeit-Datenerhebungen in der Region fortzuführen. Darüber hinaus fanden insgesamt 5 Auslegungen sowie 2 Bergungen von profilierenden Argo Tiefendriftern im Rahmen des internationalen Argo Programms statt. Insgesamt konnten 40 Stunden Stationszeit hocheffizient genutzt werden, um auf dem zweiten Fahrtabschnitt wissenschaftliche Daten auch in der Wassersäule zu erheben.

Die Expedition trug zu den Zielen des Forschungsprogrammes „Erde im Wandel – Unsere Zukunft sichern“ bei. Es ist Teil der "Programmierorientierten Förderung" (PoF IV) der Helmholtz-Gemeinschaft Deutscher Forschungszentren. Die Tätigkeiten der Expedition standen im engen Zusammenhang mit den Themen 2 (Ozean und Kyrosphäre im Klimawandel), 4 (Die Küstengebiete im globalen Wandel) sowie 6 (Marines und polares Leben).

SUMMARY AND ITINERARY

Expedition PS135 of *Polarstern* was the last leg of the 2022/23 Antarctic research season and brought back the ship to its home port of Bremerhaven. Expedition PS135 started in Punta Arenas on 9 March 2023 and ended in Bremerhaven on 11 April 2023. A scheduled stopover in Mindelo was carried out on 28 March 2023, dividing the cruise into leg PS135/1 and PS135/2. On the first leg, the focus was on *en route* measurements, which were also continued on the second leg. From Mindelo, the focus was on an academic training cruise (“Floating University”) for West African M.Sc. students, during which additional station work was carried out along the route to Bremerhaven. The training during this leg took place within the framework of the WASCAL programme (West African Science Service Centre on Climate Change and Adapted Land-Use) funded by the German Federal Ministry of Education and Research (BMBF).

The following *en route* measurements and activities were carried out throughout the cruise (sections 1 and 2):

- A swath of seabed topography was bathymetrically surveyed along the entire route using the ship’s internal hydroacoustic systems.
- Water and air samples were taken to determine persistent organic pollutants (POPs) as well as novel, not yet regulated organic contaminants.
- Atmospheric measurements of aerosols, water vapour and clouds were carried out using a sun photometer and a cloud camera.
- Biogeochemical measurements in the surface ocean were carried out using flow-through sensors (including CO₂ partial pressure, dissolved oxygen, etc.).

In Mindelo, 11 students of the WASCAL programme, 9 scientists from various institutes and a technician from the Alfred Wegener Institute (AWI) joined the team and the GEOMAR Helmholtz Centre for Ocean Research Kiel took over the scientific lead of the cruise. Daily station work with the on-board CTD rosette water sampler as well as a multinet was carried out daily from Mindelo. The two time series stations CVOO north of Cabo Verde (“Cabo Verde Ocean Observatory”) and ESTOC north of Gran Canaria (“European Station of Time-Series in the Ocean of the Canary Islands”) were sampled to continue long-term data collection in the region. In addition, a total of 5 deployments and 2 recoveries of Argo profiling floats took place as part of the international Argo programme. A total of 40 hours of station time could be used highly efficiently to collect scientific data in the water column as well on the second leg of the cruise.

The expedition contributed to the goals of the research programme “Changing Earth – Sustaining our Future”. It is part of the programme-oriented Funding (PoF IV) of the Helmholtz Association of German Research Centres. The activities of the expedition were closely related to Topics 2 (Ocean and Cyrosphere in Climate Change), 4 (Coastal Zones at a Time of Global Change) and 6 (Marine and Polar Life).

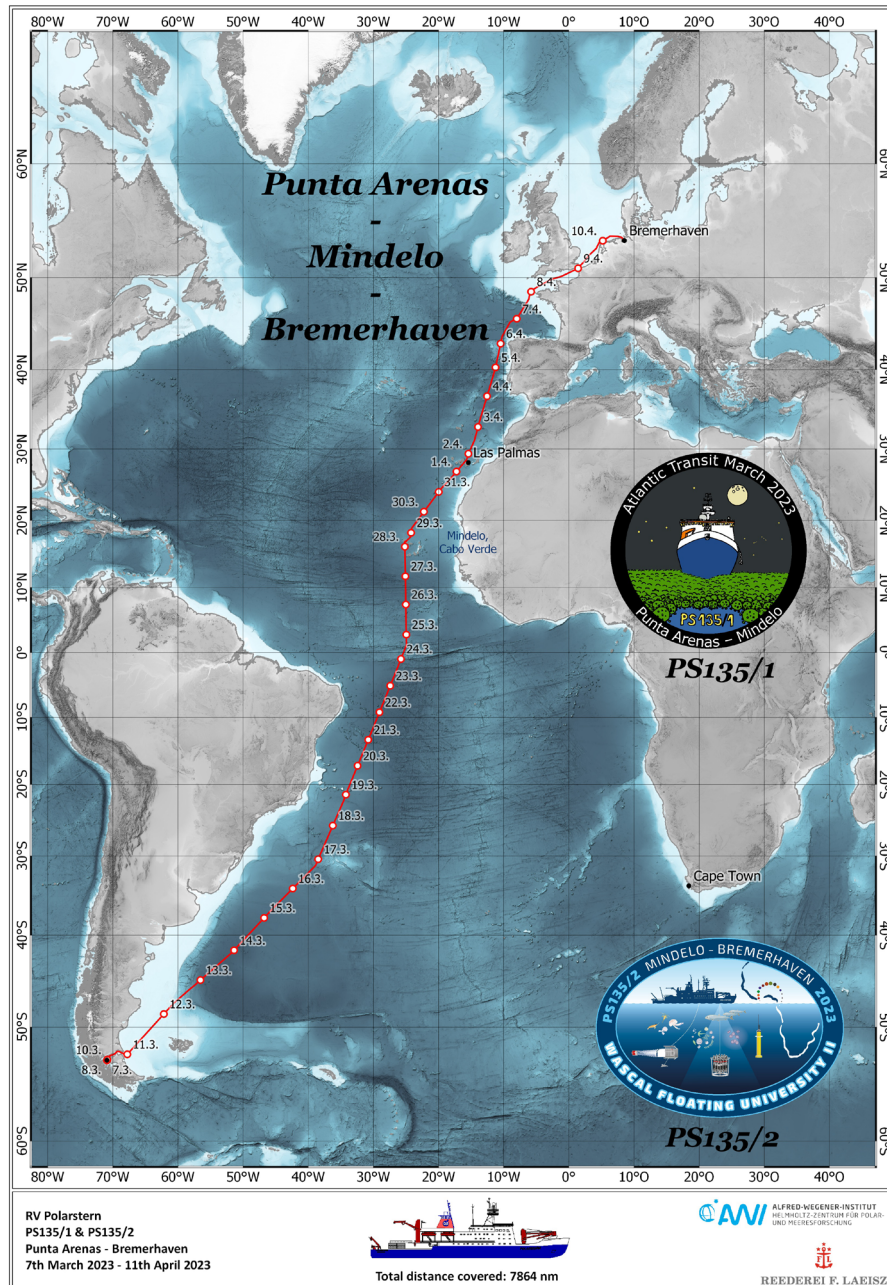


Abb. 1.1: Fahrtverlauf der Expedition PS135 von Punta Arenas nach Bremerhaven. Siehe <https://doi.pangaea.de/10.1594/PANGAEA.961682> und <https://doi.pangaea.de/10.1594/PANGAEA.961687> für eine Darstellung der master tracks in Verbindung mit den Stationslisten für PS135/1 (Punta Arenas – Mindelo) und PS135/2 (Mindelo – Bremerhaven). (Karte: I. Nasis)

Fig. 1.1: Cruise track of expedition PS135 from Punta Arenas to Bremerhaven. See <https://doi.pangaea.de/10.1594/PANGAEA.961682> and <https://doi.pangaea.de/10.1594/PANGAEA.961687> to display the master tracks in conjunction with the station lists for PS135/1 (Punta Arenas – Mindelo) and PS135/2 (Mindelo – Bremerhaven). (Map: I. Nasis)

WEATHER CONDITIONS DURING PS135/1 AND PS135/2

Julia Wenzel

¹DE.DWD

PS135/1 – from Punta Arenas to Mindelo

On the evening of 10 March, *Polarstern* started its voyage from Punta Arenas in a westerly wind of 4 to 5 Bft caused by a storm low west of the Drake Passage, temporary increasing to 6 Bft when passing through the narrows of the eastern Strait of Magellan. In the night to 12 March, the research vessel crossed the front of the southeastwards moving and weakening low pressure system, causing a temporary wind speed increase to 7 Bft.

After having crossed a convergence zone in the night to 14 March, connected to a wind shift to North and a temporary increase to 6 Bft, and additionally moderate visibility due to a very humid air mass, *Polarstern* reached the western flank of a quasi stationary subtropical high pressure system near 36°S 37°W. Thereby, the mostly moderate wind (4 Bft) first came from north and veered to east when reaching the northern flank on 16 March, the significant wave height mostly staying below 1.5 m.

Moving northnortheastwards, *Polarstern* got into an increasingly unstable air mass on the northern flank of the subtropical high and from 19 March on was travelling through the tropics where more and more isolated rain showers occurred in the humid and warm air mass. On 20 March, a swell from northeast replaced the previously prevailing swell from southeast. Due to the increase in the pressure gradient between the subtropical high and the inner-tropical convergence zone, a temporary increase in wind to 5 Bft and sea state to 2.5 m occurred on 21 March.

Due to the temporal proximity to the equinox the highest position of the sun (nearly zenith) occurred on 24 and 25 March, nearly coinciding with the crossing of the equator on 24 March.

From 24 to 25 March *Polarstern* crossed the Inertropical Covergence Zone which extended along the Atlantic Ocean between the equator and 5°North and where extended convective clouds and rain showers occurred. Due to the weak pressure differences weak variable winds prevailed with a swell from north with 1.5 m. In the night to 25 March the wind shifted to north and was growing to 4 Bft when *Polarstern* moved northwards. These trade winds forced by a northatlantic subtropical high accompagnied *Polarstern* until Mindelo, where a short stop was taken on 28 March. In the proximity of the islands a temporary and local wind speed increase to 6 Bft occurred due to the jet and edge effects due to the orography.

PS135/2 – from Mindelo to Bremerhaven

The second part of the journey started with a growing significant wave height to 3 m, caused by a swell from northwest that was created by an extended gale over the northern North Atlantic and was maintained the following days by subsequent low pressure systems. With an additional continuously intensification of the northeast trade winds to 6 Bft by 30 March by strengthening and moving of the high to Madeira cross sea occurred. When the high moved

to northeast another high that was moving eastwards to the Acores was taking over on 2 April maintaining the northerly air flow along the route.

Starting from the Cape Verde Islands (28 March) a slight reduction of visibility occurred due to Saharian dust that was transported to the sea by the wind. But on 31 March the concentration of dust increased that much that the visibility was reduced to below 7 km for the whole day and only after the passage of the Canary Islands (night to 2 April) it significantly improved again.

Between the Canary Islands the wind temporary and rapidly took up to 8 Bft in the evening of 1 April due to the jet effect between the islands.

On an eastward moving cold front of a low pressure system near Iceland on 3 April a secondary low in upper levels formed west of Cape Finisterre. It moved southward while deepening and had crossed *Polarstern* by the evening of 4 April. Thereby, rain showers, a wind speed increase to 7 to 8 Bft and a cross sea of 4 m (thereof 3 m swell from northwest) occurred.

The following days, *Polarstern* again was influenced by the Acores high. The high was moving to the northeast and was situated over the Bay of Biscay on 6 April, over the English Channel on 7 April and reached Scandinavia on 8 April. On 5 April, the northerly wind temporary increased to 7 Bft near Cape Finisterre due to the pressure gradient and the cape effect. Reaching the Bay of Biscay on 6 April, the wind veered east and decreased to 5 Bft, while the sea state reduced to below 2.5 m including a swell of 2 m from west created by a gale near Iceland. Until 9 April, the wind and sea decreased to 3 Bft and below 0.5 m in the English Channel, while fog occurred in the eastern part of the Channel (visibility temporary below 200 m).

On 9 April the eastward moving front of the Iceland low was approaching and caused a wind shift to south and increase to 6 Bft. In the night to 11 April *Polarstern* was finally crossed by the front and reached its home port Bremerhaven in the early morning of 11 April.

2. BATHYMETRIC UNDERWAY MEASUREMENTS

Yvonne Schulze Tenberge¹, Peter Konopatzky¹
not on board: Boris Dorschel¹

¹DE.AWI

Grant-No. AWI_PS135_01

Objectives

Accurate knowledge of the seafloor topography, hence high-resolution bathymetry data, is key basic information necessary to understand many marine processes. It is of particular importance for the interpretation of scientific data in a spatial context. Bathymetry, or geomorphology, is a basic parameter for the understanding of the general geological setting of an area and geological processes such as erosion, sediment transport and deposition. Even information on tectonic processes can be inferred from bathymetry. Supplementing the bathymetric data, high-resolution sub-bottom profiler data of the top 10s of meters below the seabed provide information of the sediment architecture and the lateral extension of sediment successions. This can be used to study depositional environments on larger scales in terms of space and time, of which the uppermost sediments may be sampled.

While world bathymetric maps give the impression of a detailed knowledge of worldwide seafloor topography, most of the world's ocean floor remain unmapped by hydroacoustic systems. In these areas, bathymetry is modelled from satellite altimetry with a corresponding low resolution. Satellite-altimetry derived bathymetry therefore lack the necessary resolution to resolve small- to meso-scale geomorphological features (e.g. sediment waves, glaciogenic features and small seamounts). Ship-borne multibeam data provide bathymetry information in a resolution that is sufficient to resolve those features.

Therefore, the main tasks of the bathymetry group on board *Polarstern* during PS135 were:

- Collection of bathymetric data, including calibration and correction of the data for environmental circumstances (sound velocity, systematic errors in bottom detection, etc.)
- Post processing and cleaning of the data
- Data management for on-site map creation
- Collection of sound velocity data

Work at sea

Technical description

During the PS135 cruise, the bathymetric surveys were conducted with the hull-mounted multibeam echosounder (MBES) Teledyne Reson HYDROSWEEP DS3. The HYDROSWEEP is a deep water system for continuous mapping with the full swath potential. It operates on a frequency of ~14 kHz. On *Polarstern*, the MBES transducer arrays are arranged in a

Mills cross configuration of 3 m (transmit unit) by 3 m (receive unit). The combined motion, position (Trimble GNSS), and time data comes from an iXBlue Hydrins system and the signal is directly transferred into the Processing Unit (PU) of the MBES to carry out real-time motion compensation in Pitch, Roll and Yaw. With a combination of phase and amplitude detection algorithms the PU computes the water depth from the returning backscatter signal. The system can cover a sector of up to 140° with 70° per side. In the deep sea, an angle of ~50° to both sides could be achieved.

Data acquisition and processing

Data acquisition was carried out throughout the entire cruise between Punta Arenas and the British Channel wherever permitted.

The MBES was operated with Hydromap Control and for online data visualization, Teledyne PDS was used. The collected bathymetry was stored in ASD and S7K raw files.

Subsequent data processing was performed using Caris HIPS and SIPS. For generating maps, the data were exported to QGIS in the GeoTIFF raster format.

Sound velocity profiles

For best survey results with correct depths, the HYDROSWEEP was calibrated with sound velocity profiles from CTD (Conductivity Temperature Depth) and SVP (Sound Velocity Probe) casts. This is essential, as the acoustic signal travels down the water column from the transducer to the seafloor and back to the surface through several different layers of water masses with each a different sound velocity. The sound velocity is influenced by density and compressibility, both depending on pressure, temperature and salinity. Wrong or outdated sound velocity profiles lead to refraction errors and reduced data quality.

The CTD measures conductivity, temperature, and depth in the water column while the ship is on station. And, the Valeport MIDAS SVP measures pressure and temperature. From these parameters respectively, the sound velocity is calculated.

During PS135/1, the Bathymetry group operated the MIDAS SVP. The obtained sound velocity profiles were immediately processed and applied within the MBES for correct beamforming during the survey.

During PS135/2, the other science groups conducted CTD casts with the ship-owned CTD (for details see Chapter 5). The obtained sound velocity profiles were immediately processed and applied within the MBES for correct beamforming during the survey by the Bathymetry group.

Additionally, these profiles were combined/extended with World Ocean Atlas 2018 (WOA18) data to create full ocean depth SV profiles.

Stations

The HYDROSWEEP and MIDAS SVP stations are listed in Table 2.1 (PS135/1) and Table 2.2 (PS135/2). For MIDAS SVP only station starts are listed. For a complete station list see Appendix A.4.

At station PS135/1_4-1, the MIDAS SVP malfunctioned and did not record any data.

Tab. 2.1: List of bathymetry related stations during PS135/1.

Station Number	Device	Action	Event Time [UTC]	Latitude	Longitude
PS135/1_0_Underway-13	Hydrosweep DS3	station start	12.03.2023 19:01:38	-47.556283	-60.610262
PS135/1_0_Underway-13	Hydrosweep DS3	profile start	12.03.2023 19:03:23	-47.551933	-60.602668
PS135/1_0_Underway-13	Hydrosweep DS3	profile end	28.03.2023 15:01:57	16.687633	-25.173072
PS135/1_1-1	MIDAS_SVP	station start	13.03.2023 11:55:48	-45.114966	-56.548319
PS135/1_2-1	MIDAS_SVP	station start	15.03.2023 11:59	-37.939686	-46.771646
PS135/1_3-1	MIDAS_SVP	station start	17.03.2023 10:58	-30.451051	-38.465616
PS135/1_4-1	MIDAS_SVP	station start	19.03.2023 10:56	-21.496256	-34.218806
PS135/1_5-1	MIDAS_SVP	station start	21.03.2023 11:17	-13.403489	-30.779653
PS135/1_6-1	MIDAS_SVP	station start	23.03.2023 09:59	-5.296772	-27.457148
PS135/1_7-1	MIDAS_SVP	station start	25.03.2023 09:00	2.735006	-24.939931
PS135/1_8-1	MIDAS_SVP	station start	27.03.2023 09:58	11.554829	-25.085381

Tab. 2.2: List of bathymetry related stations during PS135/2.

Station Number	Device	Action	Event Time [UTC]	Latitude	Longitude
PS135/2_0_Underway-13	Hydrosweep DS3	station start	28.03.2023 21:47	17.000343	-24.92187
PS135/2_0_Underway-13	Hydrosweep DS3	profile start	28.03.2023 21:47	17.001338	-24.920736
PS135/2_0_Underway-13	Hydrosweep DS3	profile end	09.04.2023 06:07	50.02597	-1.643421
PS135/2_0_Underway-13	Hydrosweep DS3	station end	09.04.2023 06:07	50.025947	-1.643575

Preliminary results

During 29 days of survey, a track length of 6,823 nmi (12,636 km) was surveyed by the swath bathymetry. Fig. 2.1 shows the generated bathymetry grid over the Atlantic.

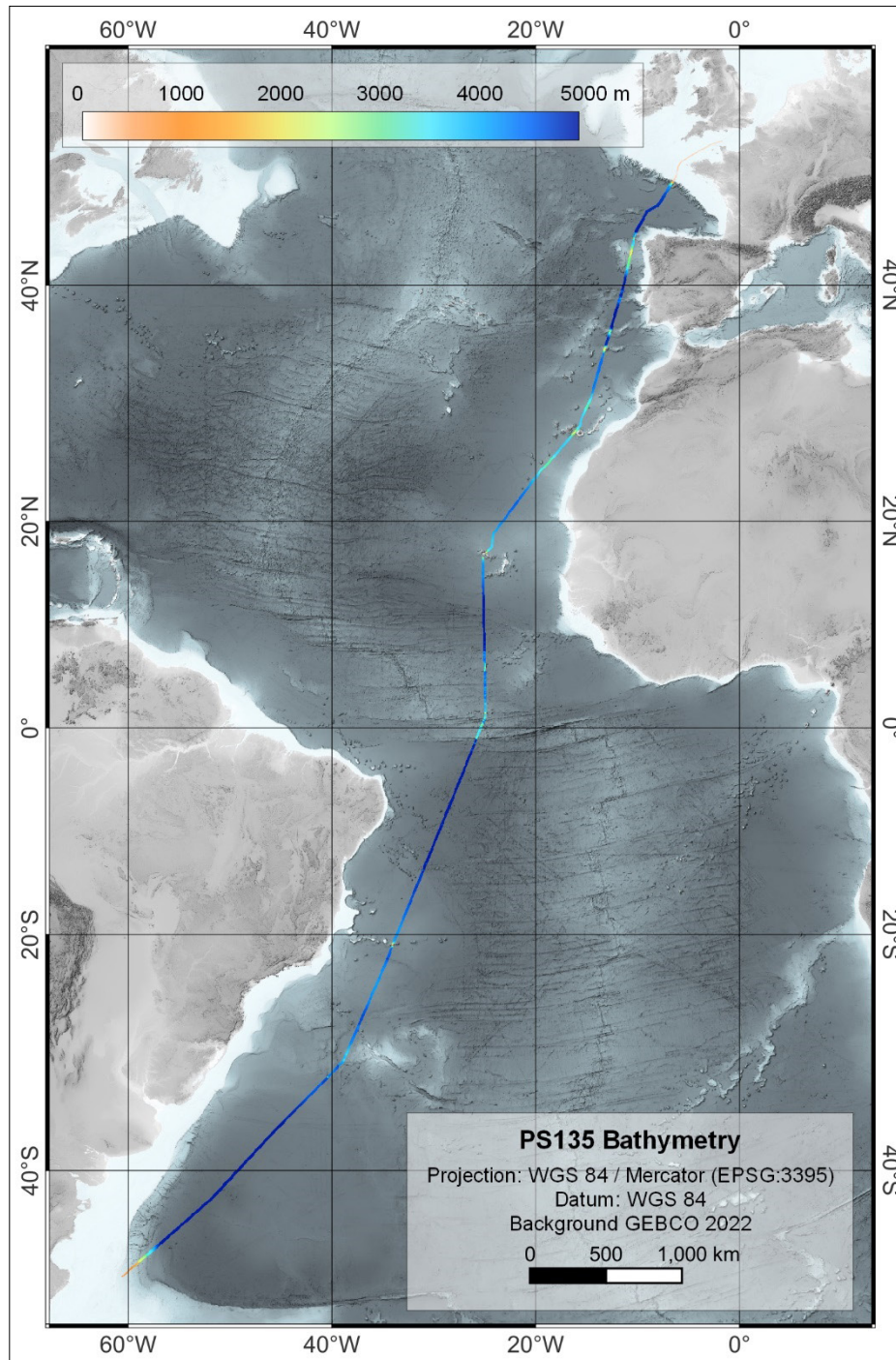


Fig. 2.1: Overview of the bathymetric data acquired during PS135

Data management

Environmental data will be archived, published and disseminated according to international standards by the World Data Center PANGAEA Data Publisher for Earth & Environmental Science (<https://www.pangaea.de>) within two years after the end of the cruise at the latest. By default, the CC-BY license will be applied. Furthermore, bathymetric data will be provided to the Nippon Foundation – GEBCO Seabed 2030 Project.

This expedition was supported by the Helmholtz Research Programme “Changing Earth – Sustaining our Future” Topic 2, Subtopic 3 Sea Level Change.

In all publications based on this expedition, the **Grant No. AWI_PS135_01** will be quoted and the following publication will be cited:

Alfred-Wegener-Institut Helmholtz-Zentrum für Polar- und Meeresforschung (2017) Polar Research and Supply Vessel POLARSTERN Operated by the Alfred-Wegener-Institute. Journal of large-scale research facilities, 3, A119. <http://dx.doi.org/10.17815/jlsrf-3-163>.

3. ATMOSPHERIC AND OCEANIC TRANSPORT OF EMERGING ORGANIC CONTAMINANTS IN THE ATLANTIC OCEAN

Zhiyong Xie¹, Freya Debler¹

¹DE.HEREON

Grant-No. AWI_PS135_02

Outline

Legacy and emerging organic contaminants can enter the coast, marine and ocean environment by a number of processes (Xie et al., 2022a). Once introduced they are subject to biogeochemical cycling, sinks, and bioaccumulation processes in the ocean. Apart from the discharge of the rivers and runoff, the atmosphere is considered to be the primary and most rapid pathway for pollutant transport to the coast and marine environment as a result of their hydrophobic and semi-volatile nature, respectively. We have participated with *Polarstern* cruise during PS135/1 and PS135/2 to determine emerging and legacy organic contaminants from the Northern and Southern hemisphere in proposal to further investigate their up to date levels and air-sea interactions in remote oceans. The research programme is focused on the determination of both persistent organic pollutants (POPs) and emerging organic contaminants (EOCs) in air and water. Considering ocean currents and fronts, the origin of air masses as well as changing air-sea gradients of pollutants, field study-based analysis of long oceanic transects from source regions to remote areas are considered a promising approach to improve the understanding of the underlying transport mechanisms (Xie et al., 2022b).

Objectives

This project aims to improve the knowledge for a better understanding of the occurrence, distribution and transport pathways of POPs and EOCs in the Atlantic, which includes perfluorinated alkyl substances (PFAS), brominated flame-retardants (BFRs) organophosphate esters (OPEs), dechlorane plus (DPs), phthalate esters, UV filters, alkyl phenols (APs), pharmaceutical and personal care products (PPCPs) and plant protection pesticides. The main objectives are providing data sets on the occurrence and distribution of POPs and EOCs in atmospheric and seawater samples along latitudinal transects in the Atlantic evaluating atmospheric and oceanic transport mechanisms of POPs and EOCs investigating atmospheric transport of new pesticides from the possible source regions, e.g. South America, Africa and Europe

Identifying alternative and transform substances of POPs and EOCs in the Atlantic to improve the understanding of air-sea interface interaction of POPs and EOCs along the south to north Atlantic transect.

Work at sea

Air sampling. Four high-volume air samplers were mounted on the upper deck of the research vessel (Fig. 3.1). Airborne particles were collected on glass fiber filters and the gaseous chemicals were trapped on PUF/XAD-2 glass cartridges. Among the four air samplers, two of them collected 24 h air samples for the determination of POPs and EOCs, and the other two air samplers were running in parallel for 48 h to collect higher air volume for measuring both classic and current used pesticides in the atmosphere (Fig. 3.2). Field blanks were prepared by espousing the PUF/ XAD-2 column and glass fiber filters shortly to the sampling site. The samples were stored at -20°C onboard and at the Helmholtz-Zentrum Hereon until further sample preparation process.



Fig. 3.1: High-volume air samplers for sampling gaseous and particle phase bound chemicals in the oceanic air

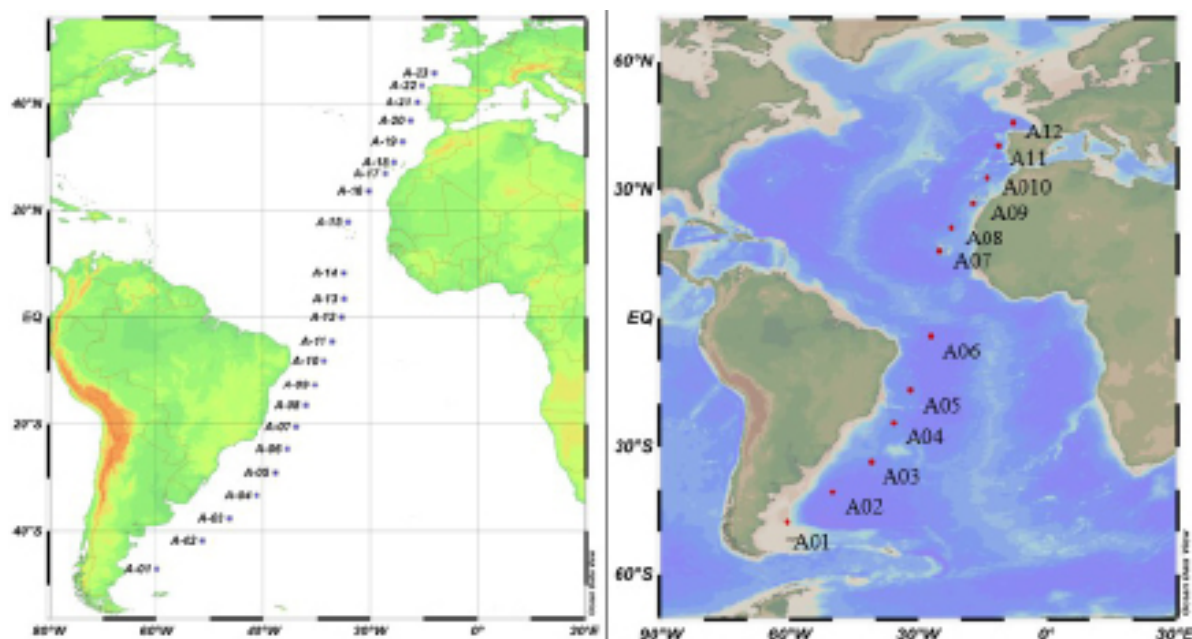


Fig. 3.2: Air sampling stations in the Atlantic Ocean, with the blue (left) and (right) red dots marked at the starting position of each air sample

High-volume water sampling. Along the entire cruise, 26 high-volume seawater samples (100 – 500 L) were collected from the ship-intake system in the water lab (Fig. 3.3). A glass fiber filter (GFC, 1.2 μm , 140 mm) was used to collect suspended particulate matter (SPM) and an XAD-2 column was used to catch organic chemicals in the dissolved phase. Samples are stored at 0°C in the cooling room onboard and at 5°C at the Helmholtz-Zentrum Hereon until further sample preparation process.

1-L water sampling. Besides high-volume water sampling, we also collected 1 L surface seawater from the ship-intake system in the water lab with polypropylene bottle and glass bottle separately at regular intervals along the cruise track for analysis of PFAS and PPCP. From Mindello to Bremerhaven, 1-L seawater samples were collected from CTD in order to determine the vertical profile of chemical contaminants in the water column.

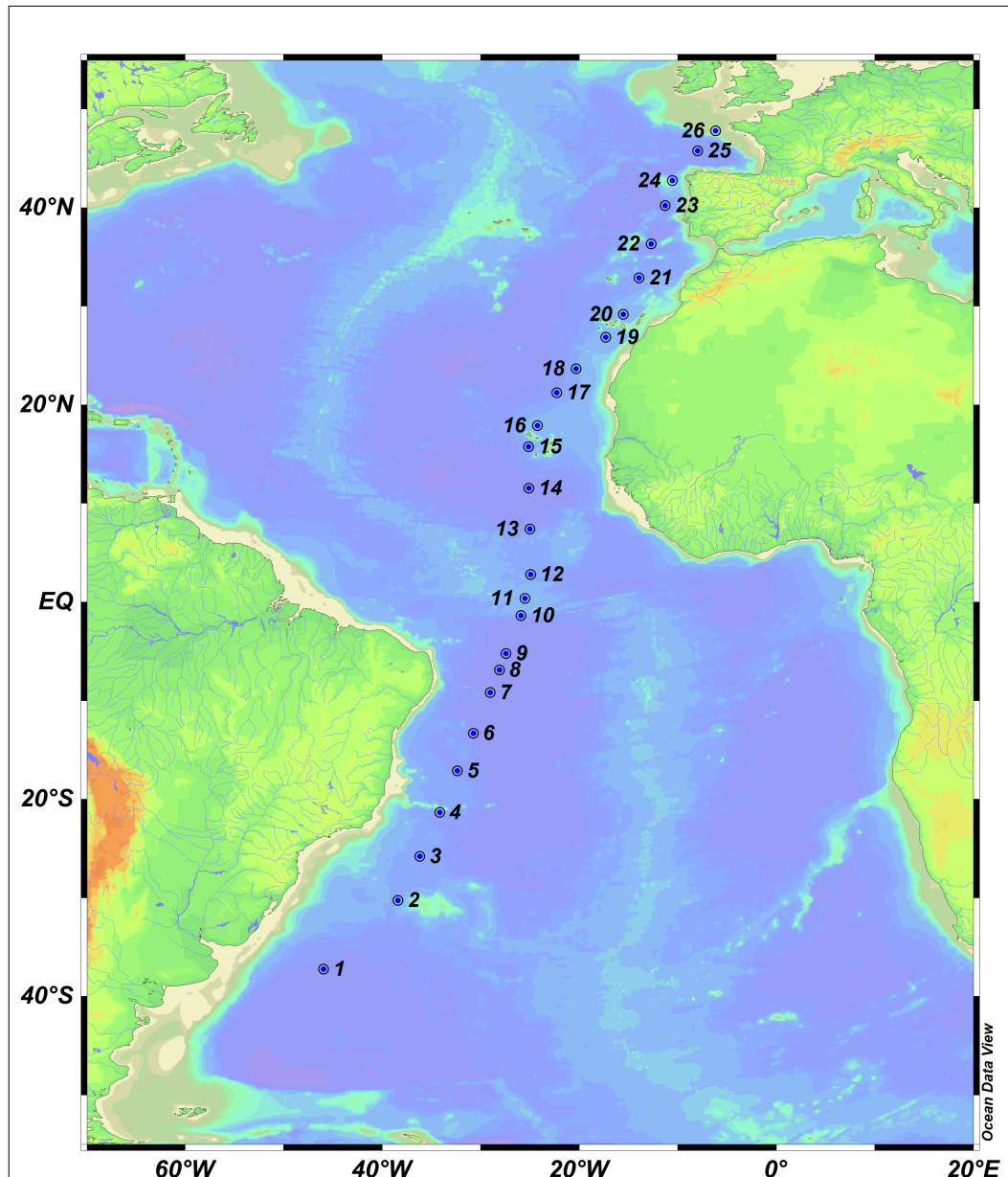


Fig. 3.3: High-volume seawater samples in the South China Sea, with the black dots marked at the starting position of each water sample

Preliminary (expected) results

All air and water samples will be processed in the analytical laboratory at the Helmholtz-Zentrum Hereon and analyzed using GC-MS/MS, GC-QTOF-MS, LC-MS/MS and LC-QTOF-MS/MS. Analytical results will show the occurrence and distribution of EOCs in seawater and air through the south to north transect in the Atlantic. Concentrations of emerging organic contaminants in ocean waters and the atmosphere from the southern Hemisphere will be investigated across several provinces of the Atlantic Ocean. Both the particulate and the gas or water phase will be analyzed to identify the partitioning behaviour in the oceans and the atmosphere. Vertical profiles deriving from CTD samples may reveal further information on sources and transport of EOCs in this area based on the data, the transport behaviour and long-range transport potential of EOCs on the southern and northern Hemisphere will

be studied, and the air-water exchange process will be estimated. Unknown substances and transformed products of chemical contaminants will be identified with non-target analysis and suspecting programmes.

Moreover, high-volume air samples will be analyzed for a broad number of pesticides ranging from organochlorine pesticides to currently-used pesticides. To investigate the partitioning behaviour, concentrations in the particulate and in the gas phase of the air will be determined. The results can give information on the transport behaviour and long-range transport of pesticides on the southern and northern Hemisphere from agricultural areas of the three different source regions South America, Africa and Europe.

Data management

Environmental data will be archived, published and disseminated according to international standards by the World Data Center PANGAEA Data Publisher for Earth & Environmental Science (<https://www.pangaea.de>) within two years after the end of the expedition at the latest. By default, the CC-BY license will be applied.

Any other data will be submitted to an appropriate long-term archive that provides unique and stable identifiers for the datasets and allows open online access to the data.

This expedition was supported by the Helmholtz Research Programme “Changing Earth – Sustaining our Future” Topic 4, Subtopic 4.1.

In all publications based on this expedition, the **Grant No. AWI_PS135_02** will be quoted and the following publication will be cited:

Alfred-Wegener-Institut Helmholtz-Zentrum für Polar- und Meeresforschung (2017) Polar Research and Supply Vessel POLARSTERN Operated by the Alfred-Wegener-Institute. Journal of large-scale research facilities, 3, A119. <http://dx.doi.org/10.17815/jlsrf-3-163>.

References

- Xie Z, Wang P, Wang X, Castro-Jiménez J, Kallenborn R, Liao C, Mi W, Lohmann R, Vila-Costa M, Dachs, J (2022a) Organophosphate ester pollution in the oceans. Nature Reviews Earth & Environment 3: 309-322. <https://doi.org/10.1038/s43017-022-00277-w>
- Xie Z, Zhang P, Wu ZL, Zhang S, Wei LJ, Mi LJ, Kuester A, Gandrass J, Ebinghaus R, Yang RQ, Wang Z, Mi W (2022b) Legacy and emerging organic contaminants in the polar regions. Science of the Total Environment 835. <https://doi.org/10.1016/j.scitotenv.2022.155376>

4. ATMOSPHERIC MEASUREMENTS

Stefan Kinne¹

¹DE.MPIC

Grant-No. AWI_PS135_03

Outline

Continuous atmospheric measurements were conducted to collect reference for satellite remote sensing and global modelling. In addition, atmospheric profiles from radiosonde data were analyzed to investigate processes in and near tropical convection and to validate wind-profiles of the AEOLUS satellite mission.

Objectives

Scientific goals were the collection of atmospheric reference data of aerosol, cloud and water vapor properties for satellite remote sensing and global modelling. Aerosol and water vapor data were collected with a sun-photometer and cloud properties were captured with visible and thermal sky imagers. These data were placed in the context to continuously sampled meteorological data and vertical atmospheric profiles from radiosonde launches. Special foci were processes in the region of tropical convection and wind-profile validations of satellite data.

Work at sea

Aerosol and water vapor atmospheric column averages were collected by a sun-photometer during the day, when the sun was not obscured by clouds, in a handheld operation. Data were transmitted each evening to NASA. These data were quality controlled and then placed on the web http://aeronet.gsfc.nasa.gov/new_web/maritime_aerosol_network_v3.html. During the voyage, all continuously recorded data were processed into hourly averages and placed into an Excel cruise summary worksheet. In particular the processing of automatically recorded sky (thermal) images into useful products was time-consuming. Sun-photometer data were added only for hours of data collections. The Excel worksheet allows to examine time-series, daily cycles and data associations, also in support of process understanding in atmospheric modeling.

Preliminary results

Crossing the Atlantic

The research cruise of the German research vessel *Polarstern* across the Atlantic from south (Punta Arenas, Chile, 53°S) to north (Bremerhaven, Germany, 53°N) provided latitudinal cross-section of atmospheric and oceanic properties for the March/April season. Hourly averages are presented as time-series for the latitude range from 47°S (after leaving the national zone of Argentina) to 47°N (when reaching the Bay of Biscayne). First, state data of automatically recorded meteorological data (available via the vessel's Dship server) are introduced. Next, aerosol properties sampled with sun-photometers are covered. Then cloud properties extracted from thermal camera images are presented. And finally, daily radiosonde data (launched at 11 UTC) inform on changes in atmospheric profiles for temperature, relative humidity, wind-speed and wind-direction.

Hourly averages of the air temperature recorded at 20 m elevation and water temperature at 5 m depth are presented in Fig. 4.1.

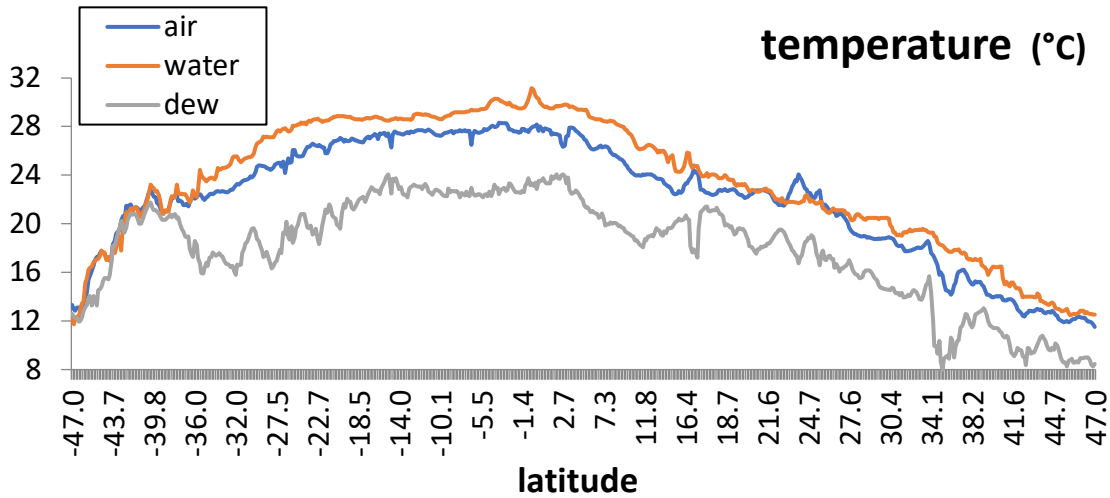


Fig. 4.1: Timeseries of hourly averages for air-, water- and dewpoint-temperature

The water temperature was generally warmer than the air temperature. Major exceptions were night- and morning-hours south of 40°S (with relative cold waters) associated with low visibility and at the peak of the dust event between 23°N and 25°N that carried warmer air from the Sahara. This air, however, was too dry for fog conditions to develop. Also presented in Figure 4.1 is the dewpoint temperature derived from the near surface relative humidity of Figure 4.3. Hereby the dry nature of the advected Sahara air is demonstrated as then the air temperature increase is associated with a dewpoint temperature decrease.

From differences between air and dewpoint temperature the low cloud condensation levels can be estimated. Figure 4.2 shows that these altitude estimates ($125 \text{ m} \cdot [T_{\text{air}} - T_{\text{dew}}]$) agree well with ceilometer detected cloud-base altitudes of cumulus clouds in the marine boundary layer (PBL).

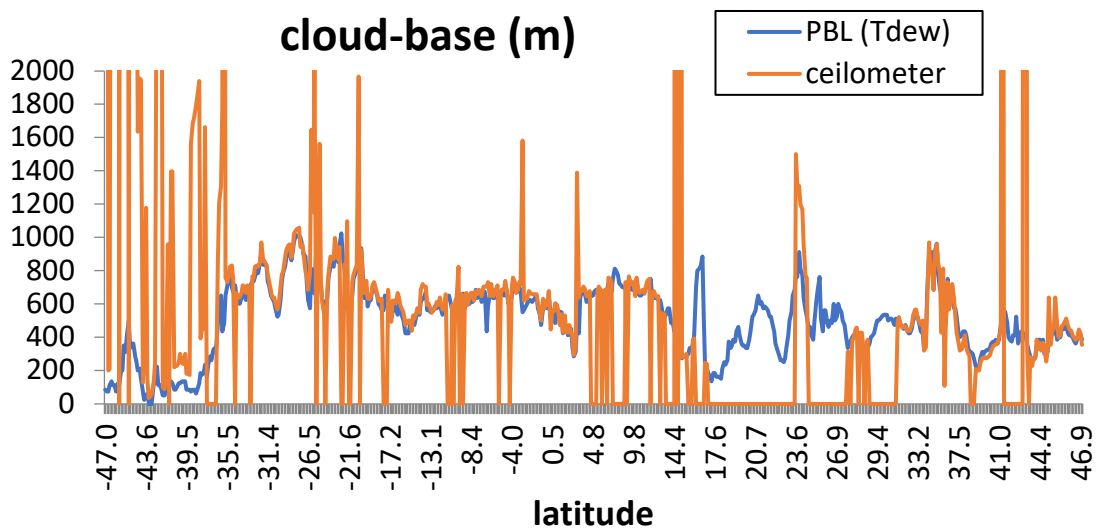


Fig. 4.2: Timeseries of hourly averages for estimates of cloud-base altitudes from $T_{\text{air}} - T_{\text{dew}}$ temperature differences ($\cdot 125 \text{ m}$) and observed cloud base altitudes with a ceilometer

Atmospheric water (vapor) properties are examined in Figure 4.3. Here surface properties of water vapor concentration and relative humidity are compared to the integrated water vapor content determined with a sun-photometer (during the day, when the sun was not obstructed by clouds).

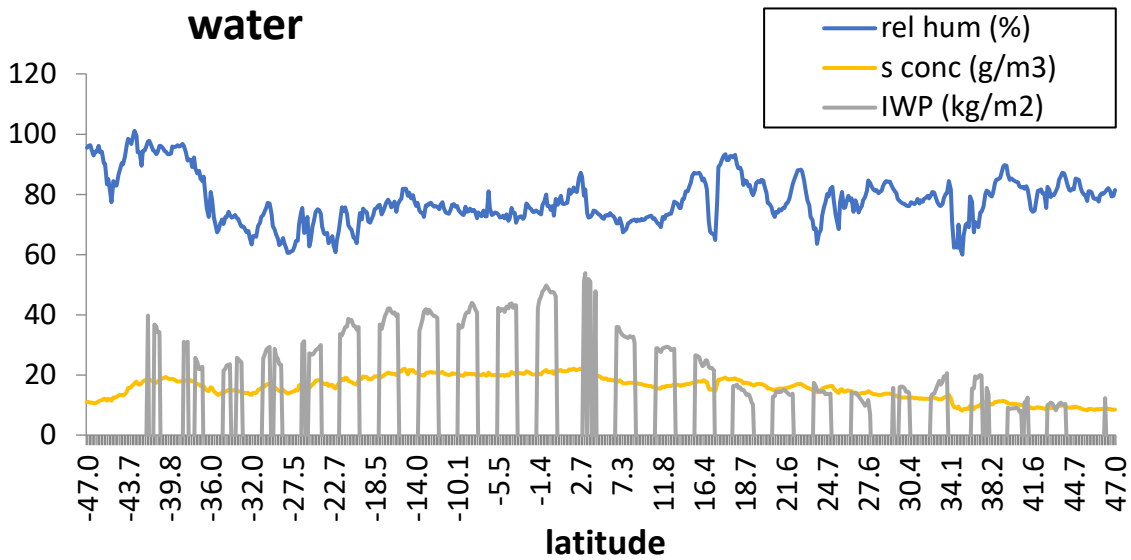


Fig. 4.3: Timeseries of hourly averages for relative humidity and water concentration at the surface as well as for integrated water vapor offered during the day by the sun-photometer

Typical values for relative humidities over oceans were near 75 %. Exceptions are relatively high values (generally above 95 %) south of 38°S and lower values near 70 % in sub-tropical regions. Particularly low values for relative humidity near 60 % are associated at 16°N with the stay in the Mindelo harbor region, at 24°N with the advection of Saharan mineral dust and at 35°N with the arrival of cold dry air after the passing of a low-pressure system with strong winds. Hourly averages of actual and relative wind speeds are presented in Figure 4.4.

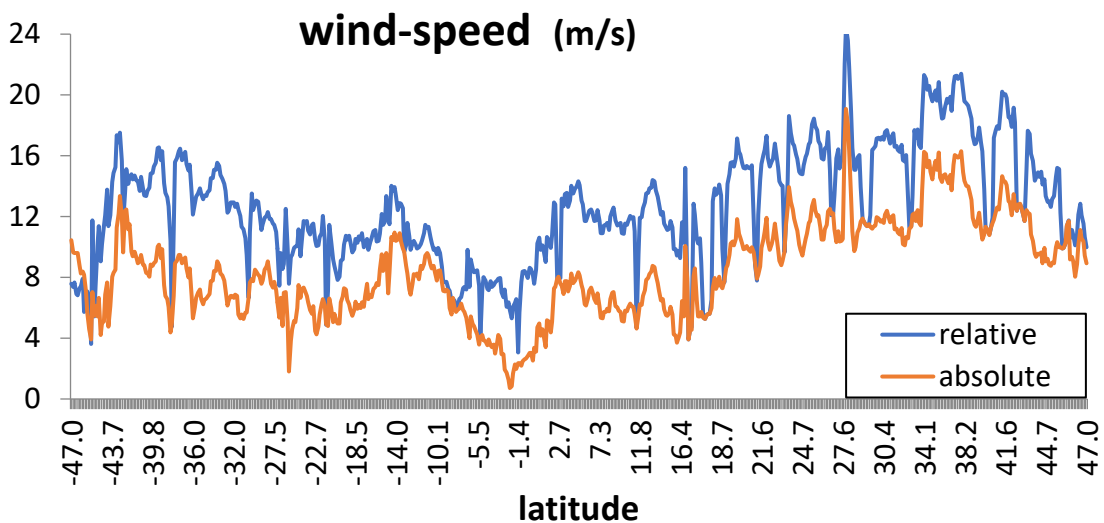


Fig. 4.4: Timeseries of relative and absolute hourly wind-speeds

For most of the voyage, the vessel moved into the winds (except during the beginning of the cruise). Thus, the relative (experienced) wind-speed was higher than actual (absolute) wind-speed. As a result, station stops are identified, when relative and absolute wind-speed are identical. The highest wind-speeds ($>15\text{m/s}$) occurred near the Canary Island (accelerations effects between island mountains) and later at and north of 34°N with a passing of a low-pressure system. The lowest wind-speeds ($<3\text{m/s}$) occurred in the low wind-speed ('doldrum') region (just south of the equator).

Hourly averages of radiative energy fluxes are examined in Figure 4.5. Only solar downward fluxes (SWdn) were recorded by instrumentation of the *Polarstern*. The SWdn hourly maxima each day resemble bell-shapes (expected for cloud-free conditions) – to indicate favorable sampling conditions with sun-photometry. To address the surface energy budget, daily averaged solar fluxes ($\langle\text{SWdn}\rangle$) fluxes are calculated (via their 24-hour running averages) and a 4 % solar surface albedo is assumed to define the solar netflux ($\langle\text{SWnet}\rangle$). For the thermal energy budget, the upward fluxes (LWup) are easily determined via the water temperature and the missing downward thermal fluxes (LWdn) were calculated from blackbody temperature statistics by the thermal camera in the thermal IR window (8-12 μm). As a result, the total (combined solar and thermal) netflux (net = $\text{SWnet} + \text{LWdn} - \text{LWup}$) imbalance at the surface now can be determined, which in the end is balanced (mainly) by releases of latent and sensible heat from the surface into the atmosphere.

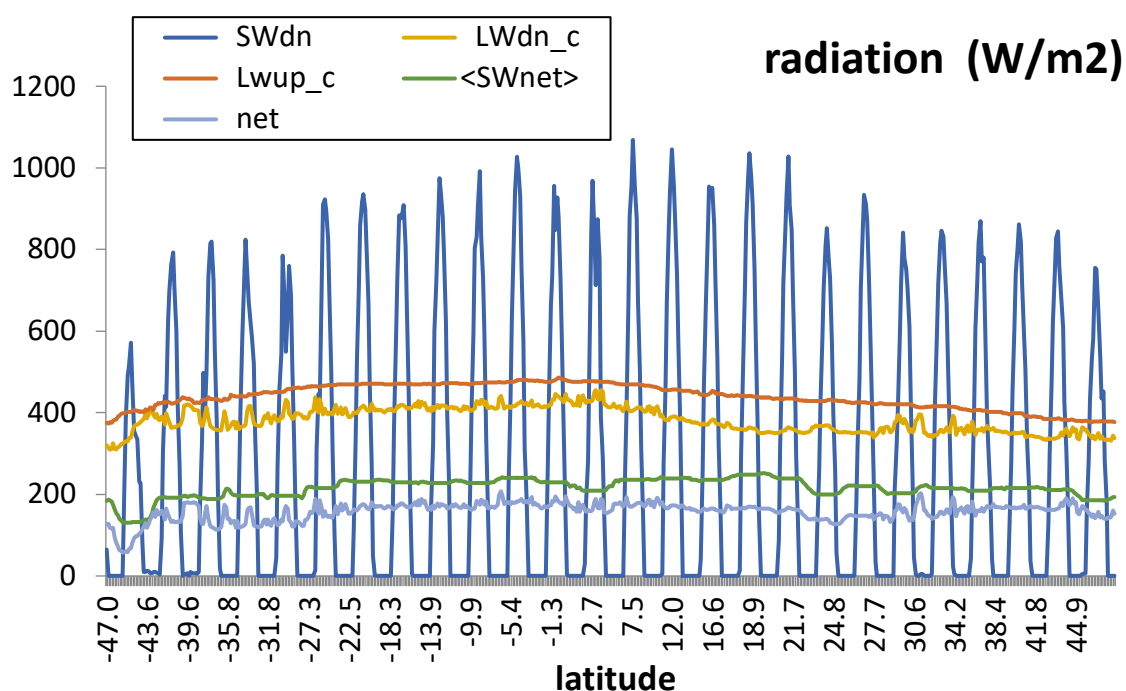


Fig. 4.5: Timeseries of measured hourly averages for the downward solar (SWdn), its day running average net ($\langle\text{SWnet}\rangle$) assuming a solar surface albedo of 4 % and thermal IR fluxes with upward fluxes (LWup) derived from the surface temperature and downward fluxes derived from blackbody temperature statistics in the IR window by the thermal camera. As a result, estimates for the radiative flux imbalance at the surface (for sensible and latent heat) are given.

The resulting daily average net-flux imbalances at the surface appear reasonable (varying between 120 and 200 W/m^2) although here the solar daily cycle is averaged out, which creates strong positive imbalances during the day and small negative imbalances during the night. Selected oceanic surface data (salinity, temperature and chlorophyll-a) are compared in Figure 4.6.

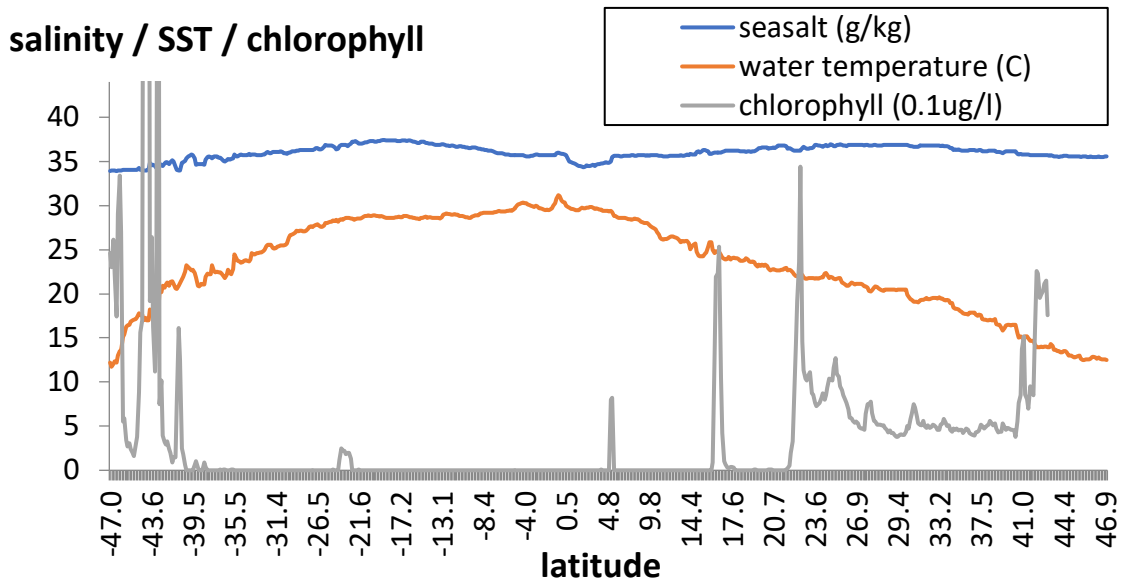


Fig. 4.6: Timeseries of hourly averages for salinity, water temperature, chlorophyll content

The highest sea surface temperatures (SST) were near the location of the overhead sun then (on 24 March) just north of the equator. For sub-tropical regions, southern hemispheric SST were higher than for the northern hemisphere, in part due to the stronger insolation during the last months and in part due to upwelling of colder waters (along the *Polarstern* path) in the northern hemisphere (indicated by higher chlorophyll-a concentrations). The sea-salt concentrations show a minimum under the region of strongest convection (and precipitation) with more fresh water.

Attenuation measurements of the direct sunlight are highly accurate, unlike interpretations of backscattered satellite data, which rely on assumptions (i.e. for aerosol on composition and the radiative background). Thus, NASA's AERONET group distributes (on an opportunity-basis) calibrated handheld MICROTUPS sun-photometers to volunteers that participate in cruises across the oceans. The volunteers are expected to sample solar spectral irradiances at times when the sun is not obscured by clouds. Since position and time defines the incoming solar radiation reference at the Top Of the Atmosphere (TOA), the smaller values measured on the ground (or vessel) define an attenuation which (if clouds do not interfere) can be attributed to aerosol, air molecules and trace-gases. The MICROTUPS records the solar intensity data at five different solar spectral intervals, to allow in combination with the TOA reference the determination of column averages for aerosol amount, for aerosol size and for water vapor. Aerosol size is derived from the spectral dependency of the aerosol amount and water vapor content is based on differences of solar attenuation in two adjacent spectral regions – one without and one with (known strength) absorption by water vapor. The MICROTUPS is paired with a GPS unit to supply the current position (of a vessel) for the determination of the needed TOA reference. As a backup to aerosol amount samples, a simpler CALITOO sun-photometer was used. Both instruments (CALITOO and MICROTUPS) are shown in Fig 4.7.



Fig. 4.7: A MICROTOPS II sun-photometer with an attached GPS for information on position (left) and a newer less pricey CALITOO sun-photometer with a built-in GPS (right);
(photos by Stefan Kinne)

All aerosol and water vapor data of the MICROTOPS are transferred at the end of each day to NASA's Marine Aerosol Network (MAN) database and are accessible within days at (https://aeronet.gsfc.nasa.gov/new_web/maritime_aerosol_network_v3.html).

For the data presentation, the lowest data sample series in each hour was selected as additional filter for outliers (e.g. cloud contamination). Time series of hourly averages are investigated for column data of aerosol amount (AOD at 550 nm), aerosol size (Angstrom parameter and AOD fine-mode fraction) and aerosol potential to modify water clouds (Aerosol Index).

AOD at 550 nm is the negative exponential attenuation coefficient normalized to a vertical view due to aerosol. The '550 nm' addition refers to the (green) solar wavelength of the observation. Only 10 % of the direct sun-light is removed under marine background conditions (AOD ~ 0.05), whereas at moderately polluted conditions (AOD ~ 0.40) about of half of the direct sunlight is removed. AOD values are highly variable with a global average AOD near 0.13. Best AOD data for the same hour between MICROTOPS and CALITOO are compared in Figure 4.8.

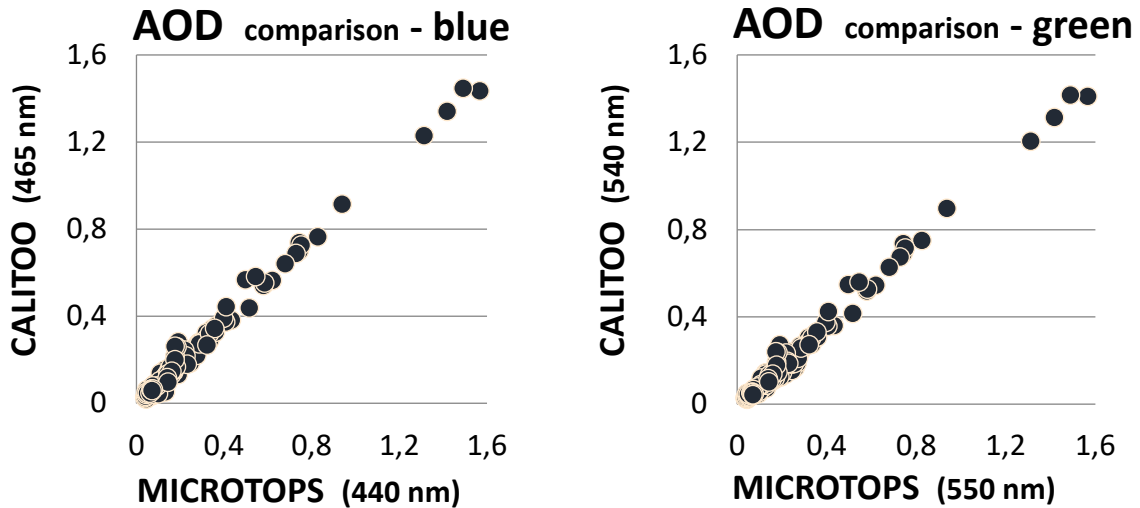


Fig. 4.8: Comparisons of lowest AOD in the same hour by MICROTOPS II and CALITOO sun-photometers for blue light (left) and for green light (right)

Low AOD data by hour between both sun-photometers agree well. The agreement, however, is better for blue than for green light. The CALITOO data for green light appear too low, as its associated 465 nm/540 nm (wavelength) AOD ratio remains large even for larger aerosol, where no significant AOD ratio should be expected. Thus, for presentation of mid-visible AOD data, MICROTOPS data are preferred.

The Angstrom parameter requires AOD data at (at least) two different solar wavelengths (here at 440 nm and 870 nm) to address the characteristic aerosol size – via the negative slope in $\ln(\text{AOD})$ and $\ln(\text{wavelength})$ space. A smaller Angstrom value (< 0.5) indicates a dominance of super-micrometer sizes (e.g. from sea-salt or mineral dust), while a larger Angstrom value (> 1.2) indicates the dominance of sub-micrometer aerosol sizes (e.g. from wildfires and pollution).

The AOD fine-mode fraction is more useful to modelling and satellite remote retrievals as they stratify aerosol in super- and sub-micrometer size-modes. The AOD fine-mode fraction can be determined from the spectral dependence of the Angstrom parameter. As a result, AOD data at four or more different wavelengths are needed for an AOD fine-mode fraction estimate.

The Aerosol Index (AI), the product of AOD and Angstrom, is a good proxy for aerosol number concentrations thus for aerosol potential to modify cloud properties and cloud processes.

The time-series of hourly AOD (amount) and associated Angstrom (size) of the MICROTOPS are presented in Figure 4.9.

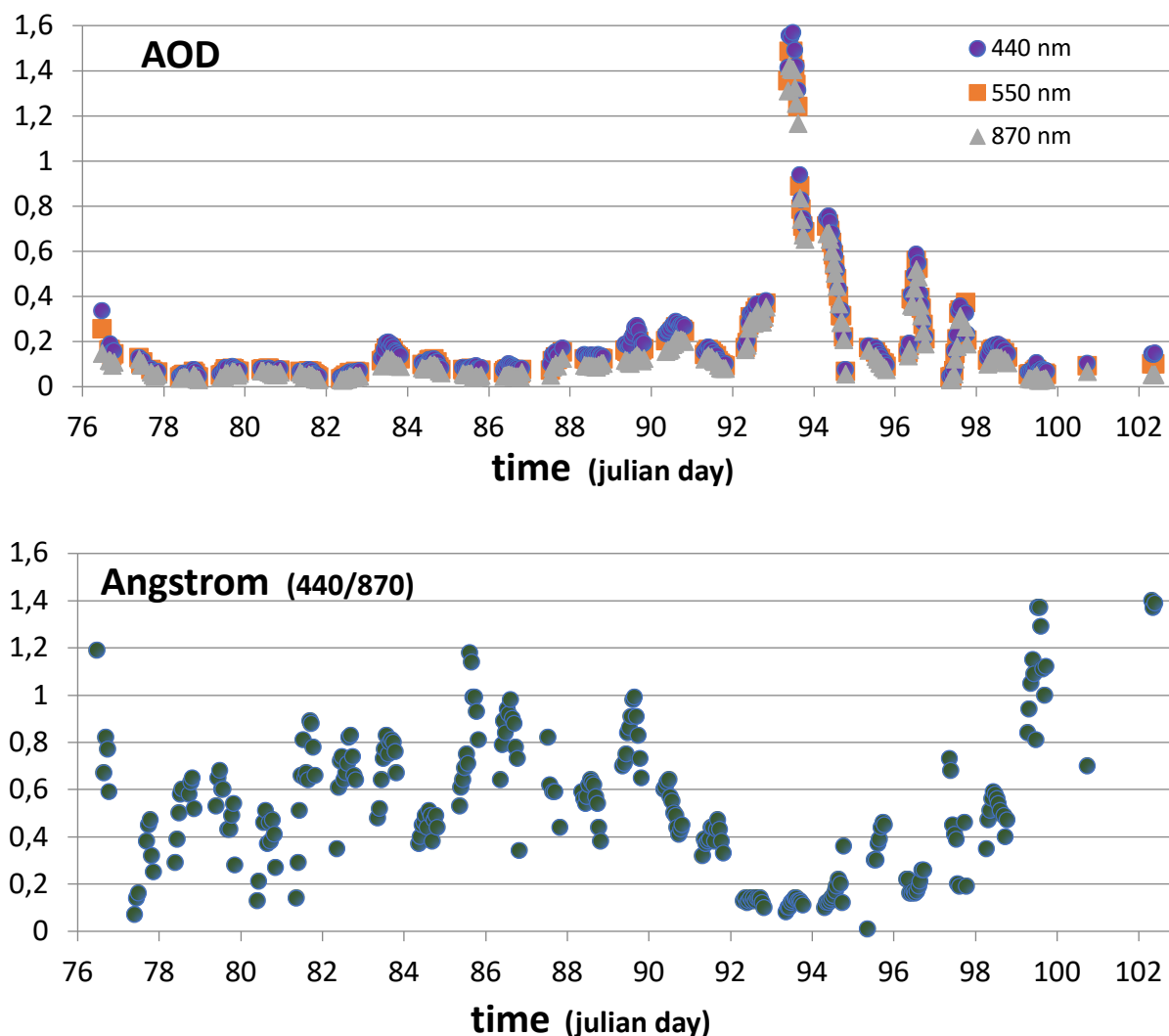


Fig. 4.9: Time-series of hourly MICROTOPS data for AOD at 440, 550 and 870 nm to inform on aerosol amount (top) and associated 440/870 Angstrom values for aerosol size info (bottom)

After leaving the EEZ of Argentina, the aerosol record starts on Julian day 76 (14 March) with foggy conditions and elevated AOD and small aerosol sizes. Then all the way across the southern hemisphere to the equator (days 77-85, 15-23 March) marine background conditions were recorded – except for day 83, when a high-pressure synoptic system advected traces of smoke or pollution from southern Africa. Once the equator was crossed AOD levels increased, although major plumes of smoke and pollution from west Africa and from Saharan dust from a few days earlier were missed. Aerosol forecast models that assimilate satellite data (i.e. <https://www.nrlmry.navy.mil/aerosol>) illustrate that these aerosol plumes frequently extend towards the equator (but without crossing the equator) on their westward path to northern S. America and the Caribic. Sampling was partly interrupted on day 87 (25 March) with convective cloud cover at the northern border of the tropical convection belt (ITCZ). There aerosols - and especially larger aerosol sizes - were removed (by wet deposition). After leaving the tropical convection slightly elevated aerosol loads on day 89 (27 March) were caused by relatively small particles from western Africa. Later, closer to and at Mindelo on day 90 (28 March) visibility was reduced by remnants of a diluting mineral dust aerosol plume. North of Mindelo over a time-period of several days (days 92 to 94) the vessel passed below a major mineral

dust plume from the Sahara with their characteristic larger aerosol sizes (identified by low Angstrom values). Maximum AOD values reached 1.5 around noontime on day 93 (31 March). As the plume spread and distributed in all directions, outflows of this plume continued to reach the vessel's northward route on days 96 to 98 (2-4 April). Later, Angstrom parameters increased to indicate a different (and smaller) aerosol type. Such higher Angstrom values of 1.4 were also associated with winds off northern France onto the western Channel on day 102 (9 April), typical for sizes associated with pollution. The AOD fine-mode fraction, the alternate aerosol size-information and corresponding to Figure 4.8, is presented Figure 4.10.

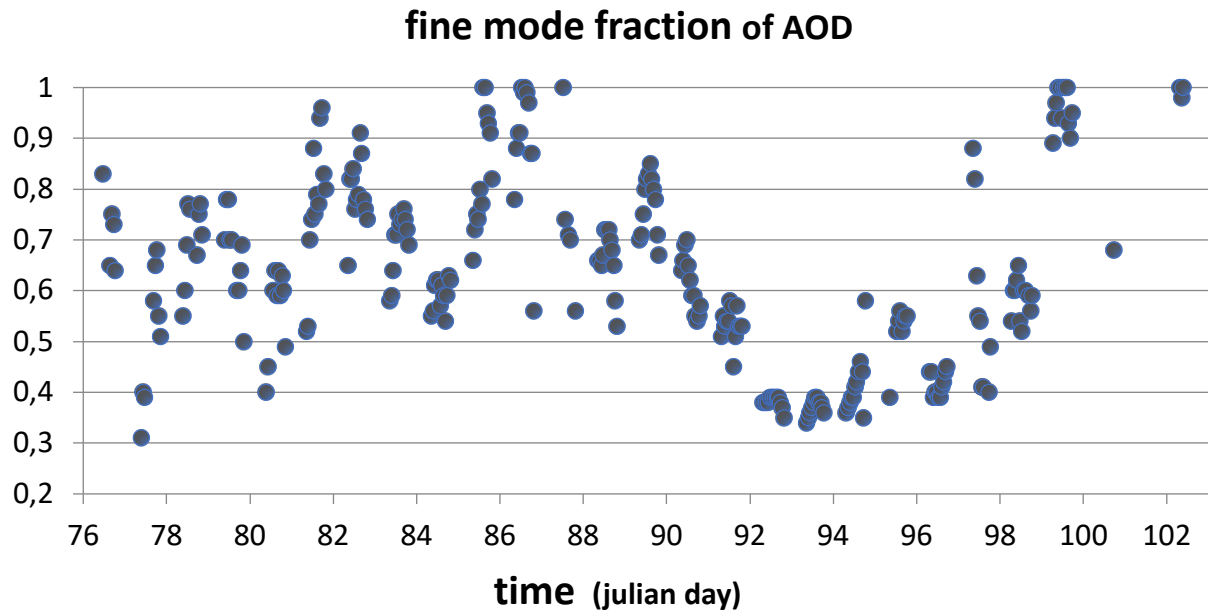


Fig. 4.10: Time-series of hourly MICROTOPS data for the AOD fine-mode fraction (using AOD data at 380, 440, 670 and 870 nm) to indicate the AOD fractions attributed to smaller sub-micrometer aerosol sizes.

The potential of aerosol to modify the microphysics of water clouds remained small, as the aerosol index ($\text{AOD} \cdot \text{Angstrom}$) remained below 0.2 – except for the high relative humidity event in the morning of day day 76 (14 March) – as illustrated in Figure 4.11.

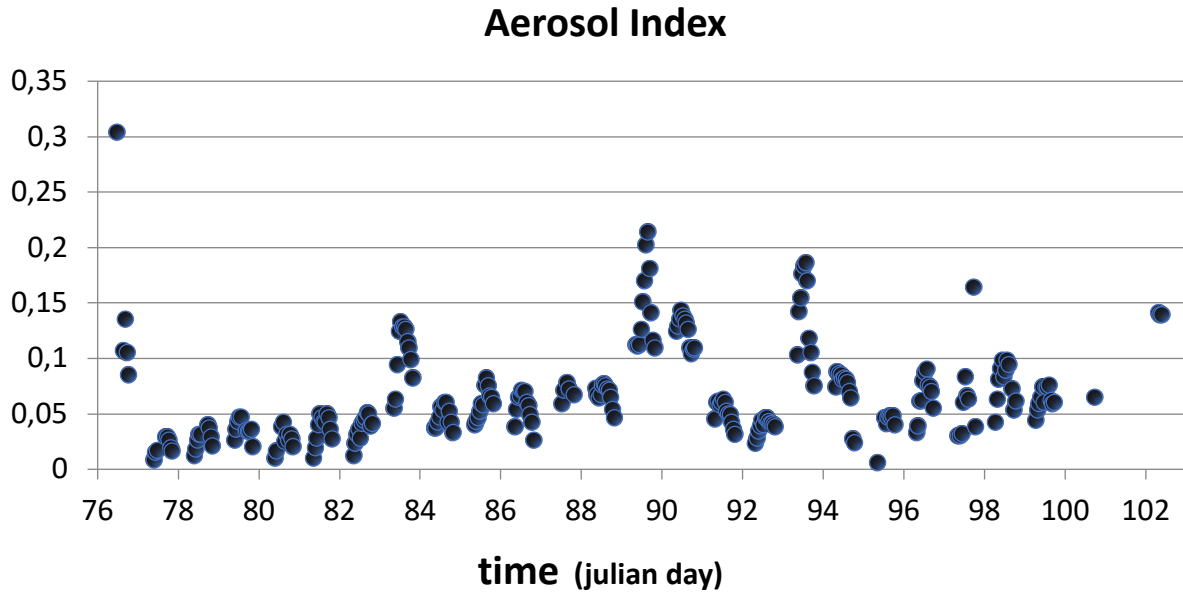


Fig. 4.11: Time-series of hourly MICROTOSPS Aerosol Indices ($AI=AOD \cdot \text{Angstrom}$) values, serves as a proxy for aerosol number concentrations and potential cloud droplet nuclei.

Via the differential absorption technique using simultaneous MICROTOSPS data samples at 870 nm (no water vapor absorption) and at 940 nm (with known strength water vapor absorption) the integrated water vapor (IWP) is determined. The time-series of hourly IWP data at cloud-free views of the sun during daytime is presented in Figure 4.12.

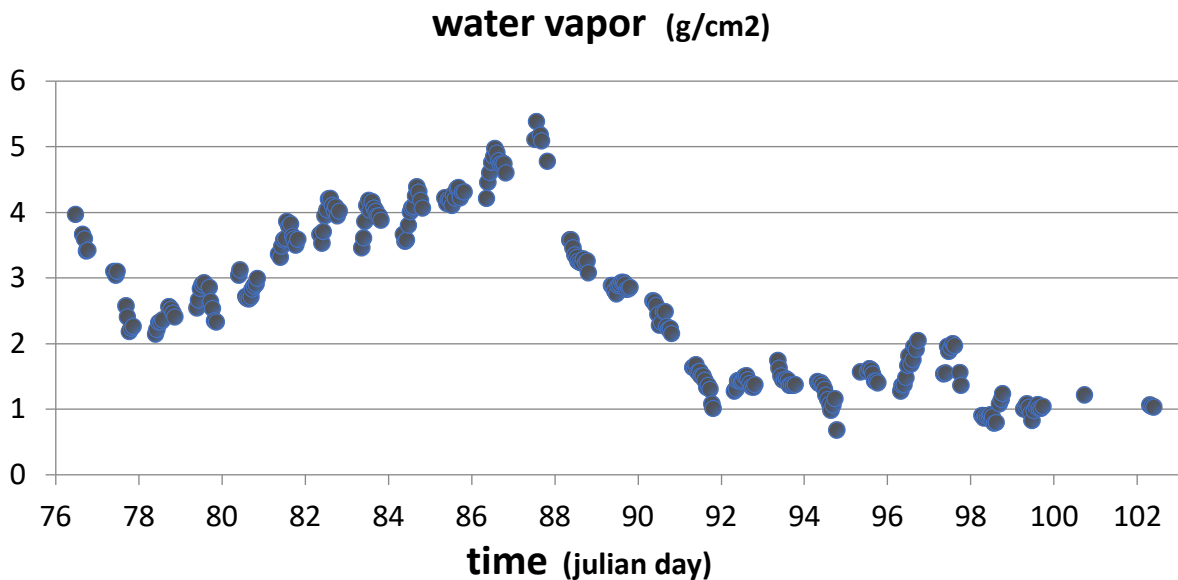


Fig. 4.12: Time-series of hourly MICROPTOSPS based data for the atmospheric integrated water vapor

After leaving the southern mid-latitude convection the Integrated Water Vapor (IWP) increased continuously from 20 kg/m² at 41°S to 55 kg/m² at the northern border of the ITCZ near 4°N. In the northern subtropics the IWP values rapidly decreased to values near 15 kg/m² at 20°N and (typical for air-masses from the Sahara and also northern mid-latitudes in spring) stayed at these and even lower values towards the end of the voyage.

The MPI-M cloud camera system consists of a mid-visible frog-eye upward hemispheric camera and a thermal (IR window) upward looking camera with a limited 30° field-of-view (FOV). Images are captured every 10 seconds. The images inform on overall cloud cover, on cloud structures (and their movement in time) and (with the thermal sensor) also on cloud base heights. Visible images are mainly used to describe general sky conditions. The actual cloud data analysis focuses on (restricted view) thermal images, because they offer aside from cloud cover and structures (even near the sun) also information on cloud-base altitude distributions—day and night. The camera box and a set of simultaneous images on a monitor are presented in Figure 4.13.

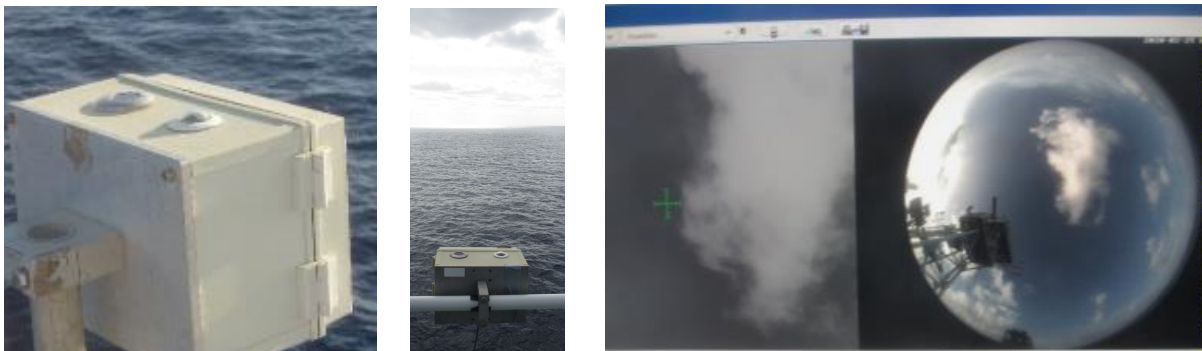


Fig. 4.13: The dual camera system onboard Polarstern (center) with a frog-eye spherical and a flat thermal sensor (left) and an example of a coincident thermal and visible image (right); (photos by Stefan Kinne)

For the data processing, first the recorded grey-images of the thermal camera are translated into (IR blackbody) temperatures (via a camera specific calibration file) in the camera's sensed thermal IR window (roughly between 8 and 12 μm wavelengths). Then, these temperatures are converted into altitudes. This task is complicated, since generally neither complementary information on the atmospheric temperature profile nor information on the atmospheric water content and its vertical distribution are available, certainly not at the same temporal resolution. The water vapor information is particularly important for warmer climates with higher water content (i.e. the tropics). There, water vapor continuum absorption (in a square dependence) reduces the thermal camera's sensitivity to clouds – especially to higher altitude clouds, so that the cloud-free sky background as well as clouds appear much warmer to the camera as the (assumed) atmospheric temperature profile would suggest. Thus, the difference between the (measured) surface temperature (T_{sur}) and the (camera-detected) cloud-free sky background temperature (T_{sky}) is applied to serve as proxy for the atmospheric Integrated Water vapor Path (IWP) content. Hereby, T_{sky} is defined by the low 2 % Probability Density Function (PDF) value of all 60.000 sensor pixels from all 360 recorded thermal images during the last hour. Only in case of persistent overcast conditions during the last hour, a T_{sky} value of the most recent cloud-free observation is substituted. For cloud-base altitude distribution information, $[T_{\text{sur}} - T_{\text{sky}}]$ difference estimates were applied to estimate blackbody temperatures at specific altitudes z (of 0.5, 1.0, 1.5, 2.0, 3.0, 6.0, 10.0 km): $T_z = [T_{\text{sur}} - T_{\text{sky}}] * z / z_{\text{tp}} ** ([T_{\text{sur}} - T_{\text{sky}}] / [T_{\text{sur}} - T_{\text{tp}}]) ** 0.5$, with 'tp' for tropopause values and by considering that with more IWP (or smaller $[T_{\text{sur}} - T_{\text{sky}}]$) water vapor induced reductions to the sensed blackbody temperature

decrease with altitude (lapse rate) are stronger at lower altitudes. Altitude assigned effective blackbody temperatures T_z are then applied to each thermal image as threshold temperature to determine its cloud cover and its cloud inhomogeneity. Cloud cover is assigned when image temperatures are warmer than the threshold temperature T_z . Cloud inhomogeneity is based on the total length of cloud borders within any image, which are easily identified by ‘multiplying’ the cloud pattern of a sensed image with its minimal shifted twin. A time-series of cloud cover (as seen by a ground-observer) with fractional contributions by cloud-base altitude range is presented in Figure 4.14.

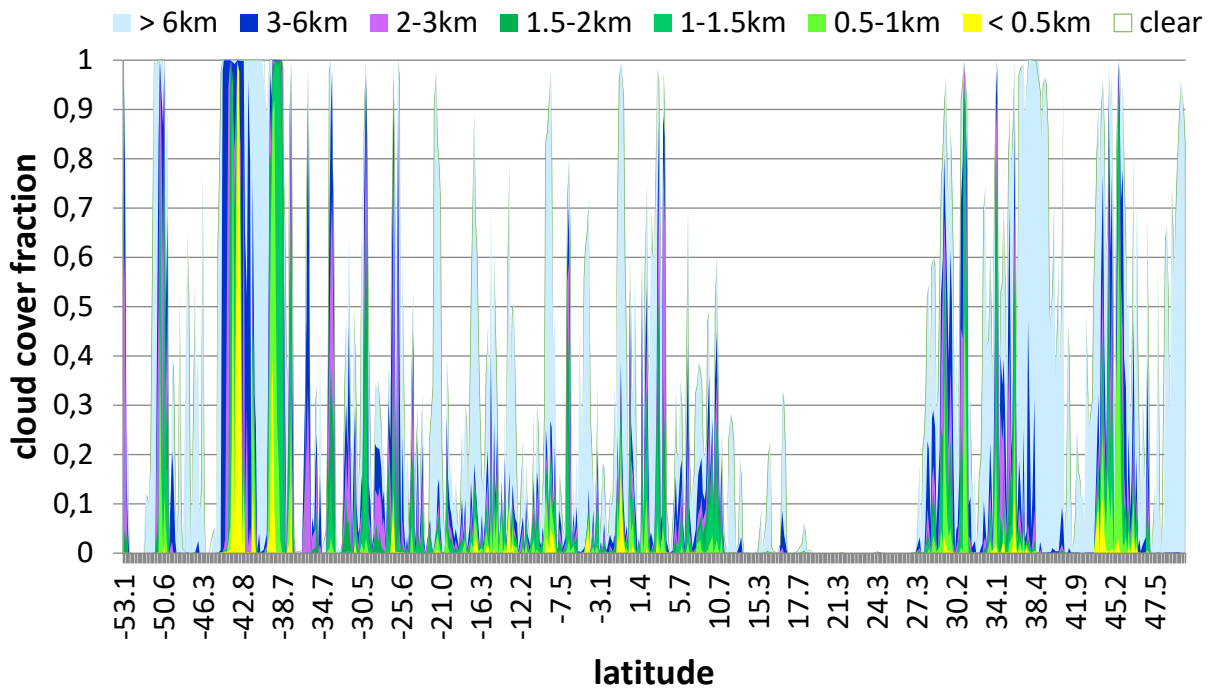


Fig. 4.14: Time-series of hourly averages for cloud-cover during PS135, with cloud-base altitude contributions for different altitude ranges: 0.0-0.5 km (yellow), 0.5-1.0 km (light green), 1.0-1.5 km (green), 1.5-2.0 km (dark green), 2.0-3.0 km (purple), 3.0-6.0 km (blue) and above 6 km (light blue)

Cloud cover during the cruise was generally low and then mainly caused by lower altitude clouds. Periods of higher cloud cover occurred in conjunction with of synoptic weather systems at mid-latitudes (i.e. 44°S-38°S, 33°N-49°N) with the passing of tropical convection (2°N-4°N). In contrast, the outflow of Saharan dust (20°N-26°N) occurred at cloud-free conditions. Cloud inhomogeneity scores as function of altitude are presented in Figure 4.15.

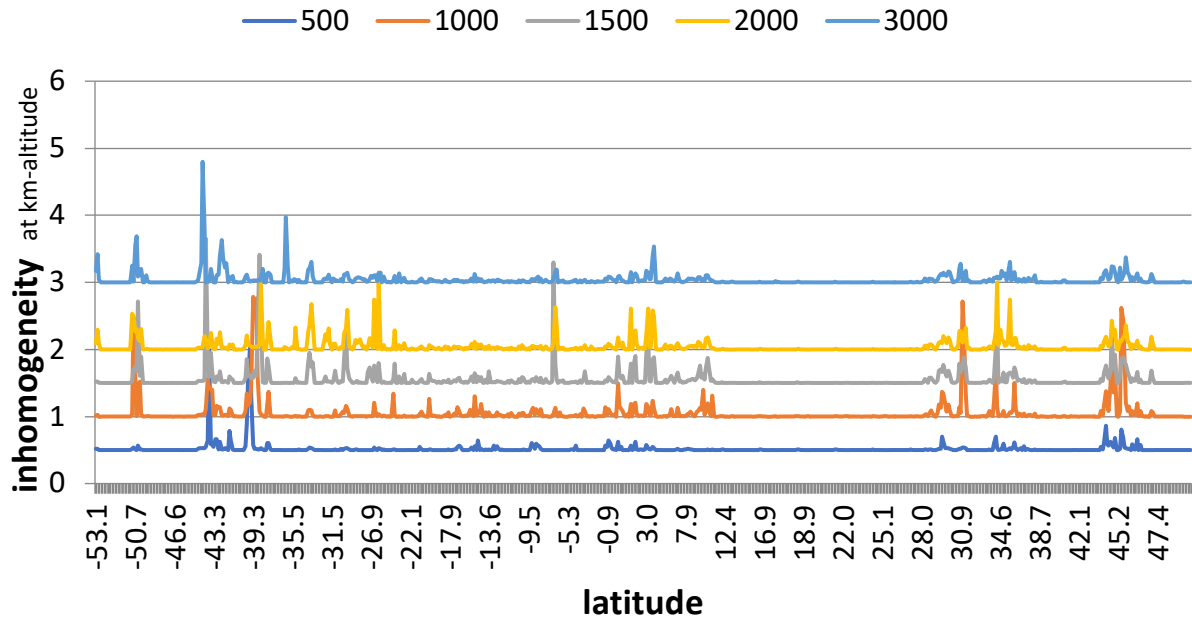


Fig. 4.15: Time-series of hourly averages for cloud inhomogeneity during PS135 as function of altitude: 0.5 km (dark blue), 1.0 km (orange), 1.5 km (grey), 2.0 km (yellow) and 3.0 km (light blue)

Major convection is indicated by inhomogeneity at higher altitudes (> 2km). In the sub-tropics this higher altitude convection was usually absent, as the dry mid-atmosphere did not allow for cloud cover. Brief precipitation, when it occurred, was not associated with an ice-phase.

In a complementary effort to the cloud cover data by the thermal imager also visual estimates of cloud cover were recorded each hour. These observations were based on meteorological charts for cloud-types and sea-state. The cloud type chart distinguishes among nine different types of clouds at high (5-12 km), mid (2-5 km) and low-level (0-2 km) altitudes – via a NOAA Sky Watcher Chart, <https://www.weather.gov/media/bmx/skywarn/cloudchart.pdf> and via a DWD cloud atlas.

Cloud cover observations (in octas) each hour during day-light were compared to hourly cloud cover averages by thermal cloud camera images and – in a rather general way – to monthly average properties of the ‘geoprof’ cloud climatology (in a ground observation mode) along the ship track. Comparisons for the total and low cloud cover are compared in Figure 4.16.

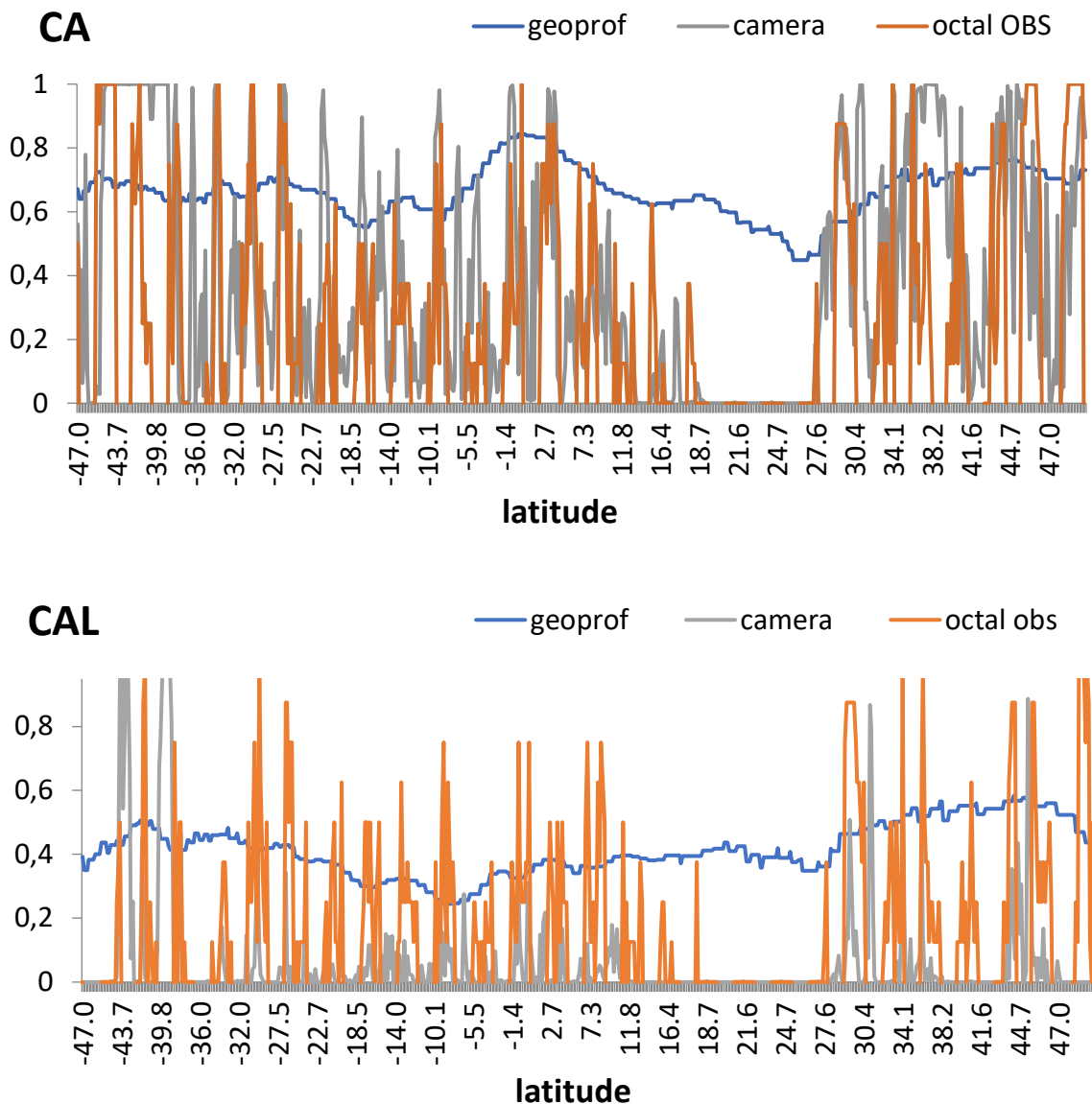


Fig. 4.16: Comparisons of total cloud cover along the ship track for total cloud cover (CA, top) and low altitude cloud cover (CAL, bottom); Octas cloud cover estimates observed every hour are compared to hourly averages by the thermal camera (camera) and to monthly averages of a cloud climatology in a ground observer mode – based on active remote sensing from space ('geoprof').

The cloud observations are in general agreement with the highly averaged data of the climatology. There is also a general agreement between spot observations and hourly averages with the camera processed cloud cover data during the day. But this comparison also reveals apparent camera processing biases (too much total cloud cover, too few low cloud cover) mainly due to the assumptions of linearly decreasing temperature with altitude, which is a poor choice in case of temperature inversions, which were quite common in the subtropics.

The DWD station on the *Polarstern* launched radiosondes on each day between 12 March and 7 April at 11 UTC (for a 12 UTC weather forecast) – except when too close to islands. All launch locations are presented in Figure 4.17.

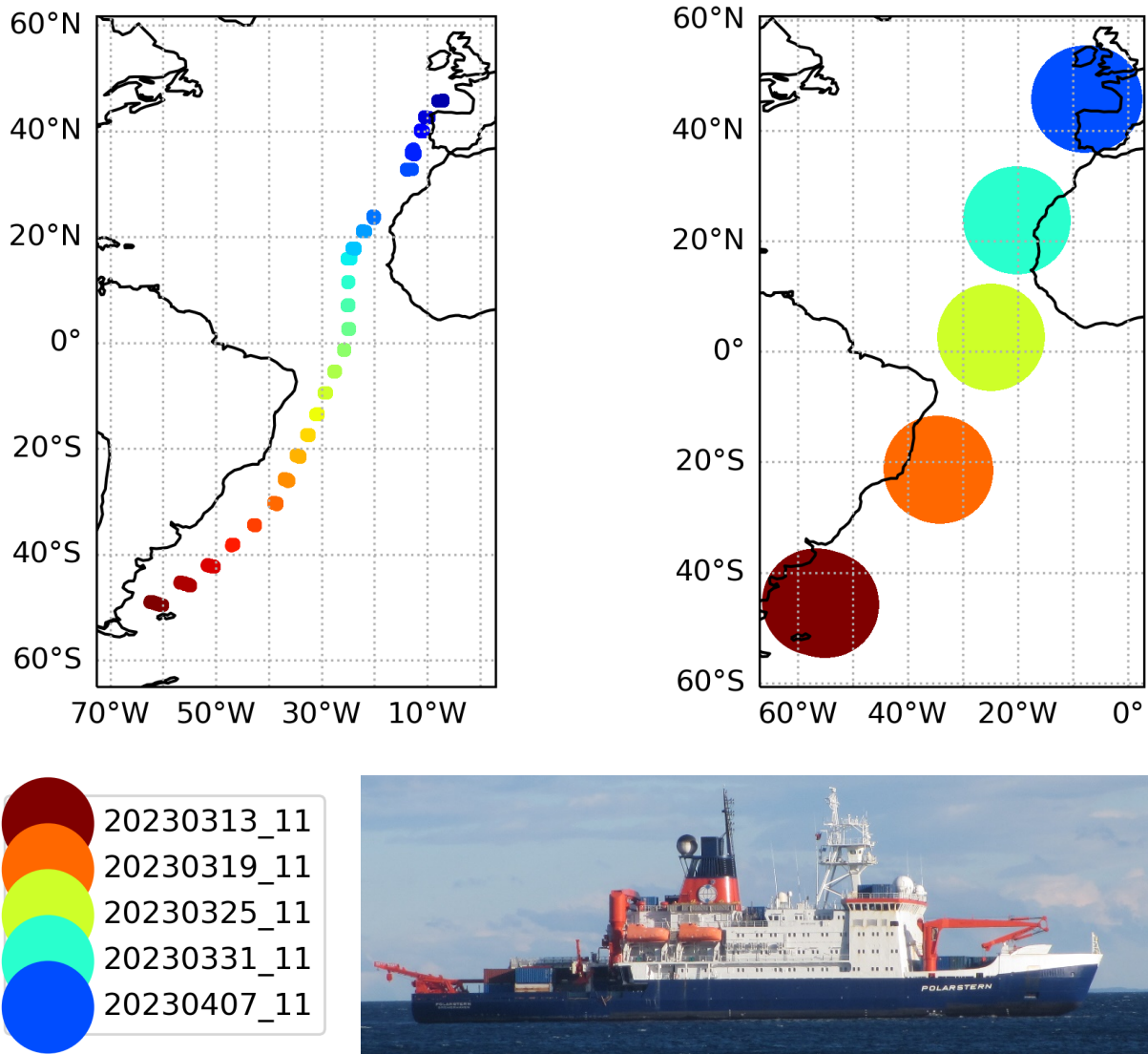


Fig.4.17: Sampling locations of the daily radiosondes (top, left) and selected five (top, right) from Polarstern (bottom) during the PS135 science cruise from 12 March to 7 April 2023; (photo of Polarstern before Punta Arenas in early March by Stefan Kinne)

Radiosondes were lifted by a helium balloon to altitudes above 30 km for atmospheric profiles of temperature, humidity, wind-speed and wind-direction. Data were recorded during ascent and descent. To illustrate profile differences with respect to climate zones, the comparison of the profiles is reduced to five, according to the locations and their colour codes of Figure 4.17. Vertical profiles for temperature, relative humidity, windspeed and wind-direction are presented in Figure 4.18 for five radiosonde ascents and subsequent descents (thus, two profiles) are for southern and northern mid-latitudes, southern and northern sub-tropics and the central tropics.

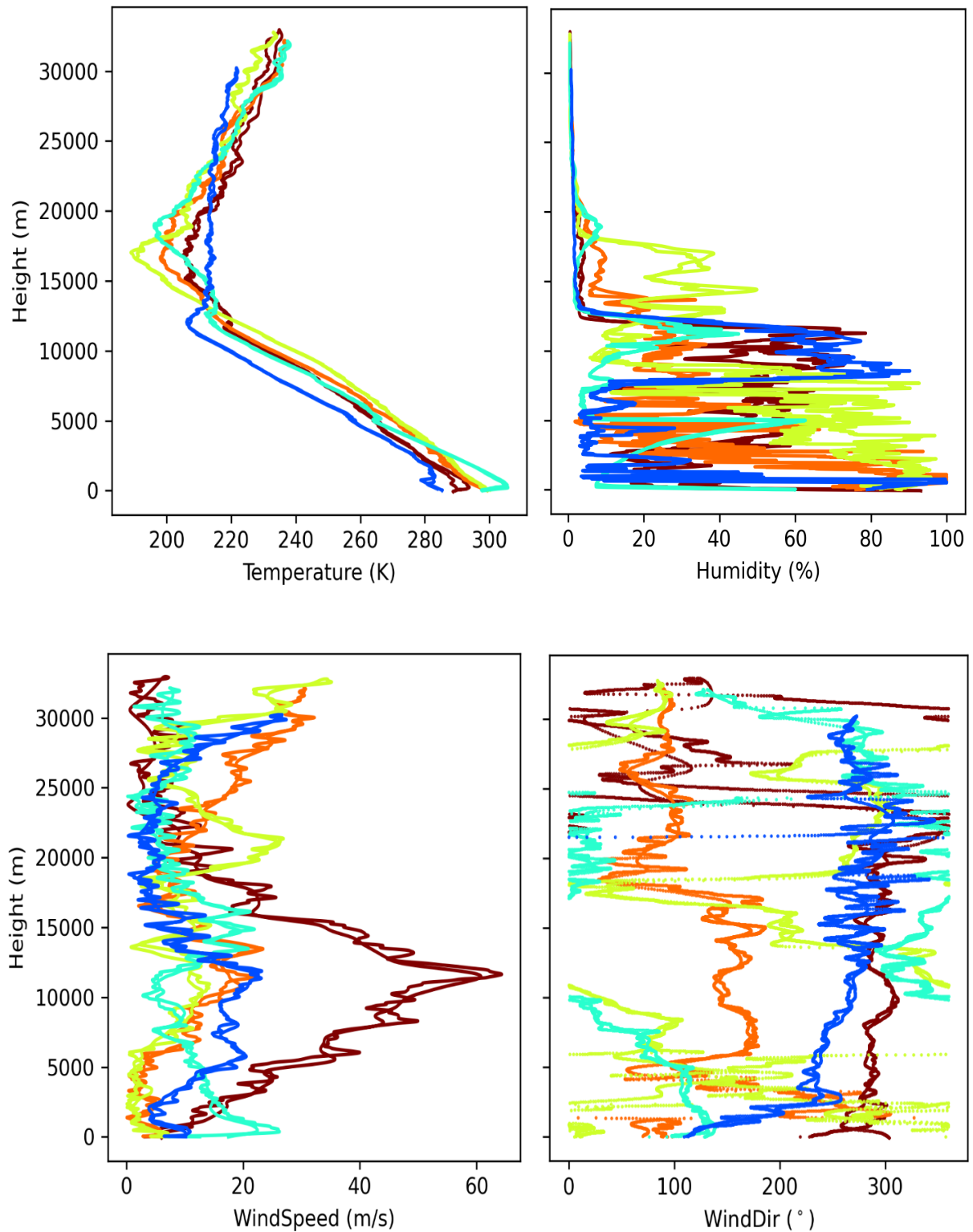


Fig. 4.18: Comparisons of vertical profiles for temperature (top, left), relative humidity (top right), wind-speed (bottom left) and wind-direction (bottom right) representing different climate zone: the southern hemispheric mid-latitudes (brown), the southern subtropics (orange), the tropics (green), northern subtropics (turquoise) and northern hemispheric mid-latitudes (blue)

Temperature: Near surface temperature inversions were detected at mid-latitudes and also for the northern subtropics with elevated warm air from the Sahara. With advection of arctic air on the backside for a low-pressure system, the temperatures for the northern mid-latitudes profile are particular low. Tropopause altitudes at mid-latitudes are near 12 km, while those for tropics and sub-tropics are well above 15 km.

Relative Humidity: The tropical profile has relative high values up to altitudes of 8 km, the mid-latitudes have relatively high values between 8 and 12 km and the subtropics are usually very dry from above the boundary layer all the way up to the tropopause. In that context, the northern sub-tropical profiles deviate with very dry conditions already from the surface but relative moist layers at 5 and 11 km linked to different air masses – as demonstrated by changes in wind-directions at those altitudes.

Wind-speed: The largest horizontal wind-speeds are associated with the zonal jet-stream near 10 km at mid-latitudes – although the jet is relatively weak for the northern mid-latitude example with the northerly advection of Arctic air. Tropical and sub-tropical profiles have relatively weak wind-speeds, particularly in the lower troposphere.

Wind-direction: Wind-direction changes are only meaningful, if wind-speeds are larger. Some wind-direction changes with altitudes, however, reveal general circulation features. For the northern subtropical dust event the easterly winds near the surface (which carried the Saharan dust) are fed by compensating westerly winds above 2 km. And for the tropical convection near the ITCZ the south-easterly winds near the surface are associated with opposite direction north-western winds between 10 and 15 km (for a flavour of the Hadley circulation).

The locations of all radiosondes released just before 11 UTC from *Polarstern* during PS135 are presented by hemisphere in Figure 4.19 and associated data in Figure 4.20 (following the colour selections of Fig. 4.19).

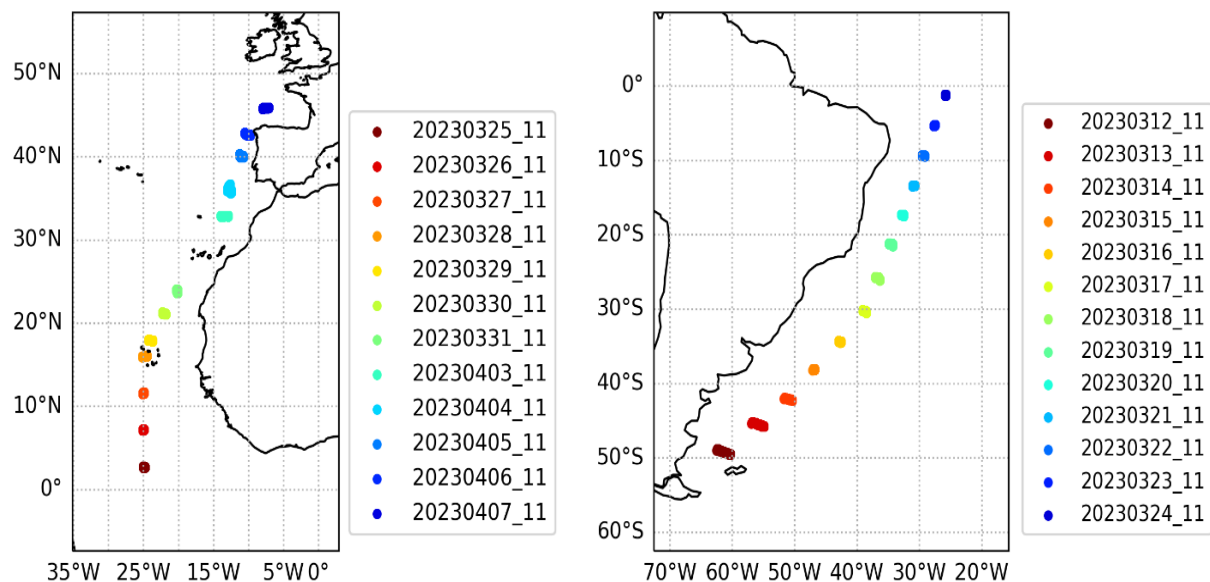


Fig. 4.19: Sampling locations of the daily radiosondes in the northern hemisphere (left) and southern hemisphere (right) during the PS135 science cruise from 12 March to 7 April 2023

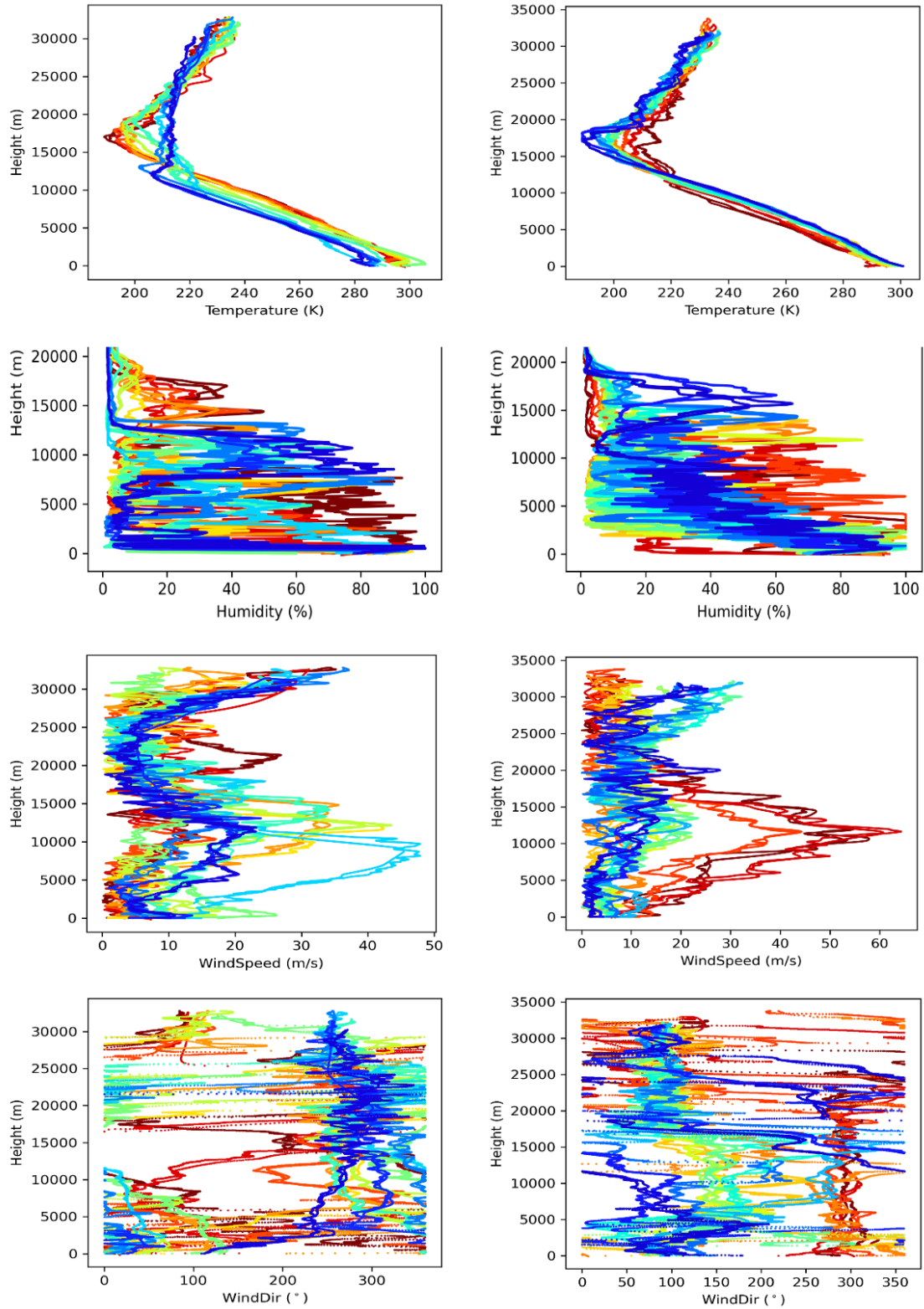


Fig. 4.20: Comparisons of vertical profiles in the northern hemisphere (left column) and in the southern hemisphere (right column) for temperature (row 1), relative humidity (row 2), wind-speed (row 3) and wind-direction (row 4) – for locations and dates by colours of Fig. 4.19

Crossing the tropical convection

Atmospheric clouds are main modulators of the Earth's energy budget, yet they are also driven by their environment. Clouds and convective cloud-systems near the equator are particularly important (e.g. for the distribution of atmospheric water). Currently, smaller scale features and processes are not adequately resolved in global modeling to the point that climate change aspects associated with convective cloud systems have remained highly uncertain. To help identify and to properly parameterize the most important unresolved processes associated with convection in global modeling (even as these models thrive to operate towards higher resolution), statistically meaningful observational data are needed. In the framework of efforts to document the structure of the convection in the tropical region (referred to as Inter-Tropical Convergence Zone, in short ITCZ) over the Atlantic and their seasonal evolution, measurements during the equator crossing with *Polarstern* (during PS135 in March-April) add to data of earlier cruises by other German research vessels (MSM82-2 in April-May, SO284 in Jun-Jul and MSM114-2 in Jan-Feb). During the recent *Merian* cruise (MSM 114-2) the Atlantic ITCZ was located in a latitude range between 7°N and 5°S and during that cruise this range was crossed three times (near 23°W). The collection of data on properties of clouds and their environment (via active and passive remote sensing from the ground and space) was enhanced by frequent radiosonde launches. During the ITCZ crossings with the *Merian*, radiosondes were launched every three hours to capture atmospheric profiles for temperature, relative humidity and horizontal wind speed and wind direction. To complement this effort during PS135, three radiosondes were launched each day, as *Polarstern* crossed the ITCZ region. The crossing was more to the west (27°W at 5°S, 25°W at 1-7°N) and the ITCZ was much wider with the weaker southern convection band already near 12°S (then at 30°W) and with the stronger convection band near 2°N. Thus, from 21 to 26 March, radiosondes were launched at 17 and 23 UTC, in addition to daily 11 UTC launches. Screen shots of ascent profiles of these launches are presented in Figure 4.22, with an added launch (for satellite validation) on 25 March at 19 UTC close to the ITCZ's northern convection band. For this extra launch, profiles of temperature, relative humidity and pressure are shown in Figure 4.21.

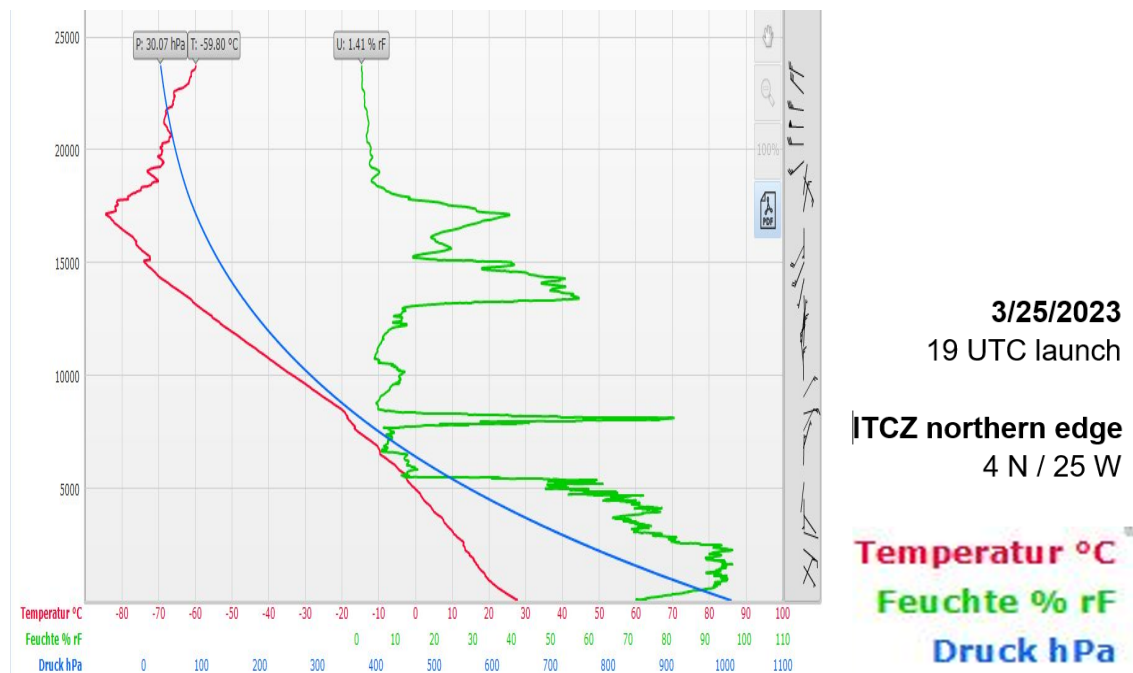


Fig. 4.21: Screen shot of a 25 March 19 UTC (near 4N/25W) radiosonde ascent showing profiles for temperature (red), relative humidity (green) and pressure (blue)

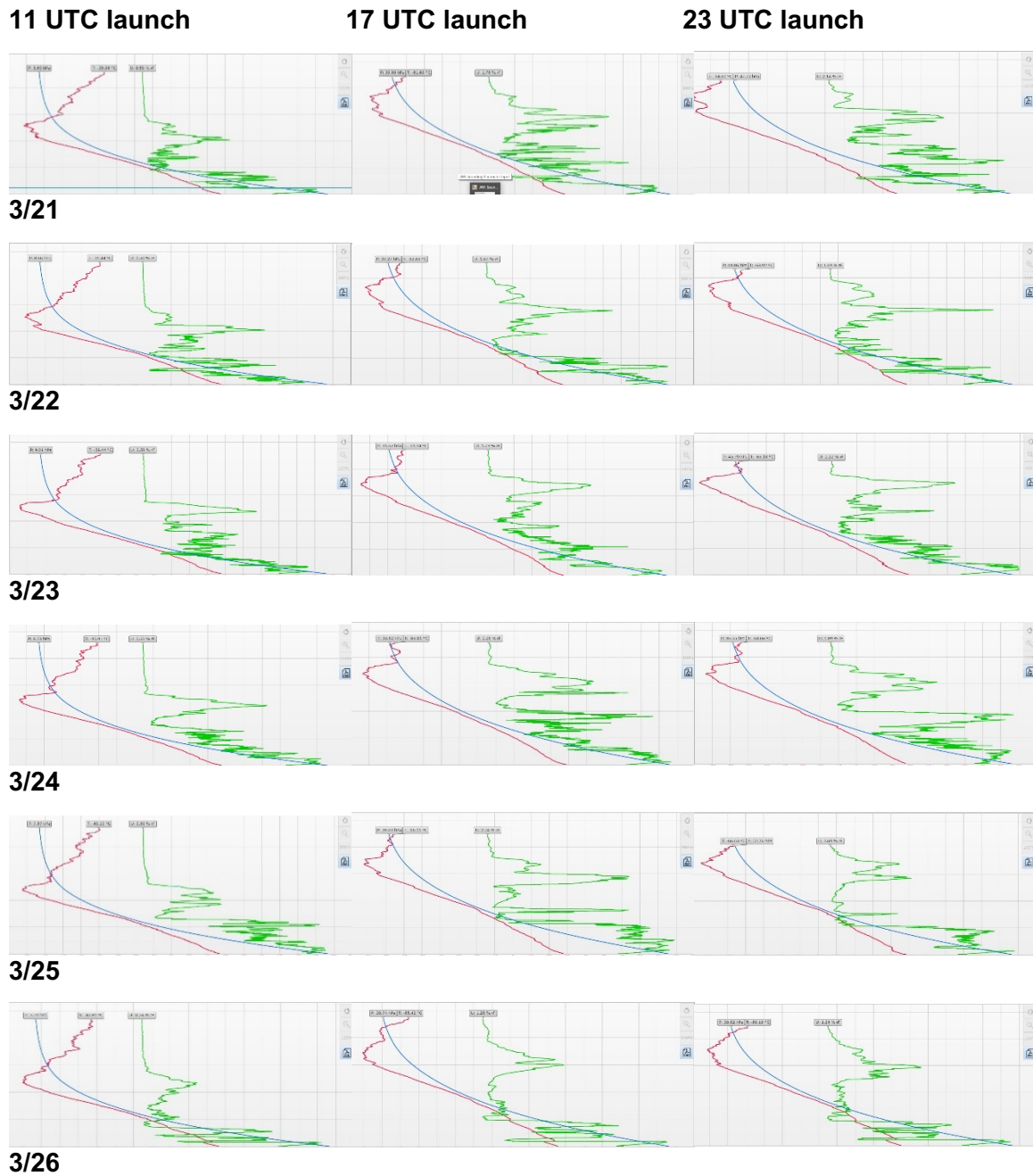


Fig. 4.22: Screen shots of radiosonde ascent showing profiles for temperature (red), relative humidity (green) and pressure (blue) in the tropical convection region with PS135 between 21 and 26 March for launches at 11 UTC (left), 17 UTC (center) and 23 UTC (right)

The southern convection band of ITCZ was crossed during the evening of 21 March (near 12°S) and the northern convection band of the ITCZ during the night from 24 to 25 March (near 3°N), as illustrated by moist layers at low and mid altitudes in Figure 4.22. Both times no precipitation occurred on the vessel although during the morning of 25 March the air temperatures cooled from nearby precipitation. Major precipitation in the ITCZ occurred far away near coastal regions of western Africa and northern S. America, while in the middle between the continents (the passing route of *Polarstern* in March) the mid-altitudes stayed relatively dry – to suppress major convection. Possible explanations are zonal circulations involving coastal convection but also the advection of very dry sub-tropical air, which contributed at the northern convection band.

Temperature, humidity and wind-profiles from all 11 UTC launches (20-29 March) and from all 11 UTC and 23 UTC launches (21-26 March) are directly compared in Figures 4.23 and 4.24.

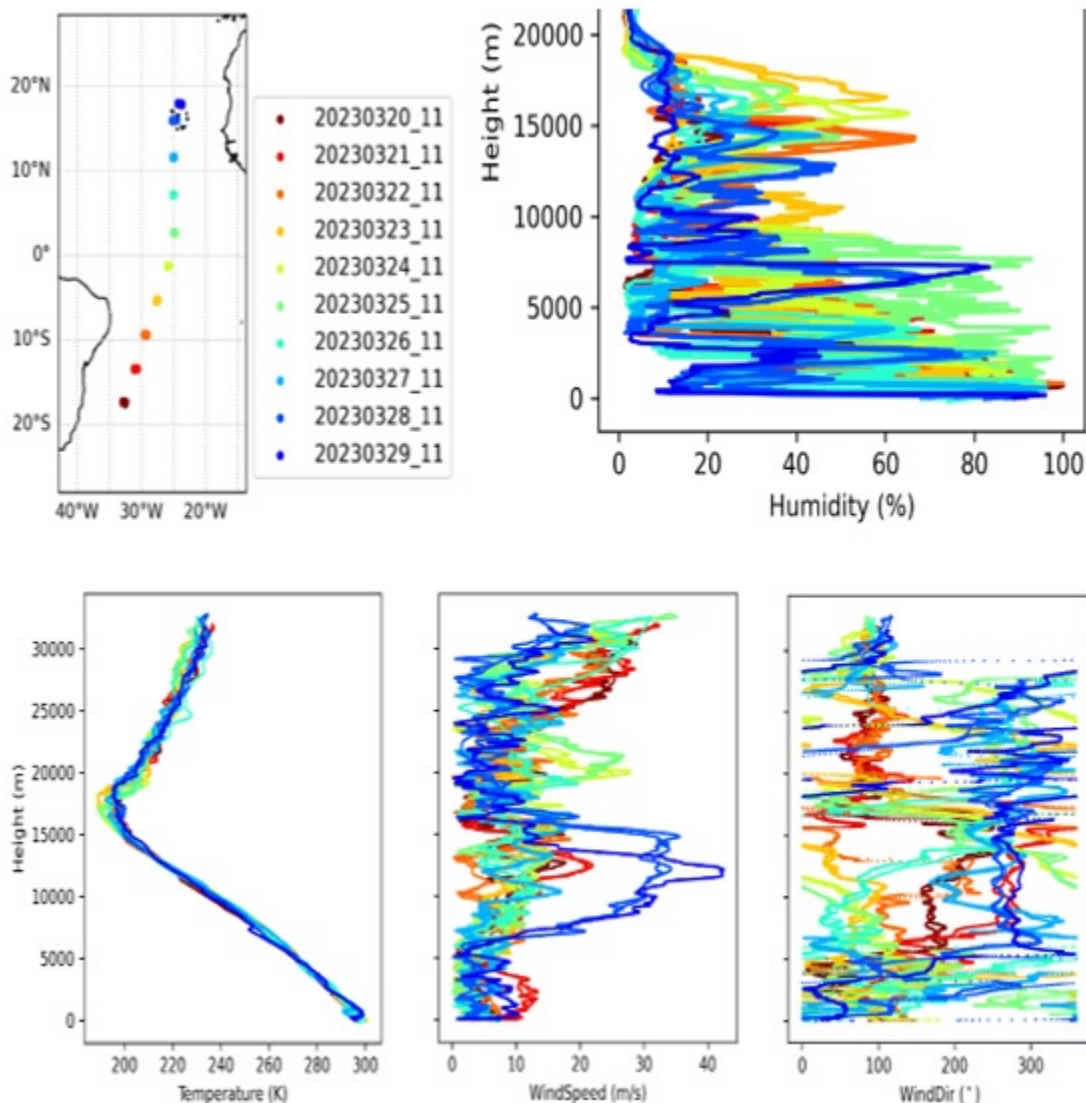


Fig. 4.23: Direct comparisons of radiosonde profiles of 11 UTC launches from the Polarstern during PS135 from 20 to 29 March 2023 in the tropics (top, left) for humidity (top, right), temperature (bottom left), wind-speed (bottom, center) and wind-direction (bottom, right)

The temperature profiles are similar. Profile differences are mainly for the atmospheric moisture in the mid-atmosphere. More mid-altitude moisture indicates convection mainly for 25 March (when passing the northern convection) and less for 21 March (when passing the southern convection). With dryer mid-atmospheres in the (low wind-speed) region between the convection bands bordering the ITCZ, local convection was limited to low altitudes. There occasional showers were rare and brief. Horizontal wind-speeds remained rather moderate, except for the northern sub-tropics with west wind maxima near altitude 12 km and for the ITCZ northern convection with north wind maxima near 20 km. In Figure 4.24 humidity and (horizontal) wind-speed profiles are compared with (a finer) 12-hour temporal resolution, separating by colour, south, central and north ITCZ as well as northern sub-tropics. For a better visualization the plotting order was also reversed to reveal hidden lines.

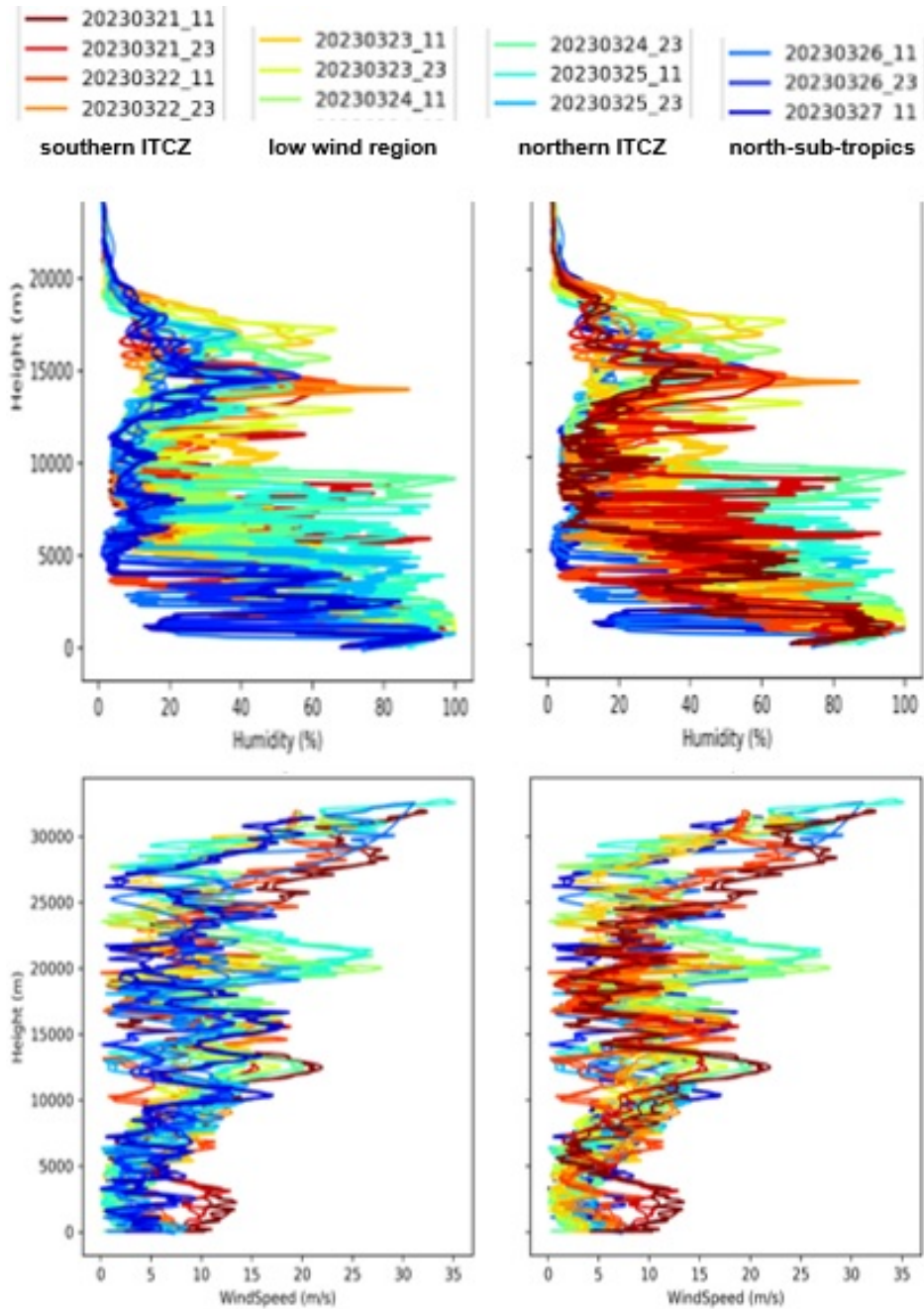


Fig. 4.24: Direct comparisons for humidity (top) and wind-speed (bottom) near and within the ITCZ of the Atlantic using all 11 and 23 UTC radiosonde launches of PS135 from 21 March to 26 March. Note, the right and left plots are identical, except that the plotting order is reversed to reveal hidden behaviour.

To illustrate the variability of the Atlantic ITCZ, hourly averages of four state variables are compared for the ITCZ latitude range between 5°S and 7°N. Data of the three crossings in early February by *Merian* (legs 1 to 3) are compared to the late March crossing by *Polarstern* (leg 4). The four investigated properties are surface temperature in Figure 4.25, horizontal wind-speed in Figure 4.26, integrated water content in Figure 4.27 and air-water temperature difference in Figure 4.28 (differences more negative than -3°C indicate nearby precipitations).

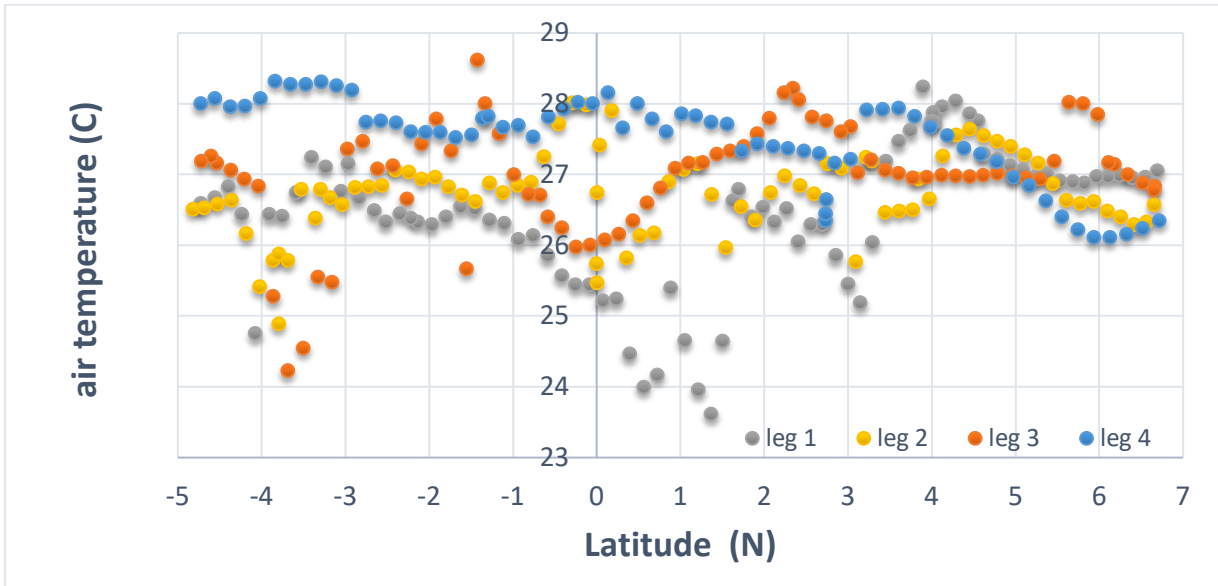


Fig. 4.25: Comparisons of air-temperatures during four different Atlantic crossings with Merian in early February (legs 1 to 3) and with Polarstern in late March (leg 4), when solar irradiance was stronger

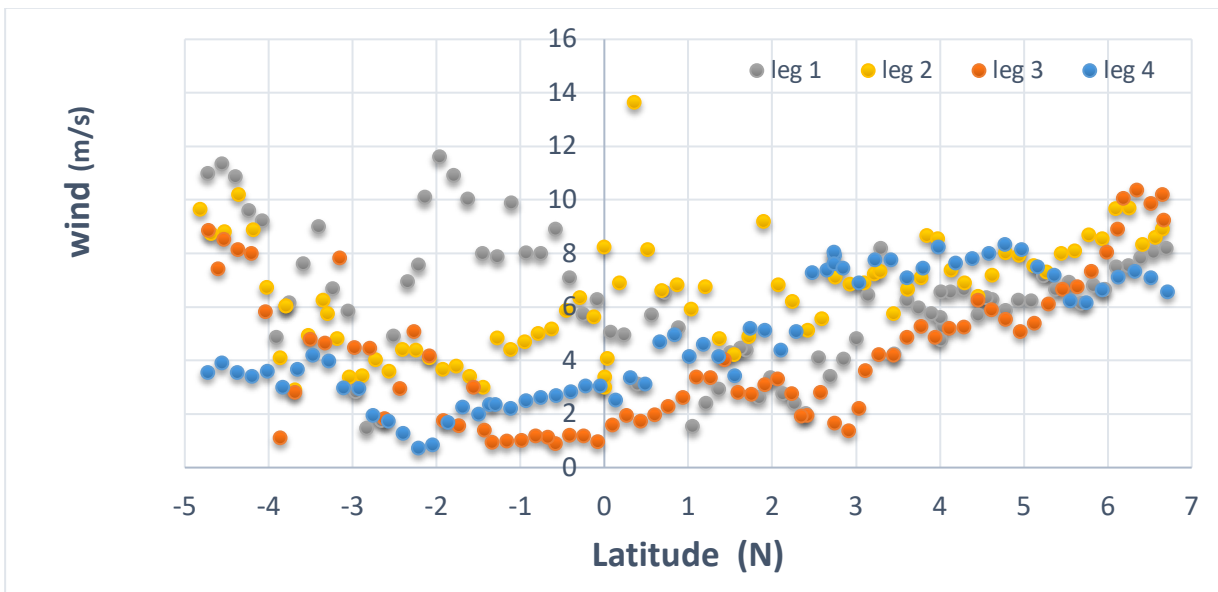


Fig. 4.26: Comparisons of horizontal wind-speeds as function of latitude during four different Atlantic crossings with Merian in early February (legs 1 to 3) and Polarstern in late March (leg4)

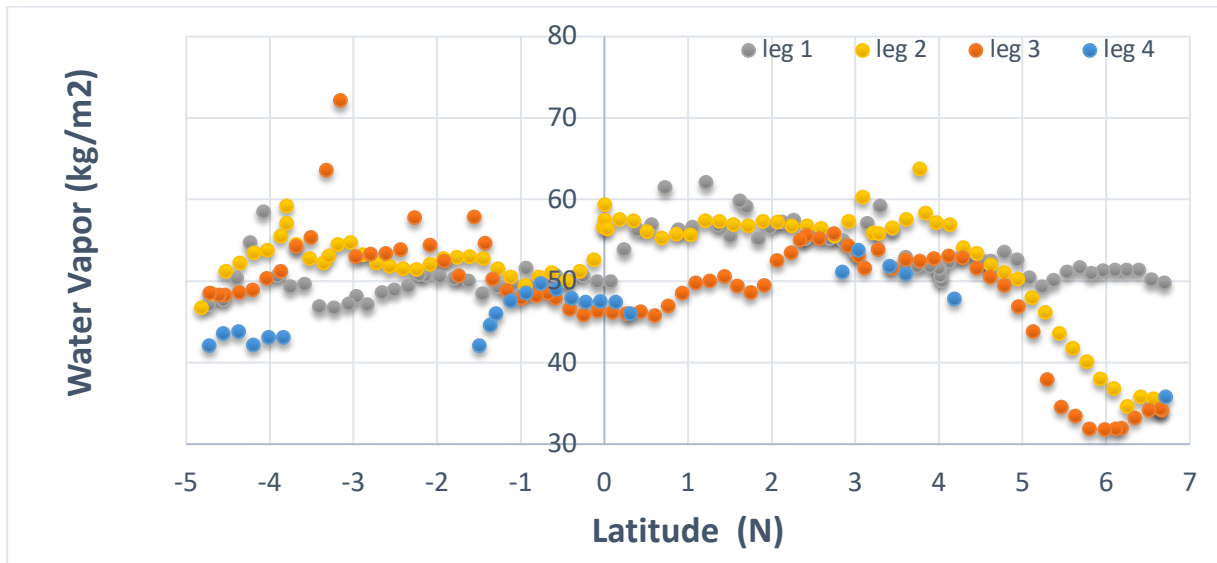


Fig.4.27: Comparisons of integrated water vapor as function of latitude during four different Atlantic crossings with Merian in early February (legs 1 to 3) based on Microwave remote sensing and Polarstern in late March based on sun-photometry (with available data only during the day)

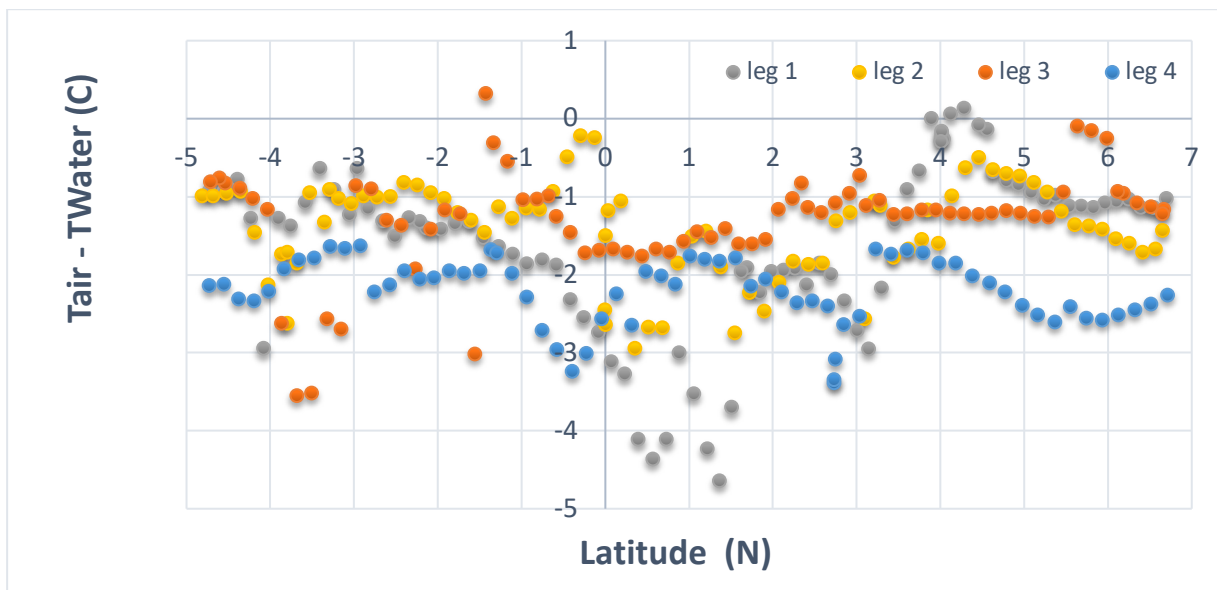


Fig. 4.28: Comparisons of differences between air temperature minus water temperatures as function of latitude during four different Atlantic crossings with Merian in early February (legs 1 to 3) and Polarstern in late March (leg 4). Differences which are more negative than -3°C (cold pools) indicate local or at least nearby precipitation.

Finally, a couple of images of convective clouds near the northern edge of the ITCZ from the late evening of 24 March (near $0.4^{\circ}\text{N} / 25^{\circ}\text{W}$) and from the morning of 25 March (near $2.8^{\circ}\text{N} / 25^{\circ}\text{W}$) are presented in Figure 4.29.

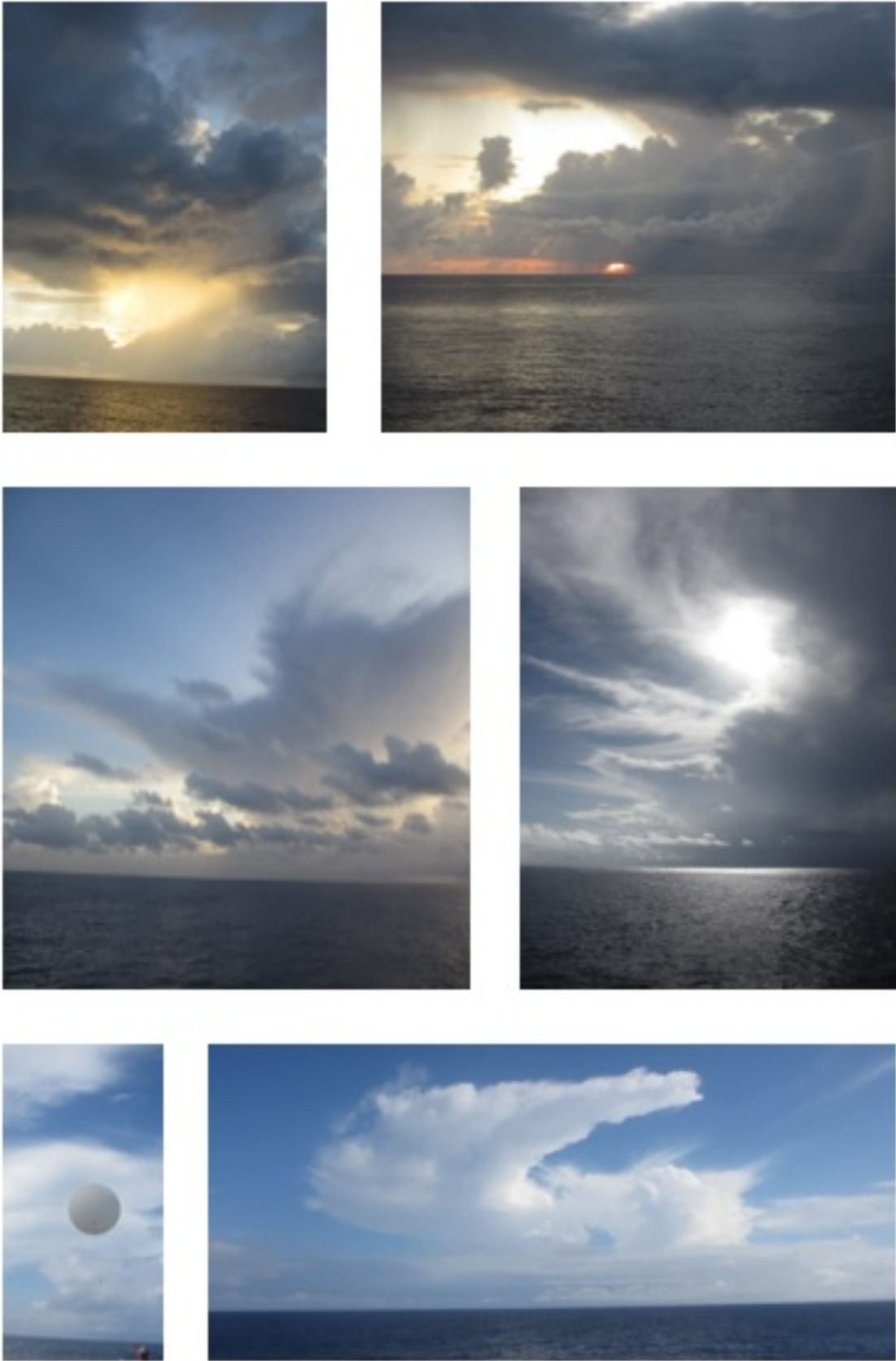


Fig. 4.29: selected cloud images of convection at the northern edge of the ITCZ on 24 and 25 March (photos by Stefan Kinne)

A major dust event off the northern African west coast

On the way from the Cape Verde Islands to the Canary Island the atmosphere above *Polarstern* was contaminated by a major dust event for several days. Warm dry air at lower altitudes carrying mineral dust was blown from the Sahara out onto the Atlantic towards the Canary Islands. Maximum aerosol loads over the vessel were reached near local noon on 31 March near 24°N/20°W. Images from that day are presented in Figure 4.30.



Fig. 4.30: Sunrise on Polarstern on 31 March 2023 (near 20°N / 24°W), when atmospheric dust loads during that day reached AOD values of 1.5. The presence of dust is indicated by sharply reduced direct sun-light, the loss of colours to sky and sun, sunrise (and sunset) above the horizon (left), dust deposits (top right) and arrivals of desert grasshoppers (bottom right); (photos by Stefan Kinne)

Clear indications of mineral dust were missing colours of sky and sun, a sunrise well above the horizon and brownish mineral dust deposits. The 31 March noon-time radiosonde data and 31 March expedited CALIPSO space lidar data at 16 UTC in Figure 4.31 show that the advected air originated from the African continent, was in the lower 5 km, was very dry and was relatively warm (warmer than the water temperature directly above a strong inversion).

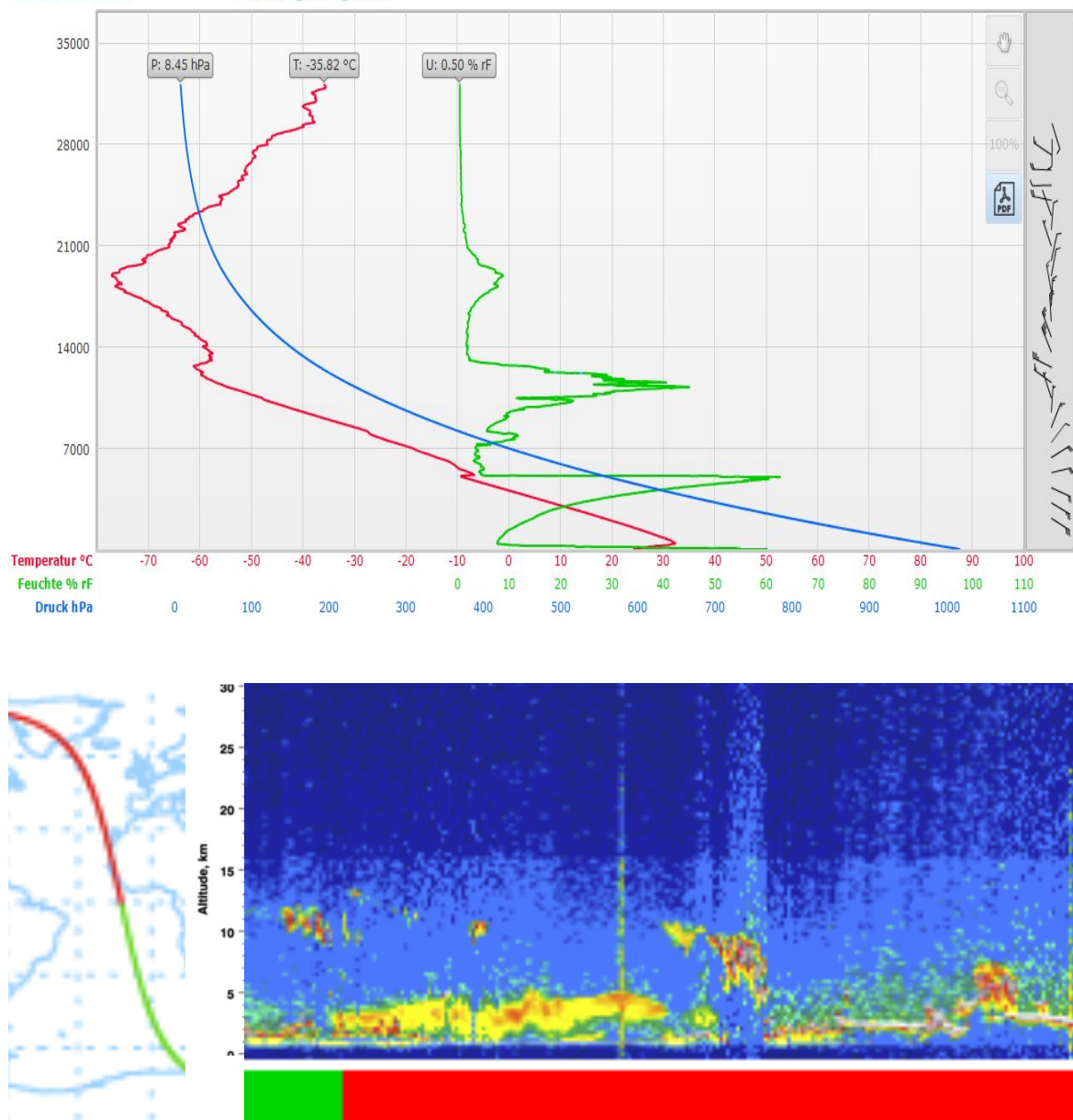


Fig. 4.31: Screen shot of radiosonde ascent profiles of a 31 March 11 UTC launch near 24°N/20°W (top) and a lidar backscatter image by the CALIPSO space lidar for 31 March at 16 UTC (bottom) from the web: https://www-calipso.larc.nasa.gov/products/lidar/browse_images/exp_index.php

This large dust event had a larger regional impact and contaminated the atmosphere above the vessel repeatedly for several days, as the plume spread and meandered. For the period from 29 March (at background conditions before the event) to 5 April (at background conditions after the event) noon-time ship positions (on its northward route to Europe) and associated values for aerosol load (via the mid-visible Aerosol Optical Depth, AOD at 550 nm) and for aerosol size (via the Angstrom parameter) are listed in Table 4.1. The regional distribution for dust AOD by the NAAPS model (<https://www.nrlmry.navy.mil/aerosol>), also for the noon-time of these days, are presented in Figure 4.32. The images explain why after the quick escape from the dust event via the northerly route for the relatively dust free day of 2 April, dust from the plume returned on 3 April and 4 April, as synoptic systems (i.e. a high over the Azores)

pushed part of the spreading plume back into the path of the vessel. The time-series of sampled AOD data is presented in Figure 4.33.

Tab. 4.1: Noon-time locations of the vessel and measured aerosol properties of the dust event

Date	Time	Lon ° (E)	Lat ° (N)	AOD ₅₅₀	Angstrom
2023/03/29	12 UTC	-24.2	18.1	0.15	0.40
2023/03/30	12 UTC	-22.2	21.3	0.30	0.15
2023/03/31	12 UTC	-20.0	24.0	1.45	0.10
2023/04/01	12 UTC	-17.2	26.9	0.56	0.15
2023/04/02	12 UTC	-15.5	29.3	0.15	0.30
2023/04/03	12 UTC	-13.9	32.9	0.52	0.15
2023/04/04	12 UTC	-12.5	36.9	0.18	0.40
2023/05/04	12 UTC	-11.3	40.3	0.15	0.60

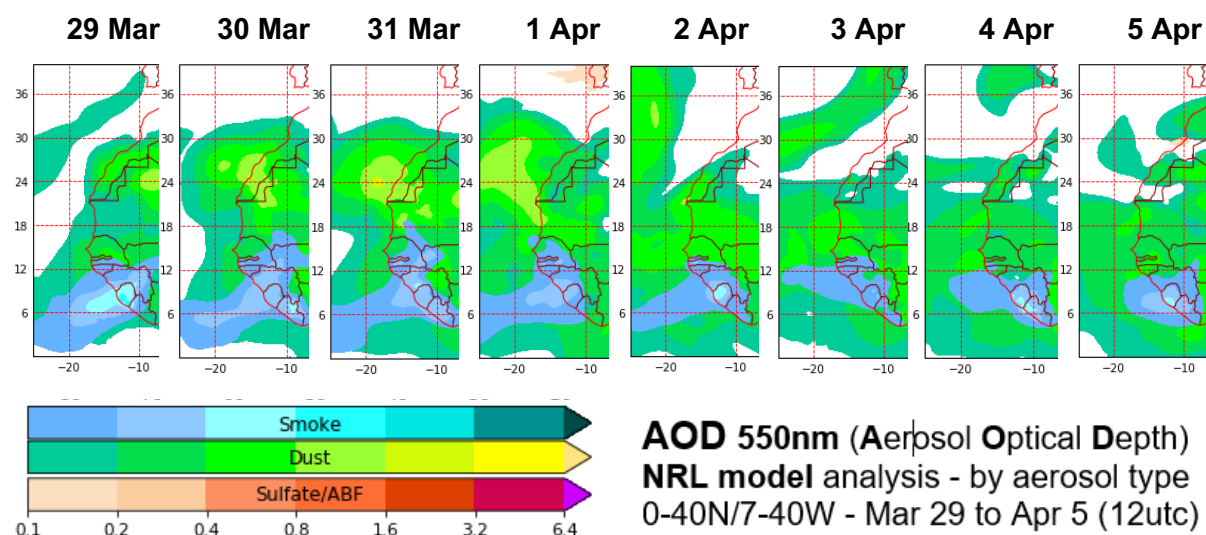


Fig. 4.32: Forecasts for the (column) aerosol optical depth (AOD) by NAAPS model of the US Navy's Research Lab in Monterey, California (<https://www.nrlmry.navy.mil/aerosol>); time-slices (in 24-hour steps) are presented for the Atlantic off northern Africa from 29 March to 5 April 2003, distinguishing dominant AOD contributions by dust, smoke or pollution

The AOD time series show that on the largest AOD (of 1.5) was sampled on the vessel on 31 March (day 93) close to noon (see Fig. 4.33). The AOD ramped up during 30 March, while on 1 April the AOD continued to decline to marine background conditions during the evening hours. The noon time maxima (then at reduced level) on 3 and 4 April were caused by branches of the spreading dust plume which occasionally crossed the northerly path of the vessel.

The expedited images of the CALIPSO space lidar in Figure 4.34 show the continued presence of the dust plume near the Canary Island. Eventually, the plume spread and reaching as far north as Iceland and far west as the northern Amazonas region.

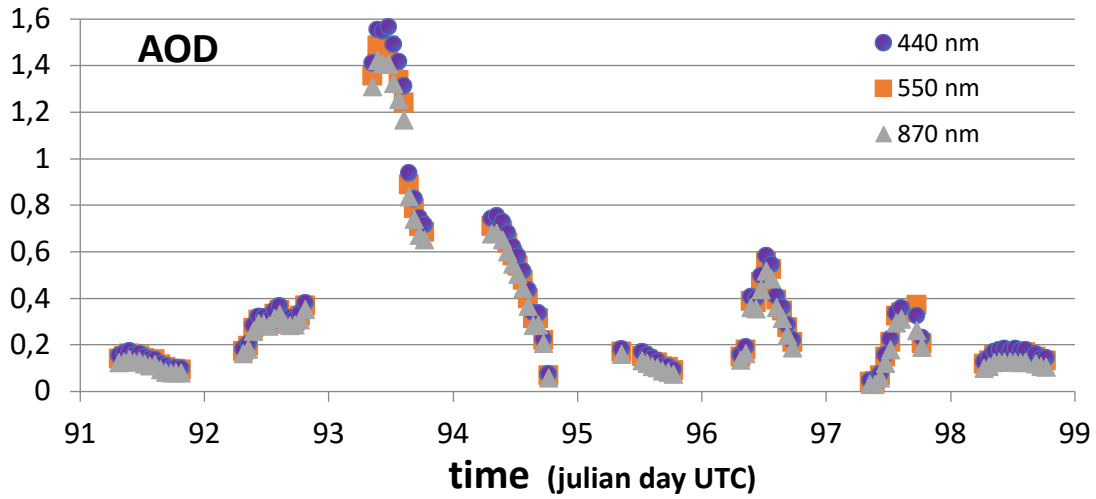


Fig. 4.33: Time-series of hourly AOD data from 29 March (day 91) to 5 April at wavelengths of 440, 550 (interpolated) and 870 nm. The lack of an AOD spectral dependence indicate an AOD contributing dominance by super-micrometer size aerosol, as expected for major dust events

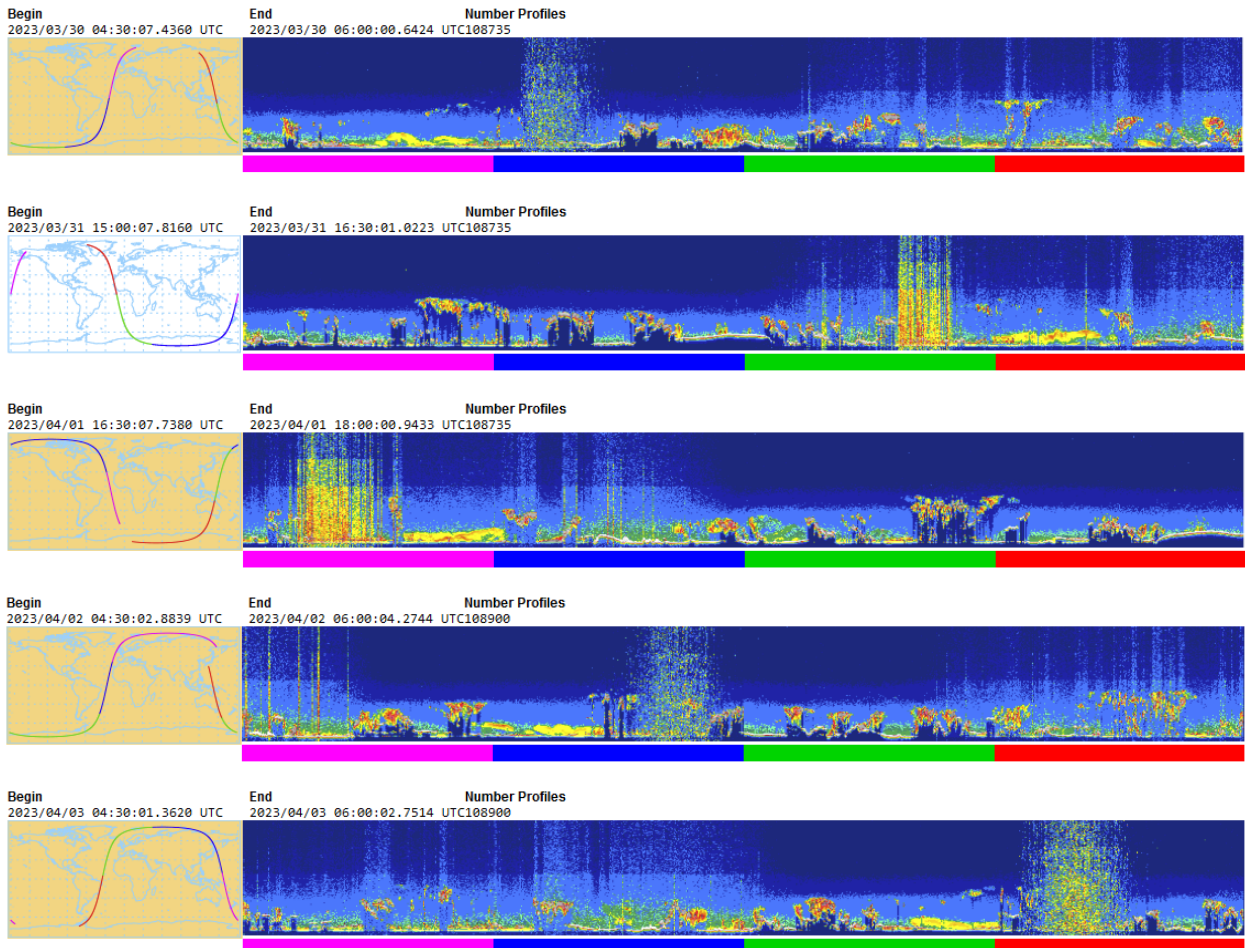


Fig. 4.34: Calipso space lidar backscattering covering the dust plume off the Sahara between 30 March and 3 April: https://www-calipso.larc.nasa.gov/products/lidar/browse_images/exp_index.php

AEOLUS wind profile data validation

The AEOLUS satellite hosts the first space-based Doppler wind lidar. The primary mission objective is to demonstrate the Doppler wind lidar technique for measuring wind profiles from space for immediate assimilation in Numerical Weather Prediction (NWP) models. Initial results have shown that with the use of these data weather forecasts have improved, especially in remote regions. To assure data quality, continued monitoring of wind retrievals are needed. Reference data over oceans can be provided by radiosonde releases from ships when positioned under (or near) an AEOLUS overpass. These overpass events are rare, due to the a specific lidar view, which covers only specific locations (in a weekly repeat cycle) as shown in Figure 4.35.

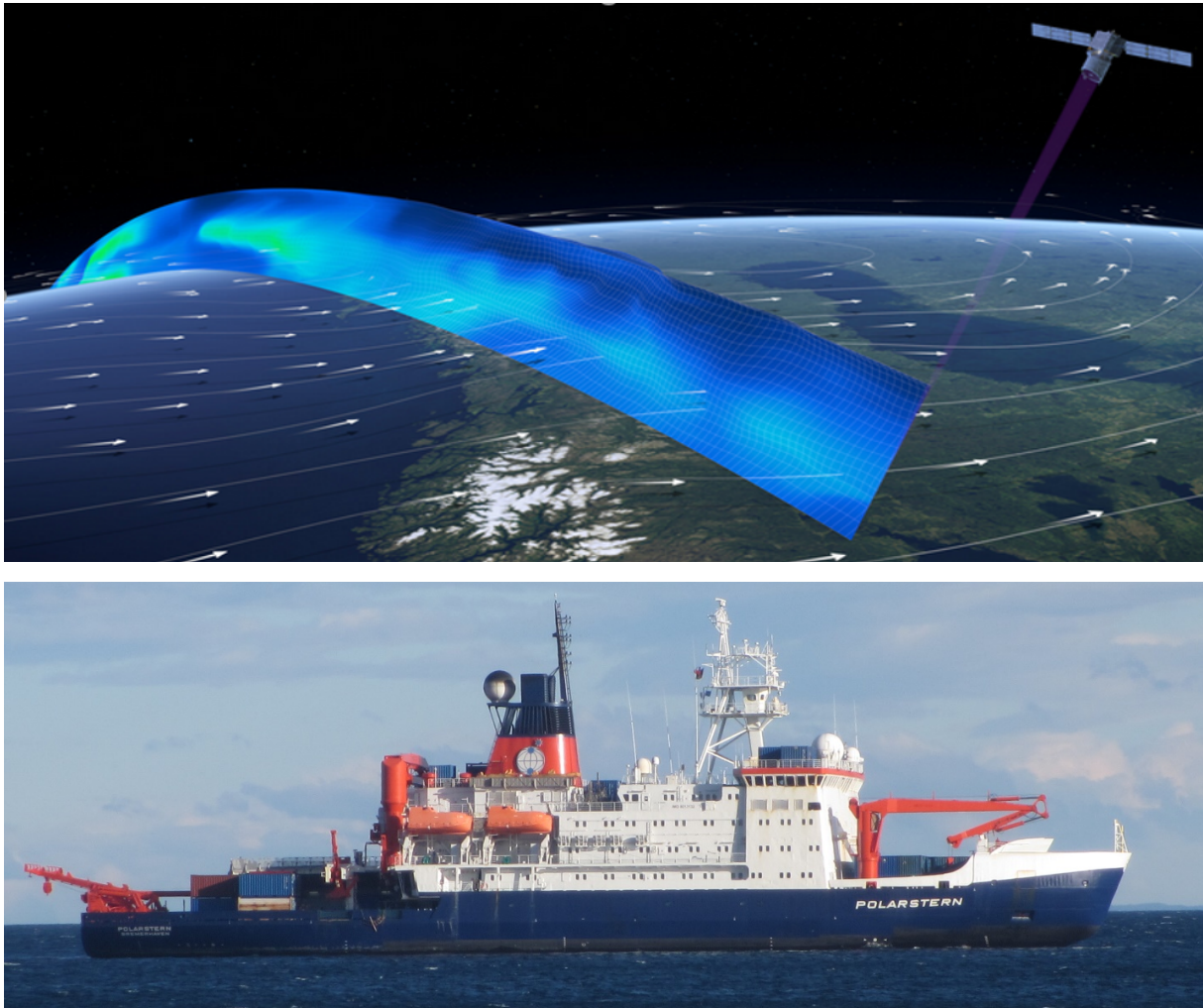


Fig. 4.35: Example of the narrow AEOLUS polar-orbiting flight track https://www.esa.int/Applications/Observing_the_Earth/FutureEO/Aeolus/Measuring_wind with its Doppler lidar to detect wind-profiles (top) and the Polarstern platform (bottom) from which radiosondes at nearby overpasses were launched for validation of satellite retrieved atmospheric winds. (Photo by Stefan Kinne)

Figure 4.35 shows the German research vessel *Polarstern*, from which a few well timed radiosondes were launched during its voyage across the Atlantic from Punta Arenas, Chile at 53°S (10 March) to Bremerhaven, Germany at 53°N (11 April), when close to AEOLUS overpasses.

The radiosondes are lifted with a helium filled balloon into the atmosphere. A radiosonde, the helium balloon preparation and a launch on the helicopter deck of *Polarstern* are shown in Figure 4.36.

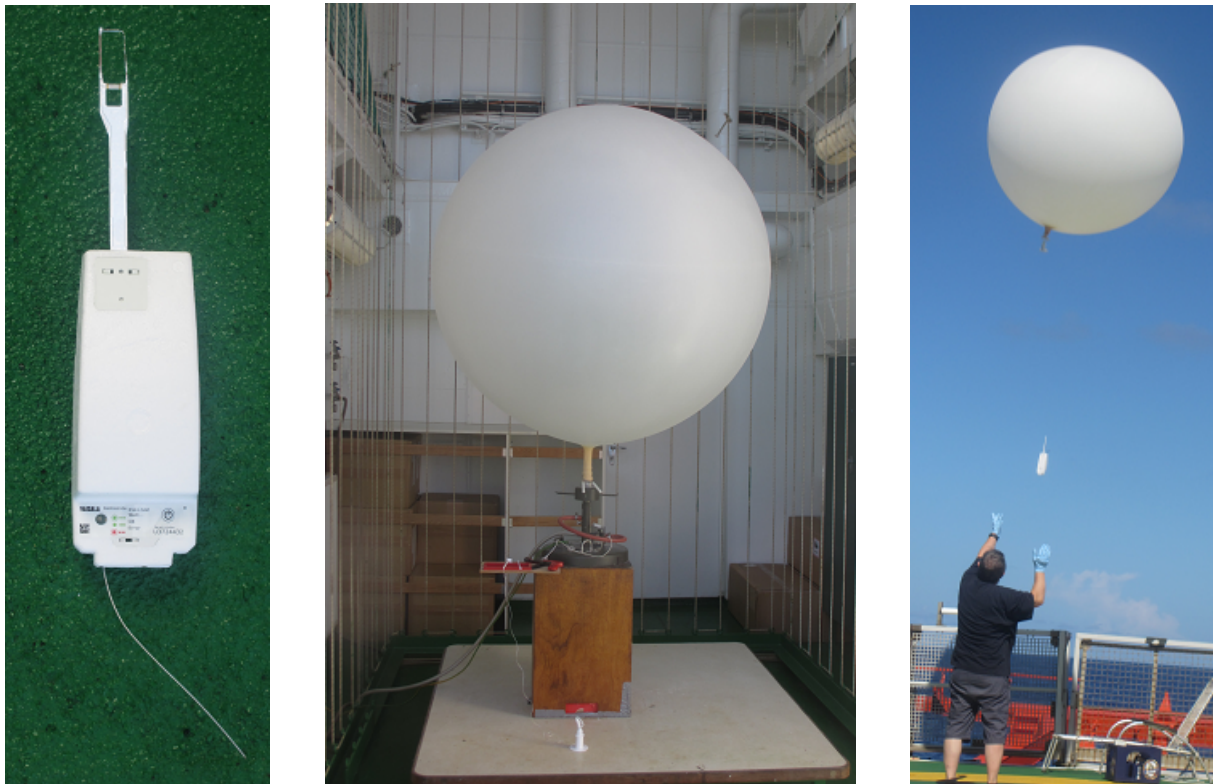


Fig. 4.36: A radiosonde (left), a helium balloon preparation (center) and a launch by Andreas Raeke (DWD) from the German research vessel *Polarstern* during PS135 (right); (photos by Stefan Kinne)

The list of launched radiosondes from *Polarstern* in support of the AEOLUS mission are summarized in Table 4.2.

Tab. 4.2: Radiosonde launches in support of AEOLUS satellite mission during PS135 1/2.

	radiosonde	lat (N)	lon (E)	date	launch time	overpass	PS
1	# 1	-29°	-38°	2023 / 03 / 17	19:10 UTC	20:55 UTC	135/1
2	# 2	-11°	-30°	2023 / 03 / 21	19:40 UTC	20:17 UTC	135/1
3	# 3	4°	-25°	2023 / 03 / 25	19:00 UTC	19:43 UTC	135/1
4	# 4	18°	-24°	2023 / 03 / 29	6:48 UTC	7:40 UTC	135/2
5	# 5	22°	-22°	2023 / 03 / 30	18:25 UTC	19:25 UTC	135/2

Profiles for temperature, humidity, wind-speed and wind-direction are compared in Figure 4.37.

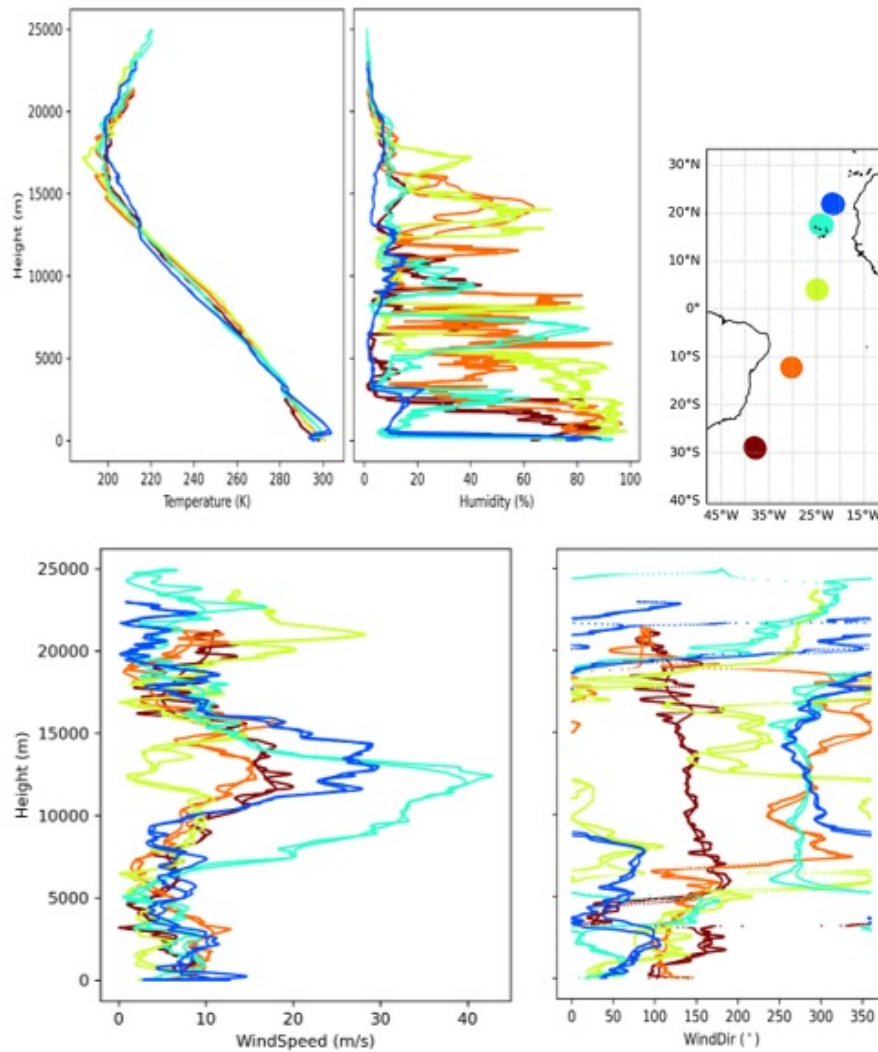


Fig. 4.37: Atmospheric profiles of five radiosondes released during PS135 for humidity, temperature, wind-speed and wind-direction in support of the AEOLUS satellite mission; for each launch (identified by colours) sampled profiles are shown for both, ascent and descent.

The AEOLUS team was particularly interested in getting radiosonde data with their very high vertical resolution for the tropical region between 20°N and 20°S , where a finer (than the ECWMF model) vertical resolved wind-profile product needs to be evaluated. As *Polarstern* could not adjust their route, the released radiosondes were only somewhat near to (and not directly under) AEOLUS overpasses with spatial mismatches of up to 200 km. Initial comparisons also to (ECMWF) modelling for 25 to 29 March cases are offered in Figure 4.38.

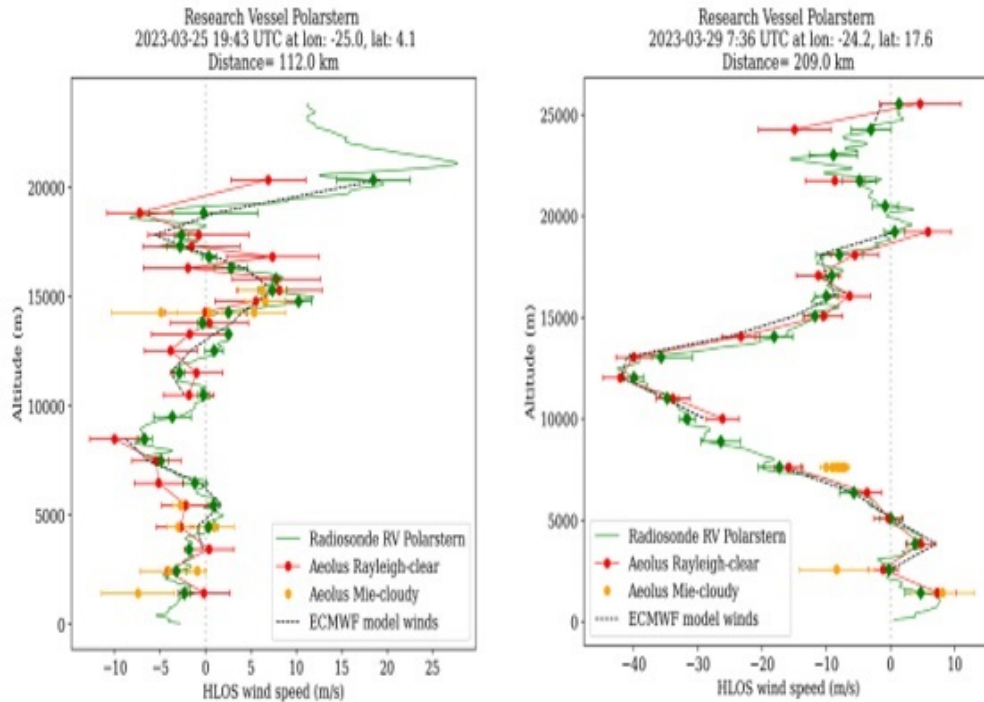


Fig. 4.38: Comparisons of the wind profile of a radiosonde (green) to an ECMWF forecast (black) and for cloud-free retrieval (red) and retrievals for clouds (yellow). These comparisons were provided by Sebastian Bley from TROPOS, as a member of the AEOLUS science team. Comparisons are presented for 25 March launch near major tropical convection (left) and for 29 March launch in the northern trade-wind region (right)

Overall, there is generally good agreement. Especially for the 29 March case up to 20 km in altitude the agreement is very impressive, even more so when considering that the radiosonde sampled ca 200 km off the AEOLUS track. The agreement for the 25 March case disappoints a bit but at the same time it also demonstrates the need for much better spatial (than 100 km) matches in highly variable environments, like the intertropical convergence zone (ITCZ). But even the 25 March comparison was useful to the AEOLUS science team as it showed that “the wind profiles shows very interesting structures and we do see some collocated Mie cloudy winds from AEOLUS additional to the Rayleigh clear winds – but we also see that the Rayleigh clear winds with 500 m vertical bin width are relatively noisy.”

Finally, the AEOLUS lidar also retrieves atmospheric aerosol loads (via the AOD at 355 nm). Thus, in addition, sun-photometer sampled aerosol properties near the time of the AEOLUS satellite overpass are summarized in Table 4.3.

Tab. 4.3: Aerosol properties during at radiosondes launches for AEOLUS during PS135-1/2

rs	lat(N)	lon(E)	day	overpass	aod,355	aod,550	ang	composition
# 1	-29°	-38°	03/17	20:55 UTC	.08	.07	.28	marine
# 2	-11°	-30°	03/21	20:17 UTC	.16	.12	.67	biomass. /mar.
# 3	4°	-25°	03/25	19:43 UTC	.17	.14	.42	dust /marine
# 4	18°	-24°	03/29	7:40 UTC	.16	.14	.32	dust /marine
# 5	22°	-22°	03/30	19:25 UTC	.38	.37	.10	dust

Data management

All data will be immediately available (via the web and/or contacts). During the voyage efforts will be made to assure a high data quality and to develop derived data products and data associations. For any data download or request, it is suggested to contact instrument PIs to understand data quality and data limitations to avoid potential data mis-interpretations. More specifically:

- at http://aeronet.gsfc.nasa.gov/new_web/maritime_aerosol_network_v3.html the sun-photometer data can be viewed and downloaded
- visible and black-body sky camera images (every 10 sec, ca 200 Gb) will be stored at an MPI-M facility and are available on request (contact: call4stefan@gmail.com)
- radiosonde profile data are stored at MPI-M (contact: call4stefan@gmail.com)
- an Excel spreadsheet with hourly averages will be offered and scientific results will be summarized in a contribution to the cruise report (contact: call4stefan@gmail.com)

There will be efforts eventually to transfer data into PANGAEA (<https://www.pangaea.de>) within next two years.

In all publications based on this expedition, the **Grant No. AWI_PS135_03** will be quoted and the following publication will be cited:

Alfred-Wegener-Institut Helmholtz-Zentrum für Polar- und Meeresforschung (2017) Polar Research and Supply Vessel POLARSTERN Operated by the Alfred-Wegener-Institute. Journal of large-scale research facilities, 3, A119. <http://dx.doi.org/10.17815/jlsrf-3-163>.

5. WASCAL FLOATING UNIVERSITY

Björn Fiedler¹, Sunke Schmidtko¹, David Needham¹, Fiona-Elaine Strasser¹, Cathy Wimart-Rousseau¹, Antonio Pinto², Avan Antia³, Henry Bittig⁴, Svenja Christiansen⁵
not on board: Arne Körtzinger¹, Corrine Almeida²

¹DE.GEOMAR

²CV.UTA

³DE.CAU

⁴DE.IOW

⁵NO.UIO

Grant-No. AWI_PS135_04

Outline

Leg PS135/2 hosted the 2nd edition of the WASCAL Floating University programme (GPF 211_041; WASCAL-II) which combined a research expedition with an academic curricular education cruise. This floating university cruise was part of the curriculum of the international master programme “Climate Change and Marine Sciences”, which is currently implemented at the Atlantic Technical University of Cabo Verde (UTA) in the framework of the BMBF-funded WASCAL programme (“West African Science Service Centre on Climate Change and Adapted Land Use”). During the cruise, several modules of the curriculum were taught theoretically as well as practically. In addition, scientists on board communicated their research to West African students and data were collected for a master thesis project. Therefore, ongoing scientific research efforts off West Africa have been integrated into the work programme (e.g. ecological and biogeochemical time-series observations). The students have benefitted, not only through the teaching component delivered by the lecturing PIs, but even more through their immersion into real individual research projects as compared to the more “staged” experience of classical field work practicals.

By combining teaching and research (“training-through-research”), the WASCAL Floating University benefitted both academic education and current research projects in the region during PS135/2.

The WASCAL programme in Cabo Verde including this expedition are endorsed by IOC-UNESCO as a Decade Project hosted by the Decade ECOP programme within the framework of the UN Decade of Ocean Research for Sustainable Development.



Fig. 5.1: Cruise logo for Polarstern expedition PS135/2

Objectives

Primary objective during this expedition is the academic education of Master's degree students in the course "Climate Change and Marine Sciences" (MRP-CCMS) during an authentic research expedition. Therefore, theoretical lecture modules were combined with practical training sessions about classical oceanographic field-sampling methods (e.g., gear deployment/recovery, analytical lab techniques, data reduction and visualization, etc.). Scientific data obtained during the cruise were instantaneously used for teaching and training purposes but also for scientific exploitation (see section "preliminary (expected) results").

The following lecture modules of the MRP-CCMS curriculum got addressed on board: 1) Ocean Observations 2), Hydroacoustics in fisheries and marine ecology and 3) Communication and scientific writing.

Beside teaching modules also research modules were carried out in order to (i) contribute to current research efforts in the region and to global ocean observing programmes, (ii) teach the students with state-of-the art oceanographic technologies and real scientific data, and (iii) collect scientific data for individual master thesis projects.

Students were split into small groups and rotated during the cruise through the following research modules:

Module 1 – Oceanography: During the cruise different assets for hydrographic measurements were used to continue and extend long-term observations in the Eastern Tropical North Atlantic to better understand physical transport processes and how they change over time. One important transport process is induced by mesoscale eddies which not only transports water masses laterally but also induces vertical processes such as up-or downwelling. In order to study this, a CTD rosette sampler was used to measure hydrographic parameters in the water column. Currents of the upper few hundred meters were investigated with an Acoustic Doppler Current Profiler (ADCP).

Module 2 – Surface ocean biogeochemistry: Underway measurements of key surface properties (temperature, salinity, CO₂ partial pressure, O₂ partial pressure, chlorophyll, and turbidity) were performed that allow to assess the saturation state for CO₂ and O₂ to deconvolute the observed disequilibrium into its physical and biological drivers and calculate air-sea CO₂ and O₂ fluxes.

Module 3 – Marine ecology: The cruise track covered different biomes and offered the opportunity to characterize the associated pelagic ecosystems as well as local communities. To facilitate integration of results, the main aim was to use methods that readily can be used to estimate zooplankton contribution to biomass, bulk metabolic rates and export flux. Specifically, the total integrated zooplankton biomass at each station as well as the contribution of larger taxonomic groups and selected sites were investigated.

Module 4 – Microbiology: Marine microorganisms form the base of the food chain and drive global biogeochemical cycles. The diversity of these organisms, which encompass all domains of life plus viruses, is enormous and their turnover times (i.e., how fast the whole community replicates/dies) is just a few days on average, largely due to biological interactions such as infection by viruses and microbial predation. On the cruise, seawater was filtered from a variety of different depths in order to characterize the diversity from a taxonomic and functional basis, as well as quantify the organisms present.

Module 5 – Science Communication: Students were taught how to communicate science to the public in an easy and understandable way. The WASCAL Floating University II cruise is embedded into the UN Decade of Ocean for Sustainable Development and connected to

the EU project EuroSea. Students reached out to these networks and shared their research experience in ocean science with others via different communication exercises in this module.

Work at sea

Overall 11 stations – two of them being the Cape Verde Ocean Observatory (CVOO) and the European Station of Time-Series in the Ocean of the Canary Islands (ESTOC) – have been sampled during the transit between Mindelo, Cabo Verde and Bremerhaven, Germany (Fig. 5.2; section A.4). During transits a variety of continuous underway measurements were performed between the stations and the port of departure and destination.

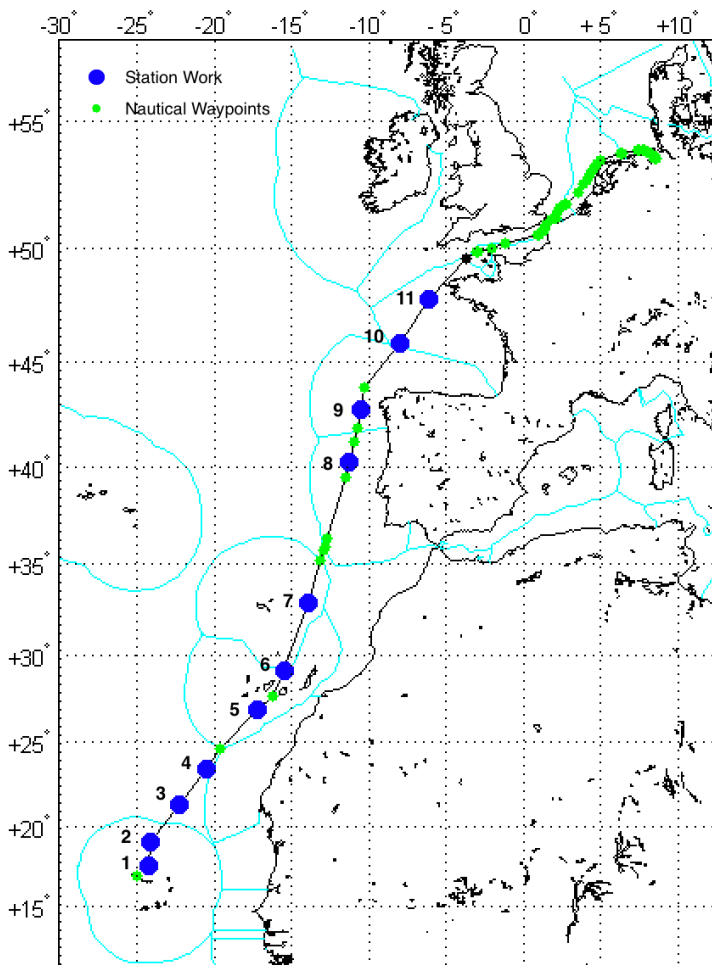


Fig. 5.2: Cruise track of PS135/2 illustrating the locations of station work (blue dots) along the transit from Mindelo, Cabo Verde to Bremerhaven, Germany

Oceanography

The rosette water sampler equipped with the Conductivity, Temperature, and Depth (CTD) instrument was deployed during every station along the track in order to collect high-resolution hydrographic data as well as discrete water samples from various depth levels (Tab. 5.1). Along with the Niskin bottles the CTD is connected with different types of sensors which collect autonomously physical and biogeochemical parameters during up- and downcasts. Temperature, oxygen, and conductivity have two sensors unlike the others parameters (Tab. 5.2).

Tab. 5.1: Maximum depths of CTD profiles and number of discrete salinity samples collected.

Station number	Depth [dbar]	Number of Salinity Samples
1	3645	11
2	1097	12
3	1012	-
4	1216	10
5	1230	9
6	3678	12
7	2026	11
8	5157	13
9	2746	5
10	4940	5
11	151	-
		Total: 88 samples

Tab. 5.2: Information on sensors mounted on *Polarstern's* rosette water sampler

Sensors	Sensors ID	Serial number	Calibration Date
Temperature sensor 1	55	2423	2021-08-21
Temperature sensor 2	55	2685	2021-08-21
Conductivity sensor 1	3	2446	2021-08-26
Conductivity sensor 2	3	2078	2021-08-26
Pressure sensor	45	485	2017-11-17
WET_LabsCStar	71	814	2011-10-24
FluoroWetlabECO_AFL_FL_Sensor	20	7239	2021-12-09
PAR_BiosphericalLicorChelseaSensor	42	2197	2021-11-30
OxygenSensor 1	38	4274	2022-05-05
OxygenSensor 2	38	880	2022-08-09
AltimeterSensor	0	51533	-
FluoroWetlabCDOM_Sensor	19	7239	2021-12-09

Water samples were also collected from the Niskin bottles to measure the salinity in the lab for CTD sensor calibration using an Optimare Ops06 instrument standardized with certified OSIL standard seawater (Batch P162, K15: 0.99983, Sal.: 34.9933; production date: 16 April 2021).

At each station, salinity samples were collected depending on the shape of the vertical salinity profile. Samples were not collected at stations 3 and 11 (Tab. 5.1).

For underway measurement of water velocities the vessel-mounted Acoustic Doppler Current Profiler (ADCP, Kongsberg, 150 kHz) was used.

Biogeochemistry

During the cruise, discrete water samples were collected from the CTD-Rosette to measure biogeochemical parameters. At all stations samples for dissolved oxygen (O_2) were collected. In addition, samples for inorganic nutrients, DIC (dissolved inorganic carbon), and TA (Total Alkalinity) analyses were collected at the CVOO and ESTOC. To collect water samples, a CTD-Rosette was deployed during either early or late stations. Water samples were collected during the ascending profile of the CTD according to a sampling pre-defined depth grid to gather the expected water sample. Underway systems (permanently installed on the vessel) including a Ferry Box (FB) and a system to measure CO_2 partial pressure (pCO_2 , General Oceanics; GO) were also used to acquire continuous measurements of physical and biogeochemical parameters from the vessel's continuous seawater supply system along the journey.

Oxygen samples: After each recovery of the CTD, O_2 samples were drawn from the Niskin bottles immediately, prior to any other sampling to avoid contamination (exchange of oxygen). Oxygen discrete samples (representing a total of 186 samples, including replicates) were sampled into 100 mL wide-necked WOCE glass bottles with glass stoppers. Each bottle was rinsed at least three times before filling to the top. Following this, 1 mL $MnCl_2$ and 1 mL KI solution were added to each bottle. The bottles were closed and then shaken for approximately one minute, stored in a dark cupboard for at least 2 hours and max. 12 hours before analysis. Oxygen samples were analysed according to the standard Winkler titration (Grasshoff et al., 1999). One duplicate or triplicate sample was collected for each CTD cast to measure sampling and titration precision ($1.9 \mu mol kg^{-1}$). Reagents for Winkler titration were checked regularly against a certified reference solution of potassium iodate (OSIL, Havant, UK).

Nutrients samples: Nutrient discrete samples (44 samples from CVOO and ESTOC stations, respectively) were collected from the CTD after O_2 and DIC/TA samplings. Samples were taken in Polyethylene vials, rinsed three times and then filled. Samples were immediately stored in a $-20^\circ C$ freezer and will be measured later.

DIC & TA samples: Discrete samples of DIC & alkalinity were taken from the Niskin bottles right after the oxygen, in order to minimize exchanges of CO_2 with the atmosphere. Glass bottles (500 mL for CVOO, 250 mL for ESTOC) were filled slowly from the bottom using a tube extending from the Niskin bottle drain to the bottom of the glass sample bottle to avoid contamination and bubbles. Once filled, samples were poisoned with aliquots of saturated $HgCl_2$ solution immediately for preservation. The samples were then stored at room temperature at a dark location. A total of 20 samples each were collected at CVOO & ESTOC stations.

Underway measurements: The vessels Ferry Box and GO pCO_2 systems acquired continuous underway measurements. The Ferry Box measured physical and biogeochemical parameters such as temperature, salinity, dissolved oxygen concentration, turbidity, chlorophyll concentration, alkalinity and pH of the seawater. The system consists of a water inlet from which seawater is pumped into the measurement circuit containing several sensors. In addition, a cooled water sampler allows bottled samples to be taken at certain positions for subsequent laboratory analysis. In addition, the GO pCO_2 system which is composed of a wet box and a dry box, measures respectively seawater and air pCO_2 , referenced against certified standard gases (Integrated Carbon Observing System, ICOS). All data from these systems were recorded within a time interval of 60 seconds.

Argo Floats: During PS135/2 a biogeochemical Argo float (WMO 7901001) was recovered north of CVOO before the float reached its end-of-life state. Data of this float will be post-processed later at GEOMAR and the float will be refurbished at the manufacturer for future redeployment. A second (core) Argo float was recovered in the Bay of Biscay for similar reason

(WMO 7900558). Beside recoveries, 5 new core-Argo floats were deployed for the German “Bundesamt für Seeschifffahrt und Hydrographie” (BSH) along the transect at stations 1, 7, 8, 9, 10 (WMO 6904216 – 6904220). For further details please refer to section A.4 (station list).

Marine Ecology

During PS135/2 a HydryBios Multi Plankton Sampler (MultiNet “Midi”, MN) was deployed at ten stations for collecting zooplankton samples in different water layers (Fig. 5.3, left; Tab. 5.3). In addition, an Underwater Vision Profiler 6 (UVP6) was mounted at the rosette water sampler and deployed together with the CTD. The shipboard EK80 echosounder collected continuous hydroacoustic data at different frequencies (Tab. 5.4). The aim of the marine ecology module was to understand the plankton community (biomass, density and diversity) at different depths and the variations in depth distributions between day and night samples as well as spatial variations along the cruise transect.

MultiNet: Twelve deployments were carried out with maximum deployment depth of 2,000 m and the shallowest at 125 m, collecting a total of 60 samples. The multinet was equipped with five nets (150 μm mesh size) attached to a steel frame (Fig. 5.3, right). The net was lowered and heaved with 0.5 m s^{-1} and stopped for the opening/closing of the nets, except at station 1 where the nets were opened/closed during heaving. See table 5.3 for details on the sampling intervals. A deck command unit controlled the opening and shutting of the individual nets with smaller depth intervals as the depth got shallower. A flowmeter recorded the sampled volume. Comparison of flow speeds between the inner and outer flow meter showed consistent values during all deployments indicating reliable flow volumes. The samples were qualitatively inspected under a stereo microscope and were then conserved in 3.7 % formaldehyde solution. The final analysis of the samples will be done in the laboratory at Thuenen Institute (PI Heino Fock) using the ZooScan method and will be identified and analysed quantitatively using EcoTaxa (<https://ecotaxa.obs-vlfr.fr/>).



Fig 5.3: Multinet sampler used during PS135/2 for the collection of zooplankton samples; photo credit: GEOMAR

Tab. 5.3: Overview over the Multinet sampling depths (opening - closing depth).

Net	Stations 1, 6 (CVOO/ESTOC)	Stations 3, 4, 5, 7, 8, 10	Station 11
1	1,000 - 600 m	800-400 m	125-100 m
2	600 – 300 m	400-200 m	100-75 m
3	300 – 200 m	200-100 m	75-50 m
4	200 – 100 m	100-50 m	50-25 m
5	100 – 0 m	50-0 m	25-0 m

Underway Hydroacoustic Observations: In order to evaluate the biomass, abundance, and population dynamics of ecosystem resources, particularly small pelagic and mesopelagic fishes, hydroacoustic methods are a standard tool. A high-precision scientific echosounder (EK80 Kongsberg Maritime AS), was used to monitor and analyse the plankton and micronekton community throughout the transect at 38, 70, 120 and 200 kHz. Transducer information and ping settings of the EK80 used are shown in Table 5.4. No calibration was done during the cruise due to lack of time. Continuous hydroacoustic data collection took place during all cruise activities: along transits and during station work. Using the EK80 software, surface data down to 1,200 m were considered usable and recorded. The raw data were transferred to the AWI data center directly after the cruise and will be published in PANGAEA.

Tab. 5.4: Overview of different transducers and their configurations used with with the EK80 echosounder during PS135/2.

Transducer model	Serial number	Nominal frequency [kHz]	Ping mode	Pulse duration (s)	Transmit power [W]
ES38-7	438	38	cw	0.004096	2000
ES70-7C	696	70	cw	0.001024	750
ES120-7C	2218	120	cw	0.000512	250
ES200-7C	879	200	cw	0.000512	45
ES38-7	438	38	cw	0.004096	2000

Underwater Vision Profiler 6 (UVP6 hf): The Underwater Vision Profiler UVP6 (serial reference number 000159HF) is a pressure-safe underwater camera that was mounted on the rosette water sampler to investigate the plankton and particle composition, distribution, and dynamics at depths of up to 6,000 m. The UVP6 records grayscale images of a defined volume (0.68 L) illuminated by red light flashes (serial number of the light unit: 000153VE2) at acquisition speeds of several images per second. Starting at a pixel size of about 73 µm, the UVP6 directly processes the abundance and image characteristics of particles.

Marine Microbiology

Samples were collected for microbial diversity. “Microbial diversity” is defined as the genetic sequence variability between all of life, plus viruses. Diverse microbial communities interact with one another and their environment. Studying this diversity is important to understand the community structure, how the ecosystem functions, and their distribution patterns.

Chlorophyll (Chl-a): *In situ* data were obtained during the cruise in the Atlantic Ocean, from Cabo Verde, CVOO (first station) to the Bay of Biscay (last station). A total of 10 stations was sampled. Chl-a samples were collected using Niskin bottles mounted on a CTD, at depths

between 10 and 200 m. The plastic bottles (2,500 mL) were rinsed three times before the final sample was taken. Seawater samples (500 – 1,000 mL; generally 1,000 mL) were filtered on GF/F filters and frozen on board at -80°C. After freezing, the samples were extracted (typically on the same day as filtration) with 5 mL of 90 % acetone and incubated at -20°C overnight. During the following day the samples were analyzed using a Turner Trilogy laboratory fluorometer (serial number 015526).

Microbial Diversity: Samples for microbial diversity were filtered by Bulk Vacuum (>0.2 µm) fractionation gravity (>3 µm), and fractionation vacuum (0.2 - 3 µm). The filters were frozen at -80°C and later transported to the lab at GEOMAR.

For downstream analyses, DNA will be extracted using filters from natural seawater samples that have been filtered through a 0.2 µm pore filter and frozen at -80°C or in liquid nitrogen until extraction (without adding a buffer to the filters before freezing). It is based on the Qiagen DNeasy Plant Mini Kit, with slight incubation times and column steps modifications. A mechanical lysis step was added based on bead beating, freezing, and thawing.

After DNA extraction, a universal rRNA gene approach will be used where 16S and 18S rRNA genes are PCR amplified and sequenced (Yeh et al., 2021), as well as full 'metagenome' sequencing. After DNA sequencing, QIIME2 pipelines will be used for data processing.

Further triplicate 12 mL samples were collected by preservation with 20 % glycerol and then stored at -80°C for single cell analyses or cultivation. Additionally, 10 mL of seawater was preserved with 2 % formaldehyde and then stored at -80°C for microscopic analyses. 20 mL samples were also taken from all stations and stored at -20°C for nutrient analysis.

Tab. 5.5: List of filtration-based samples collected in the Marine Microbiology module. Chl-a as chlorophyll a, all cell vir div as all cellular microbial and virus diversity, large particle-attached div as large particle-attached plankton diversity and free-living prokaryo viral diversity as free-living prokaryotic and viral diversity.

Station	Depth [m]	Filter Type / Filter membrane [µm]	Filtration volume [mL]	Purpose
1	10, 20, 45, 60, 100, 200	Fractionation, Vaccum / GF/F	500(3 samples) 1000(15 samples)	Chl-a
1	10, 45, 350, 450, 3500, Bottom	Bulk, Vaccum / >0.2	1000(5 samples)	all cell, vir div
1	10, 45, 350, 450, 3500, Bottom	Fractionation, Gravity / >3	1500(5 samples) 500(1 sample)	large, particle-attached div
1	10, 45, 350, 450, 3500, Bottom	Fractionation, Vaccum / 0.2-3	Variable volumes	free-living prok, vir div
3	10, 20, 45, 60, 80, 100, 200	Fractionation, Vaccum / GF/F	1000(21 samples)	Chl-a
3	10, 80, 250, 550, 750, 1200	Bulk, Vaccum / >0.2	1000(6 samples)	all cell, vir div
3	10, 80, 250, 550, 750, 1200	Fractionation, Gravity / >3	1500(4 samples) 1000(2 samples)	large, particle-attached div
3	10, 80, 250, 550, 750, 1200	Fractionation, Vaccum / 0.2-3	500(6 samples)	free-living prok, vir div

Station	Depth [m]	Filter Type / Filter membrane [µm]	Filtration volume [mL]	Purpose
4	10, 20, 50, 60, 80, 100, 200	Fractionation, Vaccum / GF/F	1000(20 samples)	Chl-a
4	10, 80, 250, 550, 750, 1200	Bulk, Vaccum / >0.2	1000(6 samples)	all cell, vir div
4	10, 80, 250, 550, 750, 1200	Fractionation, Gravity / >3	1500(6 samples)	large, particle-attached div
4	10, 80, 250, 550, 750, 1200	Fractionation, Vaccum / 0.2-3	500(6 samples)	free-living prok, vir div
5	10, 20, 45, 60, 80, 100, 200	Fractionation, Vaccum / GF/F	1000(21 samples)	Chl-a
5	12, 80, 250, 550, 750, 1200	Bulk, Vaccum / >0.2	1000(6 samples)	all cell, vir div
5	12, 80, 250, 550, 750, 1200	Fractionation, Gravity / >3	1000(6 samples)	large, particle-attached div
5	12, 80, 250, 550, 750, 1200	Fractionation, Vaccum / 0.2-3	500(6 samples)	free-living prok, vir div
6	10, 25, 50, 75, 100, 125, 200	Fractionation, Vaccum / GF/F	500(3 samples) 1000(18 samples)	Chl-a
6	10, 100, 800, 1300, 3000, bottom	Bulk, Vaccum / >0.2	1000(4samples) 500(2 samples)	all cell, vir div
6	10, 100, 800, 1300, 3000, bottom	Fractionation, Gravity / >3	1000(4 samples)	large, particle-attached div
6	10, 100, 800, 1300, 3000, bottom	Fractionation, Vaccum / 0.2-3	500(6 samples)	free-living prok, vir div
7	10, 25, 40, 60, 90, 120, 170, 200	Fractionation, Vaccum / GF/F	1000(24 samples)	Chl-a
7	10, 90, 400, 750, 1000, 2000	Bulk, Vaccum / >0.2	1000(6 samples)	all cell, vir div
7	10, 90, 400, 750, 1000, 2000	Fractionation, Gravity / >3	1000(6 samples)	large, particle-attached div
7	10, 90, 400, 750, 1000, 2000	Fractionation, Vaccum / 0.2-3	500(6 samples)	free-living prok, vir div
8	10, 25, 50, 150, 200	Fractionation, Vaccum / GF/F	1000(15 samples)	Chl-a
8	10, 50, 750, 1250, 5000, bottom	Bulk, Vaccum / >0.2	1000(5 samples) 500(1 sample)	all cell, vir div
8	10, 50, 750, 1250, 5000, bottom	Fractionation, Gravity / >3	1000(6 samples)	large, particle-attached div
8	10, 50, 750, 1250, 5000, bottom	Fractionation, Vaccum / 0.2-3	500(6 samples)	free-living prok, vir div
9	Surface, 25, 50, 100, 150, 200	Fractionation, Vaccum / GF/F	1000(18 samples)	Chl-a

Station	Depth [m]	Filter Type / Filter membrane [µm]	Filtration volume [mL]	Purpose
9	10, 50, 100, 1000, 2600, bottom	Bulk, Vaccum / >0.2	1000(6 samples)	all cell, vir div
9	10, 50, 100, 1000, 2600, bottom	Fractionation, Gravity / >3	1000(4 samples) 500(2 samples)	large, particle-attached div
9	10, 50, 100, 1000, 2600, bottom	Fractionation, Vaccum / 0.2-3	500(6 samples) ??	free-living prok, vir div
10	Surface, 25, 50, 100, 200	Fractionation, Vaccum / GF/F	1000(15 samples)	Chl-a
10	Surface, Surface, 500, 1000, 4800, bottom	Bulk, Vaccum / >0.2	1000(6 samples)	all cell, vir div
10	Surface, Surface, 500, 1000, 4800, bottom	Fractionation, Gravity / >3	1000(4 samples) 500(2 samples)	large, particle-attached div
10	Surface, Surface, 500, 1000, 4800, bottom	Fractionation, Vaccum / 0.2-3	500(6 samples)	free-living prok, vir div
11	Surface, 30	Fractionation, Vaccum / GF/F	1000(6 samples)	Chl-a
11	10, 30, 60, 120, bottom	Bulk, Vaccum / >0.2	500(5 samples)	all cell, vir div
11	10, 30, 60, 120, bottom	Fractionation, Gravity / >3	500(5 samples)	large, particle-attached div
11	10, 30, 60, 120, bottom	Fractionation, Vaccum / 0.2-3	500(5 samples)	free-living prok, vir div

Preliminary (expected) results

CTD measurements

As expected, a section of the upper layer (Fig. 5.4) shows a strong decrease in temperature and salinity with latitude associated with an inverse relationship with oxygen. An oxygen minimum zone is shown in the Cape Verdean waters from 200 to 600 meters depth due to the stratification while a high oxygen concentration is shown in the European waters due to cold water suggesting vertical ventilation and high productivity (spring bloom).

The data are also showing different water masses. The warm water is found in the upper layer (0 - 200 m) along the transects to approx. 40° N. It is characterized by high temperature near the start of the cruise, high salinity during the crossing of subtropical waters, and low temperature in the northern part of the cruise. The Mediterranean waters are found about 30° to 45° N between 600 – 1,200 m depth. North Atlantic Deep Water can be found at deeper layers which is very cold and has high salinity and high oxygen concentrations.

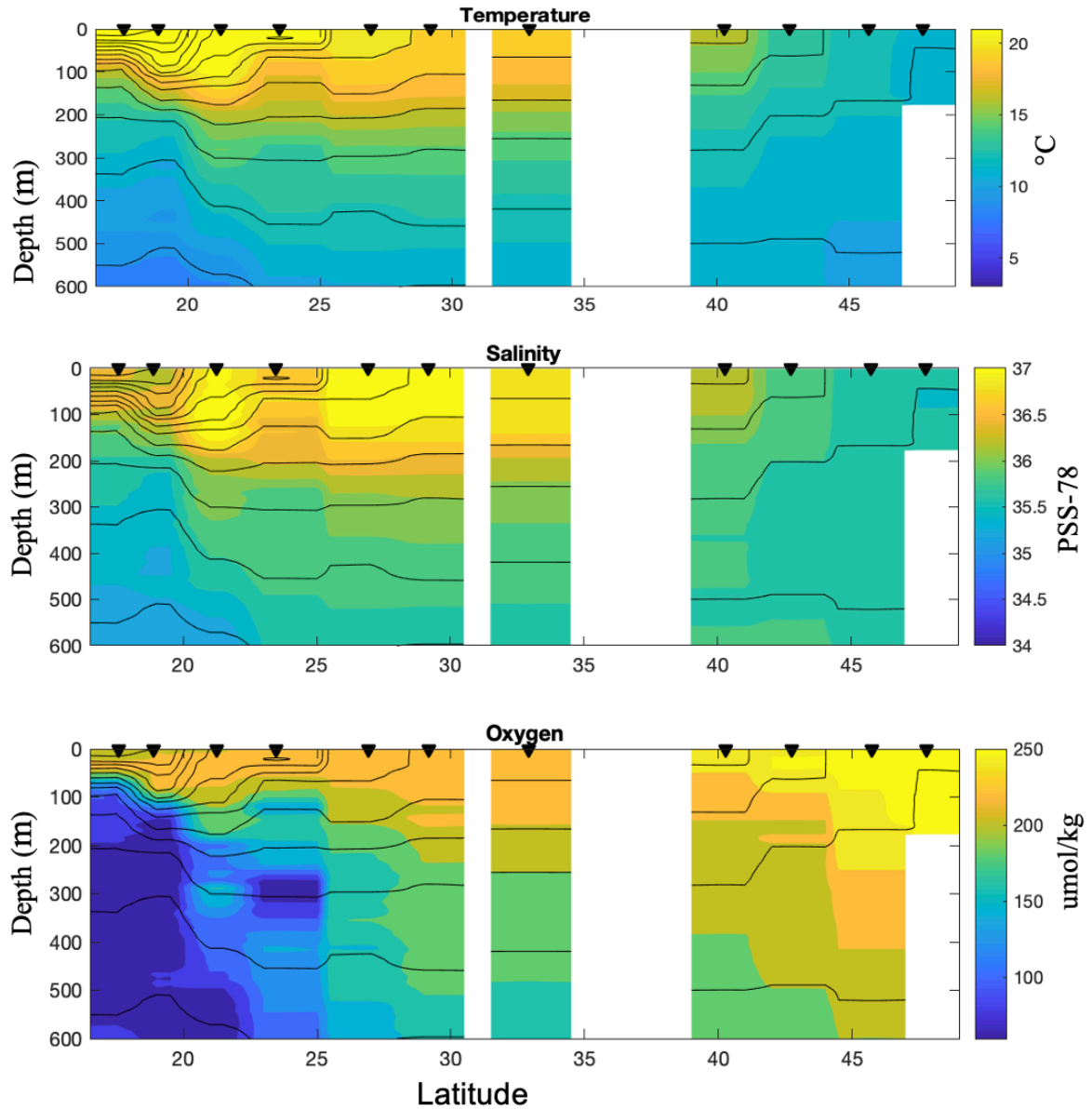


Fig. 5.4: Profiles section of Temperature, Salinity, and Oxygen (black dot on top = Stations location) per station

ADCP results

The analysis of the data collected by the ADCP (Fig. 5.5) reveals a strong mesoscale variability of zonal and meridional velocities. North of Canary Islands a pronounced cyclonic eddy has been crossed.

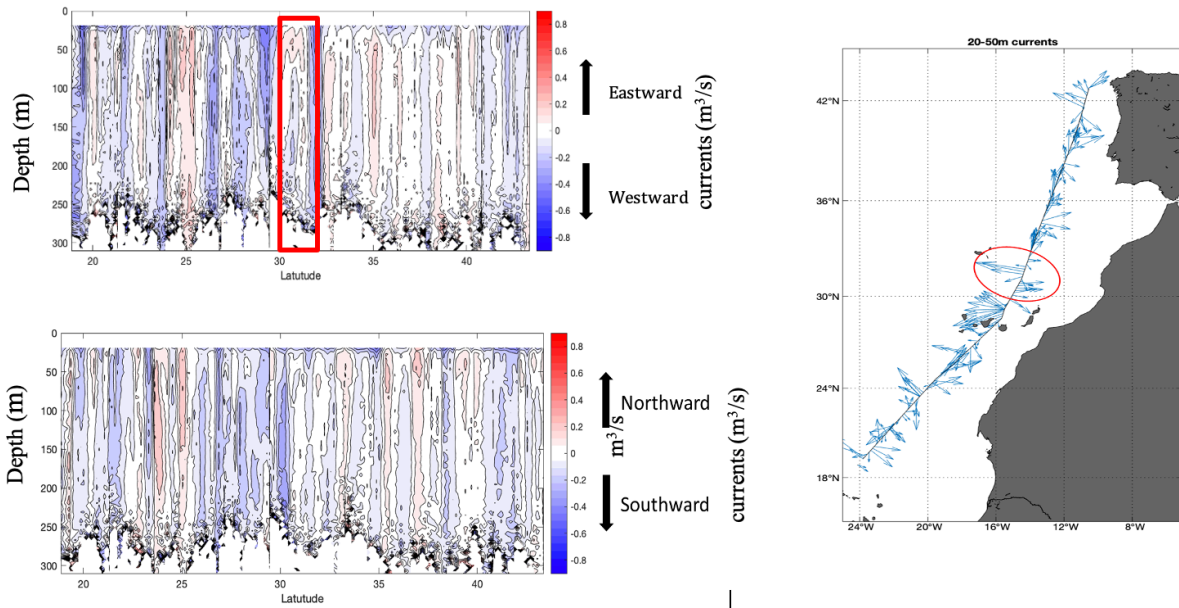


Fig. 5.5: Section of the zonal (upper left) and meridional (lower left) water velocities in the upper layer (0 - 300 m) of the water column along the cruise transect. Vectors of ocean currents along the cruise transect derived from ADCP illustrate mesoscale eddies (right, red circle).

Biogeochemistry

Measurements of dissolved O_2 (discrete samples) are needed to calibrate the O_2 sensors attached to the CTD for more accurate measurements. Figure 5.6 represents O_2 data measured in the laboratory in comparison with oxygen data measured by the CTD. The improvement in accuracy of the CTD O_2 data from before the calibration against discrete data (raw, blue dots) and after the calibration procedure (red dots) can be seen.

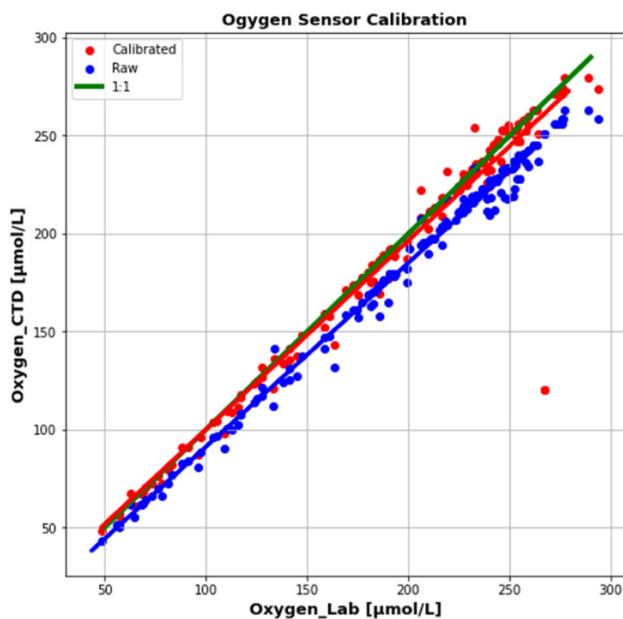


Fig. 5.6: The figure illustrates the O_2 sensor calibration (red dots represent O_2 data after the calibration and blue dots correspond to raw sensor data).

Variations in the biogeochemical parameters are described in Figure 5.7 with the time-series of 36,200 data points (from 12 March 2023 until 8 April 2023) along the meridional transect. The two red boxes in this figure correspond to the stations in tropical waters (1-6) and stations near the Mediterranean outflow waters (9 and 10). A decrease in temperature and salinity was observed while moving from tropical warm waters to temperate cold waters, compared to an increase of dissolved oxygen concentration. This contrast can be explained by the fact that the solubility of dissolved oxygen increases at colder water temperatures. Positive peaks in O_2 together with a drawdown of pCO_2 towards the end of the cruise provide clear indication of a pronounced spring bloom event in the Bay of Biscay.

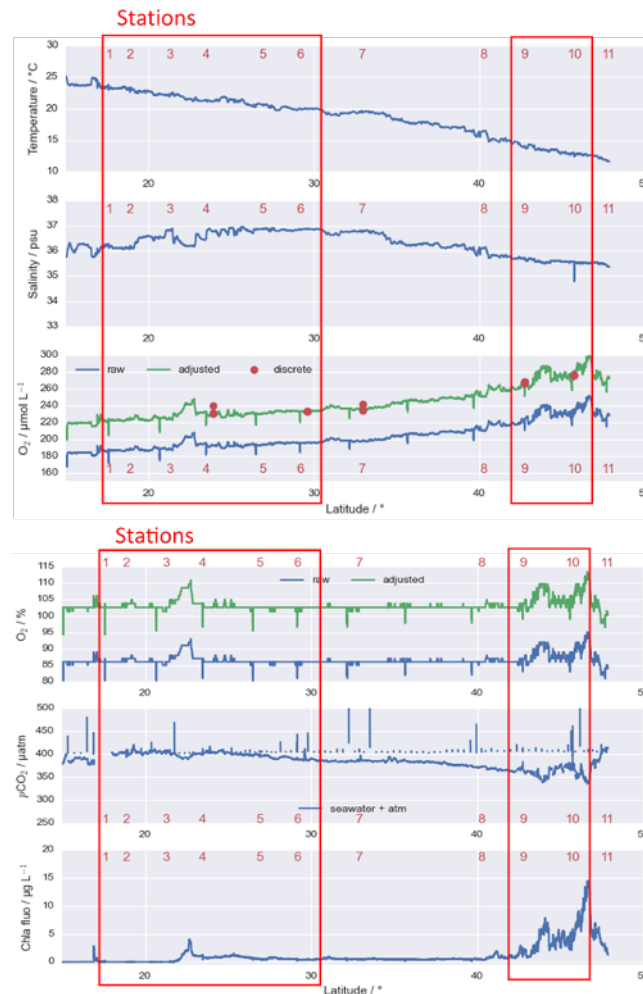


Fig. 5.7: Underway measurements for temperature ($^{\circ}\text{C}$), salinity (psu), dissolved oxygen concentration ($\mu\text{mol L}^{-1}$), dissolved Oxygen saturation (%), pCO_2 (μatm) and Chlorophyll-a ($\mu\text{g L}^{-1}$) reveal different biogeochemical provinces passed during PS135/2. Blue lines represent raw data, the discrete samples are represented by red dots and green lines represent data adjusted using discrete data; the two red boxes correspond to the stations in tropical waters (1-6) and the stations near the Bay of Biscay (9 and 10).

Marine Ecology

Net hauls: Along the transect three major scenarios were observed qualitatively. From station 1 to 6 an oligotrophic subtropical gyre setting was observed, with a generally high diversity of different taxa, an apparently high diversity of copepods, comparatively strong occurrence of large Rhizaria and occasional catches of small decapod shrimps, krill and mesopelagic fishes (mostly *Cyclothone* sp.). At station 7 to 9, a transition scenario apparently dominated by gelatinous zooplankton was observed, with large numbers of salps, larvaceans, pteropods and foraminifera. At station 10 and 11 a spring bloom was observed and the zooplankton was apparently dominated by North Atlantic species with high abundances of early live stages and inclusion of large phytoplankton (particularly *Phaeocystis*) in the Multinet samples. At station 11 (shelf station with 125 m maximum sampling depth), high abundances of salp fecal pellets and *Trichodesmium* colonies were additionally observed.

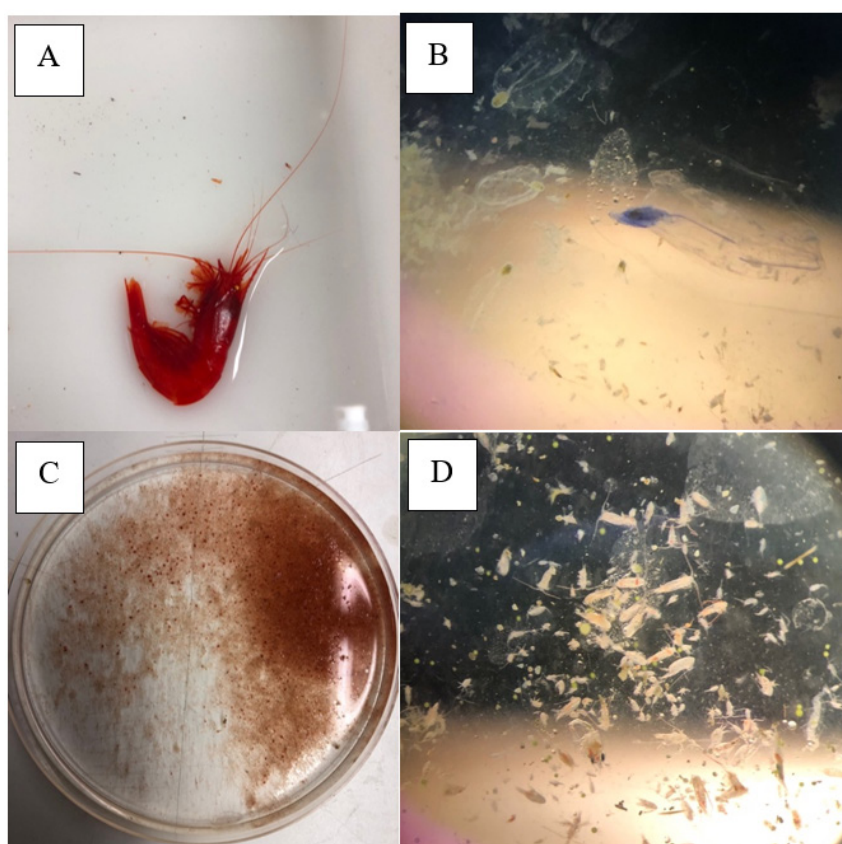


Fig. 5.8: A) A shrimp caught with the Multinet between 1,000 and 600 m at Station 1 (CVOO)
 B) Gelatinous zooplankton caught at station 9
 C) The surface sample (50 - 0 m) at station 10
 D) Sample collected from station 11 with a mixture of copepods, early live stage zooplankton, phytoplankton and *Trichodesmium* colonies.

Over the first eight days of the transect, the EK80 data illustrated typical sound scattering layers at different depths. A notable, persistent deep scattering layer was recorded and observed in depths of around 500 m. Diel vertical migration of organisms from the deep layers to the surface layers at night and back into the deep layers at dawn was observed, with some migrations

extending beyond 1,000 m depth. Furthermore, concentrations of backscatter organisms in the surface layer, particularly in the upper 100 m, were alternately increased due to the difference in migration between day and night (Fig. 5.9). On 5 and 6 April 2023, surface backscatter was particularly high. After 7 April 2023, scattering layers became more diffuse, distributions more dynamic and diel vertical migration patterns less clear.

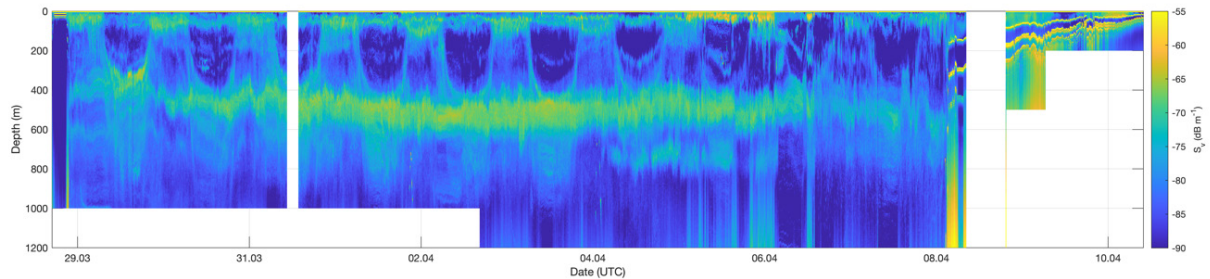


Fig. 5.9: Echogram showing the 38 kHz data from the EK80 for the whole transect

Underwater Vision Profiler 6 (UVP6 hf): The UVP6 data (particle abundances in different size bins and image data, examples in Fig. 5.10) will be stored in Ecotaxa (<https://ecotaxa.obs-vlfr.fr/>), where also the taxonomic identification and sorting of the images will take place.

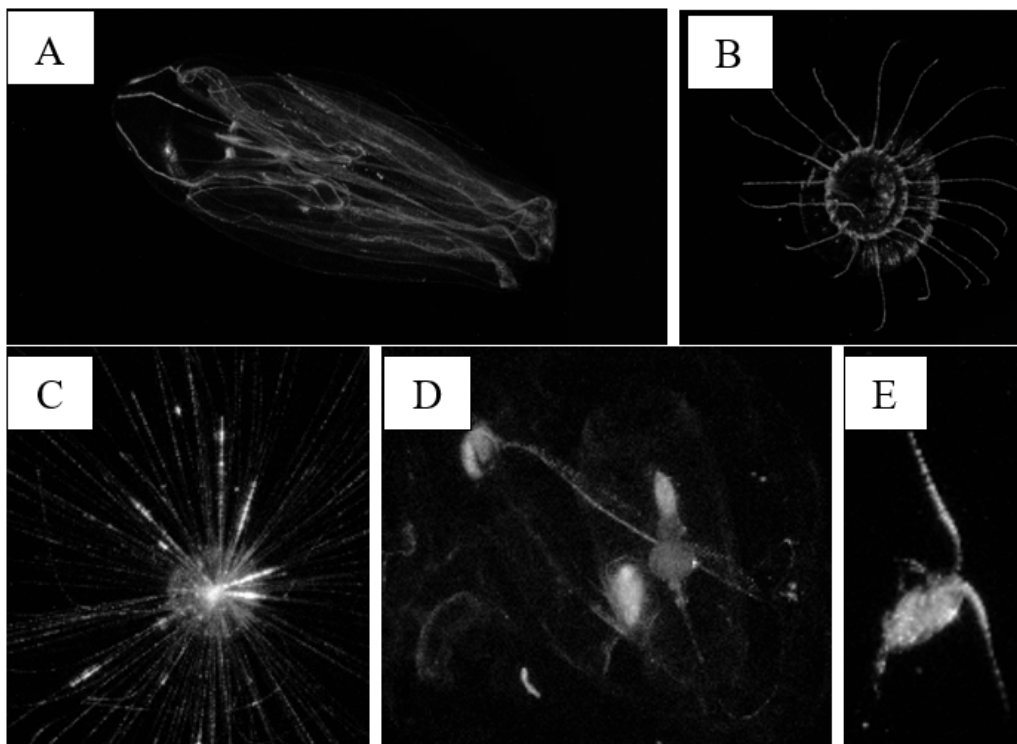


Fig. 5.10: Some examples of the UVP6 images:
A) ctenophore, B) medusa, C) Rhizaria, D) salp, E) copepod

Marine Microbiology

The samples taken for Microbial Diversity will be analyzed later in the laboratory, so the results can't be presented in this report. The results obtained for the chlorophyll measurements present two types of regimes, the oligotrophic regime (from stations 1 to 6) and the spring bloom regime (from stations 9 to 10).

Oligotrophic Open Sea Regime:

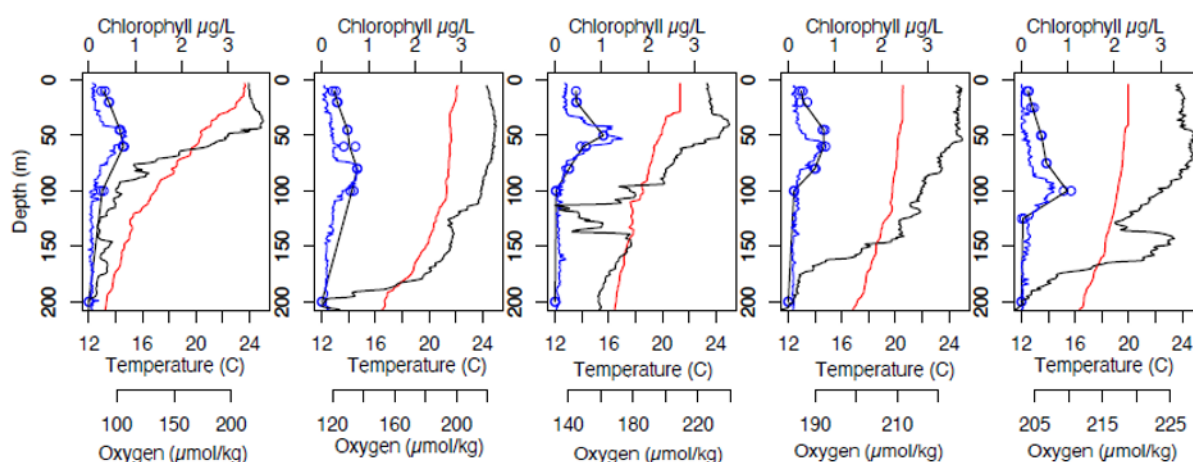


Fig. 5.11: Final results of oligotrophic open sea regime from stations 1, 3, 4, 5, and 6 (from left to right panel). Vertical profiles illustrate discrete chl-a (blue circles and black line as an average) data, as well as high-resolution chl-a (blue line), oxygen (black line) and temperature (red) data from the CTD sensors.

Spring Bloom Regime:

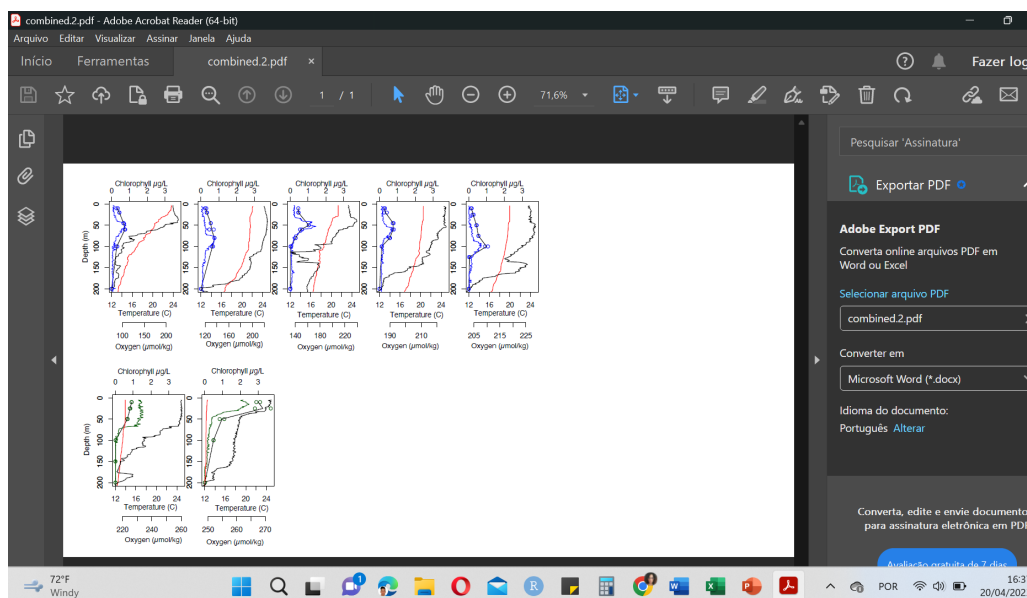


Fig. 5.12: Final results of spring bloom regime from stations 9 and 10 (from left to right). Vertical profiles illustrate chl-a, oxygen and temperature data. Colours as above except chl-a as green to reflect the spring bloom regime

Scientific Communication

This module focused on the important role of communication in science, including informing policy, creating public awareness, and promoting interest in science studies. Students were introduced to various communication theories and strategies and were challenged to apply them practically by creating short films using advanced camera and editing software. Each student group developed their own script and targeted a specific audience group, thereby enhancing their understanding of the motives behind effective science communication.

Tab. 5.6: The table below highlights the various groupings and the themes worked on.

Groups	Members	Modules filmed	Title of Video
A	Wise Goodluck Datsomor & Christelle Bôla-nlé Christelle	Oceanography	The contribution of Ocean Observations to Climate Change Studies
B	Almoustapha Amadou Malam Lacho & Amadou Biteye	Biogeochemistry	Marine Biogeochemistry
C	Kodjo Olivier Assokpa, Sienfoungo Troare & Mayara Jany Sousa Lourenço	Ecology	Zooplankton Sampling
D	Amie Ndure & Osvaldina Julião Soares	Microbiology	A day with the Microbiology group
E	Sarah Sofia Dias Dos Santos & Dembele Massitan Beny	Day on Board	A research day on <i>Polarstern</i>

Group A highlighted the relevance of CTD and Argo float data measurements in the context of global ocean observations and its contribution to studying climate change. Group B emphasized the importance of the ocean in oxygen production and outlined the steps involved in data acquisition and analysis. Group C and D described the methods used in collecting and analyzing data on zooplankton distribution and microbiology during the cruise. Meanwhile, Group E provided an overview of daily life onboard a research vessel.

Overall, the module equipped students with essential communication skills needed to effectively convey scientific concepts and practices to a wider audience.



Fig. 5.13: Image depicting students filming (left) and editing their work (right); photo credit: GEOMAR

Data management

Environmental data will be archived, published and disseminated according to international standards by the World Data Center PANGAEA Data Publisher for Earth & Environmental Science (<https://www.pangaea.de>) within two years after the end of the expedition at the latest. By default, the CC-BY license will be applied.

Any other data will be submitted to an appropriate long-term archive that provides unique and stable identifiers for the datasets and allows open online access to the data.

This expedition was supported by the Helmholtz Research Programme “Changing Earth – Sustaining our Future” topics 2 (Ocean and Cyrosphere in Climate Change) and 6 (Marine and Polar Life).

In all publications based on this expedition, the **Grant No. AWI_PS135_04** will be quoted and the following publication will be cited:

Alfred-Wegener-Institut Helmholtz-Zentrum für Polar- und Meeresforschung (2017) Polar Research and Supply Vessel POLARSTERN Operated by the Alfred-Wegener-Institute. Journal of large-scale research facilities, 3, A119. <http://dx.doi.org/10.17815/jlsrf-3-163>.

References

Grasshoff K, Kremling K, Ehrhardt M (1999) Methods of Seawater Analysis. Weinheim, Germany: Wiley-VCH Verlag GmbH.

Yeh YC, McNichol J, Needham DM, Fichot E B, Berdjeb L, Fuhrman JA (2021) Comprehensive single-PCR 16S and 18S rRNA community analysis validated with mock communities, and estimation of sequencing bias against 18S. Environmental Microbiology 23(6):3240–3250. <https://doi.org/10.1111/1462-2920.15553>

APPENDIX

A.1 TEILNEHMENDE INSTITUTE / PARTICIPATING INSTITUTES

A.2 FAHRTTEILNEHMER:INNEN / CRUISE PARTICIPANTS

A.3 SCHIFFSBESATZUNG / SHIP'S CREW

A.4. STATIONSLISTE / STATION LIST

A.1 TEILNEHMENDE INSTITUTE / PARTICIPATING INSTITUTES

Affiliation	Address
CV.UTA	Universidade Técnica do Atlântico Institute of Engineering and Marine Sciences CP.163 - Campus de Ribeira de Julião Mindelo, São Vicente Cabo Verde
DE.AWI	Alfred-Wegener-Institut Helmholtz-Zentrum für Polar- und Meeresforschung Postfach 120161 27515 Bremerhaven Germany
DE.CAU	Christian-Albrechts-Universität zu Kiel Christian-Albrechts-Platz 4 24118 Kiel Germany
DE.DWD	Deutscher Wetterdienst Seewetteramt Bernhard Nocht Str. 76 20359 Hamburg Germany
DE.GEOMAR	GEOMAR Helmholtz Zentrum für Ozeanforschung Kiel Wischhofstr. 1-3 24148 Kiel Germany
DE.HEREON	Helmholtz-Zentrum Hereon GmbH Max-Planck-Str. 1 21502 Geesthacht Germany
DE.IOW	Leibniz-Institut für Ostseeforschung Warnemünde Seestraße 15 18119 Rostock-Warnemünde Germany
DE.MPIC	Max-Planck-Institut für Chemie Hahn-Meitner-Weg 1 55128 Mainz Germany
NO.UIO	Universitetet i Oslo Boks 1072 Blindern 0316 Oslo Norway

A.2 FAHRTTEILNEHMER:INNEN / CRUISE PARTICIPANTS

PS135/1: Punta Arenas – Mindelo				
Name/ Last name	Vorname/ First name	Institut/ Institute	Beruf/ Profession	Fachrichtung/ Discipline
Debler	Freya	DE.HEREON	PhD student	Chemistry
Kinne	Stefan	DE.MPIC	Scientist	Meteorology
Konopatzky	Peter	DE.AWI	Scientist	Geophysics
Raeke	Andreas Wolfgang	DE.DWD	Scientist	Meteorology
Schulze Tenberge	Yvonne	DE.AWI	Scientist	Geophysics
Wenzel	Anna Julia	DE.DWD	Scientist	Meteorology
Xie	Zhiyong	DE.HEREON	Scientist	Chemistry

PS135/2: Mindelo – Bremerhaven				
Name/ Last name	Vorname/ First name	Institut/ Institute	Beruf/ Profession	Fachrichtung/ Discipline
Akonde	Bôla-Nlé Christelle	CV.UTA	M.Sc. Student	Marine Sciences
Antia	Avan	DE.CAU	Scientist	Biology
Assokpa	Kodjo Olivier	CV.UTA	M.Sc. Student	Marine Sciences
Biteye	Amadou	CV.UTA	M.Sc. Student	Marine Sciences
Bittig	Henry	DE.IOW	Scientist	Chemistry
Christiansen	Svenja	NO.UIO	Scientist	Biology
Datsomor	Wise Goodluck	CV.UTA	M.Sc. Student	Marine Sciences
Debler	Freya	DE.HEREON	Scientist	Chemistry
Dembele	Massitan Beny Dite Kanta	CV.UTA	M.Sc. Student	Marine Sciences
Dos Santos	Sarah Sofia Dias	CV.UTA	M.Sc. Student	Marine Sciences
Fiedler	Björn	DE.GEOMAR	Scientist	Chemistry
Kinne	Stefan	DE.MPIC	Scientist	Meteorology
Konopatzky	Peter	DE.AWI	Scientist	Geophysics
Lacho	Almoustapha Amadou Malan	CV.UTA	M.Sc. Student	Marine Sciences
Lourenço	Mayara Jany Sousa	CV.UTA	M.Sc. Student	Marine Sciences
Ndure	Amie	CV.UTA	M.Sc. Student	Marine Sciences
Needham	David	DE.GEOMAR	Scientist	Biology
Pinto	Antonio	CV.UTA	Scientist	Biology
Raeke	Andreas Wolfgang	DE.DWD	Scientist	Meteorology
Schmidtco	Sunke	DE.GEOMAR	Scientist	Physics
Schulze Tenberge	Yvonne	DE.AWI	Scientist	Geophysics
Soares	Osvaldina Julião Fernandes	CV.UTA	M.Sc. Student	Marine Sciences

PS135/2: Mindelo – Bremerhaven				
Strasser	Fiona-Elaine	DE.GEOMAR	Scientist	Biology
Tippenhauer	Sandra	DE.AWI	Technician	AWI Logistics
Traore	Sienfoungo	CV.UTA	M.Sc. Student	Marine Sciences
Wenzel	Julia	DE.DWD	Scientist	Meteorology
Wimart-Rousseau	Cathy	DE.GEOMAR	Scientist	Chemistry
Xie	Zhiyong	DE.HEREON	Scientist	Chemistry

A.3 SCHIFFSBESATZUNG / SHIP'S CREW 135/1

	Name	Vorname	Master
1	Schwarze	Stefan	Master
2	Kentges	Felix	C/M
3	Grafe	Jens	C/E
4	Falk	Stefan	2/M
5	Fallei	Holger	3/M
6	Hering	Igor	2/M
7	Müller	Andreas	E/E Com.
8	Haack	Michael Detlev	2/E
9	Brose	Thomas Christian Gerhard	2/E
10	Beyer	Mario	2/E
11	Kliemann	Olaf	E/E Brücke
12	Zohrabyan	David Rubeni	E/E Brücke
13	Hüttebräucker	Olaf	E/E Labor
14	Redmer	Jens Dirk	E/E SET
15	Nasis	Ilias	E/E System
16	Jäger	Vladimir	E/E Winde
17	Cornelsen	Rober	MPR
18	Münzenberger	Börge	MPR
19	Schwarz	Uwe	MPR
20	Rhau	Lars-Peter	MPR
21	Meier	Jan	MPR
22	Klinger	Dana Maria	MPR
23	Denzer	Florian	MPR
24	Claasen	Thies	MPR
25	Rhau	Lars-Peter	MPR
26	Hänert	Ove	MPR
27	Neisner	Winfried Wolfgang	Carp.
28	Kistenmacher	Mario André	AB
29	Wende	Uwe	AB
30	Burzan	Gerd-Ekkehard	AB
31	Bäcker	Andreas	AB
32	Preussner	Jörg	Fitter/E

	Name	Vorname	Master
33	Schnieder	Sven	Cook
34	Silinski	Frank	2./Cook
35	Pieper	Daniel	C/Stew.
36	Braun	Maja Alexandra	Stew./Nurse
37	Cheng	Qi	2./Stew.
38	Silinski	Carmen Viola	2./Stew.
39	Arendt	Rene	2./Stew.
40	Krause	Tomasz	2./Stew.
41	Chen	Dansheng	2./Stew.
42	Gößmann-Lange	Petra	Dr.

SCHIFFSBESATZUNG / SHIP'S CREW PS135/2

	Name	Vorname	Master
1	Schwarze	Stefan	Master
2	Kentges	Felix	C/M
3	Grafe	Jens	C/E
4	Falk	Stefan	2/M
5	Fallei	Holger	3/M
6	Hering	Igor	2/M
7	Müller	Andreas	E/E Com.
8	Haack	Michael Detlev	2/E
9	Brose	Thomas Christian Gerhard	2/E
10	Beyer	Mario	2/E
11	Kliemann	Olaf	E/E Brücke
12	Zohrabyan	David Rubeni	E/E Brücke
13	Hüttebräucker	Olaf	E/E Labor
14	Redmer	Jens Dirk	E/E SET
15	Nasis	Ilias	E/E System
16	Jäger	Vladimir	E/E Winde
17	Cornelsen	Rober	MPR
18	Münzenberger	Börge	MPR
19	Schwarz	Uwe	MPR
20	Rhau	Lars-Peter	MPR
21	Meier	Jan	MPR
22	Klinger	Dana Maria	MPR
23	Denzer	Florian	MPR
24	Claasen	Thies	MPR
25	Haenert	Ove	MPR
26	Neisner	Winfried Wolfgang	Carp.
27	Kistenmacher	Mario André	AB
28	Wende	Uwe	AB
29	Burzan	Gerd-Ekkehard	AB
30	Bäcker	Andreas	AB
31	Preussner	Jörg	Fitter/E
32	Schnieder	Sven	Cook

	Name	Vorname	Master
33	Hammelmann	Louisa	2./Cook
34	Silinski	Frank	2./Cook
35	Pieper	Daniel	C/Stew.
36	Braun	Maja Alexandra	Stew./Nurse
37	Cheng	Qi	2./Stew.
38	Silinski	Carmen Viola	2./Stew.
39	Dibenau	Torsten Karl	2./Stew.
40	Arendt	Rene	2./Stew.
41	Krause	Tomasz	2./Stew.
42	Chen	Dansheng	2./Stew.
43	Gössmann-Lange	Petra	Dr.

A.4 STATIONSLISTE / STATION LIST PS135/1

Station list of expedition PS135/1 from Punta Arenas – Mindelo; the list details the action log for all stations along the cruise track.

See <https://www.pangaea.de/expeditions/events/PS135/1> to display the station (event) list for expedition PS135/1. This version contains Uniform Resource Identifiers for all sensors listed under <https://sensor.awi.de>. See <https://www.awi.de/en/about-us/service/computing-centre/data-flow-framework.html> for further information about AWI's data flow framework from sensor observations to

Event label	Optional label	Date/Time	Latitude	Longitude	Depth [m]	Gear	Action	Comment
PS133/1-track		2022-10-02T00:00:00	-33.90680	18.43370		CT	Station start	
PS133/1-track		2022-11-17T00:00:00	-53.14470	-70.90910		CT	Station end	
PS135/1_0 Underway-1		2023-03-12T19:05:30	-47.54668	-60.59366	451.0	ADCP	Station start	
PS135/1_0 Underway-1		2023-03-28T15:01:57	16.68763	-25.17307		ADCP	Station end	
PS135/1_0 Underway-6		2023-03-12T19:04:51	-47.54837	-60.59644	442.8	MYON	Station start	
PS135/1_0 Underway-6		2023-03-28T15:01:57	16.68763	-25.17307		MYON	Station end	
PS135/1_0 Underway-7		2023-03-12T19:04:25	-47.54946	-60.59827	441.9	FBOX	Station start	
PS135/1_0 Underway-7		2023-03-28T15:01:57	16.68763	-25.17307		FBOX	Station end	
PS135/1_0 Underway-11		2023-03-12T19:04:01	-47.55044	-60.59999	442.5	MAG	Station start	
PS135/1_0 Underway-11		2023-03-28T15:01:57	16.68763	-25.17307		MAG	Station end	
PS135/1_0 Underway-12		2023-03-12T19:03:35	-47.55149	-60.60187	438.8	GRAV	Station start	

* Comments are limited to 130 characters. See <https://www.pangaea.de/expeditions/events/PS135/1> to show full comments in conjunction with the station (event) list for expedition PS135/1.

Event label	Optional label	Date/Time	Latitude	Longitude	Depth [m]	Gear	Action	Comment
PS135/1_0_Underway-12		2023-03-28T15:01:57	16.68763	-25.17307		GRAV	Station end	
PS135/1_0_Underway-13		2023-03-12T18:56:07	-47.57000	-60.63300		DS3	Station start	Event shows start/end point (date/time & coordinates) of first/last data record using Atlas Hydrographic Hydrosweep DS 3 multibeam...
PS135/1_0_Underway-13		2023-03-28T14:30:50	16.59620	-25.17100		DS3	Station end	Event shows start/end point (date/time & coordinates) of first/last data record using Atlas Hydrographic Hydrosweep DS 3 multibeam...
PS135/1_0_Underway-14		2023-03-12T19:00:59	-47.55792	-60.61302	437.1	NEUMON	Station start	
PS135/1_0_Underway-14		2023-03-28T15:01:57	16.68763	-25.17307		NEUMON	Station end	
PS135/1_0_Underway-17		2023-03-12T19:00:47	-47.55843	-60.61386	434.6	pCO2	Station start	
PS135/1_0_Underway-17		2023-03-28T15:01:57	16.68763	-25.17307		pCO2	Station end	
PS135/1_0_Underway-18		2023-03-12T19:00:27	-47.55928	-60.61526	431.8	pCO2	Station start	
PS135/1_0_Underway-18		2023-03-28T15:01:57	16.68763	-25.17307		pCO2	Station end	

Event label	Optional label	Date/Time	Latitude	Longitude	Depth [m]	Gear	Action	Comment
PS135/1_0_Underway-22		2023-03-12T18:59:42	-47.56122	-60.61838	428.1	SNDVELPR	Station start	
PS135/1_0_Underway-22		2023-03-28T15:01:57	16.68763	-25.17307		SNDVELPR	Station end	
PS135/1_0_Underway-23		2023-03-12T18:57:11	-47.56768	-60.62886	125.0	TSG	Station start	Keel 1
PS135/1_0_Underway-23		2023-03-28T15:01:57	16.68763	-25.17307		TSG	Station end	Keel 1
PS135/1_0_Underway-24		2023-03-12T18:56:30	-47.56938	-60.63166	178.0	TSG	Station start	Keel 2
PS135/1_0_Underway-24		2023-03-28T15:01:57	16.68763	-25.17307		TSG	Station end	Keel 2
PS135/1_0_Underway-28		2023-03-09T08:00:00	-53.17407	-70.88645	18.2	SWEAS	Station start	
PS135/1_0_Underway-28		2023-03-28T15:01:57	16.68763	-25.17307		SWEAS	Station end	
PS135/1_0_Underway-29		2023-03-12T19:00:00	-47.56040	-60.61707	428.3	HVAIR	Station start	
PS135/1_0_Underway-29		2023-03-28T15:01:57	16.68763	-25.17307		HVAIR	Station end	
PS135/1_0_Underway-30		2023-03-12T19:00:26	-47.55928	-60.61526	431.8	HVAIR	Station start	
PS135/1_0_Underway-30		2023-03-28T15:01:57	16.68763	-25.17307		HVAIR	Station end	
PS135/1_0_Underway-31		2023-03-12T19:00:00	-47.56040	-60.61707	428.3	HVAIR	Station start	
PS135/1_0_Underway-31		2023-03-28T15:01:57	16.68763	-25.17307		HVAIR	Station end	
PS135/1_0_Underway-32		2023-03-12T19:01:00	-47.55784	-60.61288	437.1	HVAIR	Station start	
PS135/1_0_Underway-32		2023-03-28T15:01:57	16.68763	-25.17307		HVAIR	Station end	

Event label	Optional label	Date/Time	Latitude	Longitude	Depth [m]	Gear	Action	Comment
PS135/1_0_Underway-33		2023-03-12T19:00:12	-47.55988	-60.61624	431.2	UWS	Station start	
PS135/1_0_Underway-33		2023-03-28T15:01:57	16.68763	-25.17307		UWS	Station end	
PS135/1_0_Underway-34		2023-03-12T19:00:54	-47.55809	-60.61330	436.0	MICROTOPS-II	Station start	
PS135/1_0_Underway-34		2023-03-28T15:01:57	16.68763	-25.17307		MICROTOPS-II	Station end	
PS135/1_0_Underway-35		2023-03-12T19:00:47	-47.55839	-60.61379	434.6	CAME	Station start	MPI-M sky camera
PS135/1_0_Underway-35		2023-03-28T15:01:57	16.68763	-25.17307		CAME	Station end	MPI-M sky camera
PS135/1_1-1		2023-03-13T11:55:48	-45.11497	-56.54832	5229.9	SVP	Station start	
PS135/1_1-1		2023-03-13T13:33:39	-45.11734	-56.54895	5228.8	SVP	Station end	
PS135/1_2-1		2023-03-15T11:59:29	-37.93969	-46.77165	5151.0	SVP	Station start	
PS135/1_2-1		2023-03-15T13:15:17	-37.94922	-46.75890	5151.3	SVP	Station end	
PS135/1_3-1		2023-03-17T10:58:11	-30.45105	-38.46562	3701.9	SVP	Station start	
PS135/1_3-1		2023-03-17T12:15:18	-30.44447	-38.46454	3704.9	SVP	Station end	
PS135/1_4-1		2023-03-19T10:56:46	-21.49626	-34.21881	4470.4	SVP	Station start	
PS135/1_4-1		2023-03-19T12:25:14	-21.49685	-34.21989	4469.5	SVP	Station end	
PS135/1_5-1		2023-03-21T11:17:32	-13.40349	-30.77965	5249.5	SVP	Station start	
PS135/1_5-1		2023-03-21T12:26:30	-13.40418	-30.77930	5246.0	SVP	Station end	
PS135/1_6-1		2023-03-23T09:59:05	-5.29677	-27.45715	5588.2	SVP	Station start	
PS135/1_6-1		2023-03-23T11:13:15	-5.29835	-27.45830	5591.0	SVP	Station end	
PS135/1_7-1		2023-03-25T09:00:07	2.73501	-24.93993	4078.6	SVP	Station start	
PS135/1_7-1		2023-03-25T10:27:55	2.73427	-24.94350	4068.4	SVP	Station end	
PS135/1_8-1		2023-03-27T09:58:23	11.55483	-25.08538	5325.5	SVP	Station start	
PS135/1_8-1		2023-03-27T11:15:45	11.55555	-25.08665	5324.7	SVP	Station end	

* Comments are limited to 130 characters. See <https://www.pangaea.de/expeditions/events/PS135/1> to show full comments in conjunction with the station (event) list for expedition PS135/1.

Abbreviation	Method/Device
ADCP	Acoustic Doppler Current Profiler
CAME	Camera
DS3	Swath-mapping system Atlas Hydrosweep DS-3
FBOX	FerryBox
GRAV	Gravimetry
HVAIR	High volume air sampler
MAG	Magnetometer
MICROTOPS-II	Sun photometer, Microtops II
MYON	DESY Myon Detector
NEUMON	Neutron monitor
SNDVELPR	Sound velocity probe
SVP	Sound velocity profiler
SWEAS	Ship Weather Station
TSG	Thermosalinograph
UWS	Underway water sampling
pCO ₂	pCO ₂ sensor

STATIONSLISTE / STATION LIST PS135/2

Station list of expedition PS135/2 from Mindelo – Bremerhaven; the list details the action log for all stations along the cruise track.

See <https://www.pangaea.de/expeditions/events/PS135/2> to display the station (event) list for expedition PS135/2. This version contains Uniform Resource Identifiers for all sensors listed under <https://sensor.awi.de>. See <https://www.awi.de/en/about-us/service/computing-centre/data-flow-framework.html> for further information about AWI's data flow framework from sensor observations to

Event label	Optional label	Date/Time	Latitude	Longitude	Depth [m]	Gear	Action	Comment
PS135/2_0_Underway-1		2023-03-28T18:00:00	16.76391	-25.17955	754.0	ADCP	Station start	
PS135/2_0_Underway-1		2023-04-10T10:03:29	52.82037	4.23381	15.7	ADCP	Station end	
PS135/2_0_Underway-6		2023-03-28T18:00:00	16.76270	-25.17930	769.0	MYON	Station start	
PS135/2_0_Underway-6		2023-04-10T09:59:56	52.81111	4.22726	15.3	MYON	Station end	
PS135/2_0_Underway-7		2023-03-28T18:00:00	16.76165	-25.17908	637.0	FBOX	Station start	
PS135/2_0_Underway-7		2023-04-10T10:02:28	52.81778	4.23166	15.7	FBOX	Station end	
PS135/2_0_Underway-11		2023-03-28T18:00:00	16.75986	-25.17873	434.0	MAG	Station start	
PS135/2_0_Underway-11		2023-04-10T10:00:13	52.81187	4.22766	15.3	MAG	Station end	
PS135/2_0_Underway-12		2023-03-28T18:00:00	16.75870	-25.17849		GRAV	Station start	
PS135/2_0_Underway-12		2023-04-10T10:00:36	52.81291	4.22820	15.2	GRAV	Station end	

* Comments are limited to 130 characters. See <https://www.pangaea.de/expeditions/events/PS135/2> to show full comments in conjunction with the station (event) list for expedition PS135/2.

Event label	Optional label	Date/Time	Latitude	Longitude	Depth [m]	Gear	Action	Comment
PS135/2_0_Underway-13		2023-03-28T21:46:12	16.99870	-24.92300		DS3	Station start	Event shows start/end point (date/time & coordinates) of first/last data record using Atlas Hydrographic Hydrosweep DS 3 multibeam...
PS135/2_0_Underway-13		2023-04-09T06:06:52	50.02580	-1.64410		DS3	Station end	Event shows start/end point (date/time & coordinates) of first/last data record using Atlas Hydrographic Hydrosweep DS 3 multibeam...
PS135/2_0_Underway-14		2023-03-28T18:00:00	16.75716	-25.17816		NEUMON	Station start	
PS135/2_0_Underway-14		2023-04-10T10:00:57	52.81385	4.22873	15.3	NEUMON	Station end	
PS135/2_0_Underway-17		2023-03-28T18:00:00	16.75624	-25.17797		pCO2	Station start	
PS135/2_0_Underway-17		2023-04-10T10:02:53	52.81884	4.23255	15.6	pCO2	Station end	
PS135/2_0_Underway-18		2023-03-28T18:00:00	16.75508	-25.17772		pCO2	Station start	
PS135/2_0_Underway-18		2023-04-10T10:03:12	52.81965	4.23322	15.8	pCO2	Station end	
PS135/2_0_Underway-22		2023-03-28T18:00:00	16.75358	-25.17743		SNDVELPR	Station start	

Event label	Optional label	Date/Time	Latitude	Longitude	Depth [m]	Gear	Action	Comment
PS135/2_0_Underway-22		2023-04-10T09:59:22	52.80962	4.22630	15.1	SNDVELPR	Station end	
PS135/2_0_Underway-23		2023-03-28T18:00:00	16.75119	-25.17708		TSG	Station start	Keel 1
PS135/2_0_Underway-23		2023-04-10T10:01:52	52.81625	4.23041	15.3	TSG	Station end	Keel 1
PS135/2_0_Underway-24		2023-03-28T18:00:00	16.75042	-25.17698		TSG	Station start	Keel 2
PS135/2_0_Underway-24		2023-04-10T10:02:09	52.81697	4.23099	15.6	TSG	Station end	Keel 2
PS135/2_0_Underway-26		2023-03-28T18:01:00	16.88752	-25.00931	10.1	UWS	Station start	
PS135/2_0_Underway-26		2023-04-10T06:10:00	52.35096	3.43389	21.7	UWS	Station end	
PS135/2_0_Underway-28		2023-03-28T18:00:00	16.74786	-25.17658		SWEAS	Station start	
PS135/2_0_Underway-28		2023-04-09T06:55:37	50.05994	-1.43466		SWEAS	Station end	
PS135/2_0_Underway-29		2023-03-28T18:00:00	16.88754	-25.00929	10.0	MICROTOPS-II	Station start	NASA supplied
PS135/2_0_Underway-29		2023-04-10T10:01:32	52.81539	4.22976	15.5	MICROTOPS-II	Station end	NASA supplied
PS135/2_0_Underway-30		2023-03-28T18:00:00	16.88754	-25.00929	10.0	CAME	Station start	MPI-M sky camera
PS135/2_0_Underway-30		2023-04-09T06:55:37	50.05994	-1.43466	61.0	CAME	Station end	MPI-M sky camera
PS135/2_0_Underway-31		2023-03-28T18:00:00	16.88754	-25.00929	10.0	HVAIR	Station start	
PS135/2_0_Underway-31		2023-04-09T06:47:29	50.05254	-1.46303	52.9	HVAIR	Station end	

Event label	Optional label	Date/Time	Latitude	Longitude	Depth [m]	Gear	Action	Comment
PS135/2_0_Underway-32		2023-03-28T18:00:00	16.88754	-25.00929	10.0	HVAIR	Station start	
PS135/2_0_Underway-32		2023-04-09T06:50:07	50.05442	-1.45132	52.6	HVAIR	Station end	
PS135/2_0_Underway-33		2023-03-28T18:00:00	16.88754	-25.00929	10.0	HVAIR	Station start	
PS135/2_0_Underway-33		2023-04-09T06:31:30	50.04253	-1.53210	58.7	HVAIR	Station end	
PS135/2_0_Underway-34		2023-03-28T18:00:00	16.88754	-25.00929	10.0	HVAIR	Station start	
PS135/2_0_Underway-34		2023-04-09T06:31:26	50.04249	-1.53239	58.8	HVAIR	Station end	
PS135/2_1-2		2023-03-29T04:10:59	17.58261	-24.28225	3605.6	MSN	max depth	
PS135/2_1-4		2023-03-29T06:15:00	17.58372	-24.28281	3604.6	GSCRS	Station start	
PS135/2_1-4		2023-03-29T07:18:27	17.58346	-24.28300	3603.6	GSCRS	Station end	
PS135/2_1-1		2023-03-29T07:20:18	17.58340	-24.28303	3604.7	CTD-RO	max depth	
PS135/2_1-3	WMO 6904220	2023-03-29T08:52:00	17.58819	-24.28266	3605.5	ARGOFL	Station start	
PS135/2_1-3	WMO 6904220	2023-03-29T08:52:42	17.58867	-24.28257	3603.2	ARGOFL	Station end	
PS135/2_2-1	WMO 7901001	2023-03-29T15:34:15	18.87137	-24.12376	3930.8	ARGOFL	Station start	
PS135/2_2-1	WMO 7901001	2023-03-29T15:49:30	18.86861	-24.12034	3929.1	ARGOFL	Station end	
PS135/2_2-2		2023-03-29T16:33:00	18.86577	-24.12118	3926.2	CTD-RO	max depth	CTD incl. UVP
PS135/2_2-3		2023-03-29T17:01:28	18.86415	-24.12071	3925.8	GSCRS	Station start	
PS135/2_2-3		2023-03-29T17:18:47	18.86383	-24.12049	3924.6	GSCRS	Station end	
PS135/2_3-1		2023-03-30T11:05:26	21.25859	-22.23688	4479.6	CTD-RO	max depth	CTD incl. UVP
PS135/2_3-2		2023-03-30T11:06:28	21.25856	-22.23697	4479.2	GSCRS	Station start	
PS135/2_3-2		2023-03-30T11:34:01	21.25871	-22.23847	4482.6	GSCRS	Station end	

Event label	Optional label	Date/Time	Latitude	Longitude	Depth [m]	Gear	Action	Comment
PS135/2_3-3		2023-03-30T11:59:49	21.25779	-22.24086	4481.8	MSN	Station start	
PS135/2_3-3		2023-03-30T13:12:08	21.25604	-22.24691	4481.4	MSN	Station end	
PS135/2_4-1		2023-03-31T05:00:12	23.46919	-20.46340	4082.2	MSN	Station start	
PS135/2_4-1		2023-03-31T06:11:18	23.47008	-20.46496	4085.5	MSN	Station end	
PS135/2_4-3		2023-03-31T06:40:18	23.47027	-20.46493	4084.9	GSCRS	Station start	
PS135/2_4-3		2023-03-31T07:08:36	23.46997	-20.46564	4085.2	GSCRS	Station end	
PS135/2_4-2		2023-03-31T06:54:36	23.46995	-20.46548	4086.4	CTD-RO	max depth	
PS135/2_5-2		2023-04-01T10:14:52	26.92184	-17.23438	3673.0	GSCRS	Station start	
PS135/2_5-2		2023-04-01T10:54:31	26.92256	-17.23646	3674.0	GSCRS	Station end	
PS135/2_5-1		2023-04-01T10:26:00	26.92210	-17.23451	3674.8	CTD-RO	max depth	CTD incl. UVP
PS135/2_5-3		2023-04-01T11:14:41	26.92238	-17.23772	3675.0	MSN	Station start	
PS135/2_5-3		2023-04-01T12:32:16	26.91740	-17.23752	3674.3	MSN	Station end	
PS135/2_6-1		2023-04-02T04:30:36	29.16612	-15.50065	3628.2	MSN	max depth	
PS135/2_6-2		2023-04-02T04:52:45	29.16363	-15.50505	3628.4	GSCRS	Station start	
PS135/2_6-2		2023-04-02T05:27:51	29.16267	-15.50699	3627.7	GSCRS	Station end	
PS135/2_6-3		2023-04-02T07:33:54	29.16391	-15.50790	3629.9	CTD-RO	max depth	CTD incl. UVP
PS135/2_6-4		2023-04-02T09:11:33	29.16481	-15.50827	3629.1	MSN	Station start	
PS135/2_6-4		2023-04-02T10:45:35	29.16883	-15.51319	3635.6	MSN	Station end	
PS135/2_6-5		2023-04-02T09:28:25	29.16537	-15.50955	3631.5	GSCRS	Station start	
PS135/2_6-5		2023-04-02T10:14:47	29.16744	-15.51171	3632.6	GSCRS	Station end	
PS135/2_6-6		2023-04-02T09:46:44	29.16615	-15.51058	3628.9	APN	Station start	
PS135/2_6-6		2023-04-02T10:15:42	29.16751	-15.51177	3629.5	APN	Station end	
PS135/2_7-2		2023-04-03T10:06:27	32.89030	-13.92940	4301.9	GSCRS	Station start	
PS135/2_7-2		2023-04-03T10:43:04	32.89195	-13.93197	4302.9	GSCRS	Station end	
PS135/2_7-1		2023-04-03T10:24:59	32.89126	-13.93055	4302.2	CTD-RO	max depth	CTD incl. UVP
PS135/2_7-3		2023-04-03T11:24:36	32.89364	-13.93405	4305.8	MSN	max depth	
PS135/2_7-4	WMO 6904219	2023-04-03T12:43:34	32.89624	-13.93873	4308.7	ARGOFL	max depth	

Event label	Optional label	Date/Time	Latitude	Longitude	Depth [m]	Gear	Action	Comment
PS135/2_8-2		2023-04-05T09:24:34	40.26271	-11.25306	5073.5	GSCRS	Station start	
PS135/2_8-2		2023-04-05T10:09:21	40.26288	-11.25297	5074.3	GSCRS	Station end	
PS135/2_8-1		2023-04-05T10:20:17	40.26280	-11.25308	5070.1	CTD-RO	max depth	CTD incl. UVP
PS135/2_8-3		2023-04-05T12:36:24	40.26530	-11.25188	5070.0	MSN	max depth	
PS135/2_8-4	WMO 6904218	2023-04-05T13:55:04	40.26705	-11.25628	5072.9	ARGOFL	max depth	
PS135/2_9-1		2023-04-06T04:00:09	42.74464	-10.54007	2722.9	MSN	Station start	
PS135/2_9-1		2023-04-06T05:15:15	42.74527	-10.54007	2724.0	MSN	Station end	
PS135/2_9-2		2023-04-06T06:21:36	42.74448	-10.54043	2719.9	CTD-RO	max depth	CTD incl. UVP
PS135/2_9-3		2023-04-06T07:35:46	42.74439	-10.54065	2720.0	MSN	Station start	
PS135/2_9-3		2023-04-06T10:17:53	42.74394	-10.53977	2716.5	MSN	Station end	
PS135/2_9-4		2023-04-06T07:43:39	42.74403	-10.54064	2720.1	GSCRS	Station start	
PS135/2_9-4		2023-04-06T08:21:59	42.74403	-10.54076	2716.1	GSCRS	Station end	
PS135/2_9-5	WMO 6904217	2023-04-06T10:21:01	42.74392	-10.53943	2716.4	ARGOFL	Station start	
PS135/2_9-5	WMO 6904217	2023-04-06T10:24:56	42.74442	-10.53893	2719.3	ARGOFL	Station end	
PS135/2_10-1	WMO 7900558	2023-04-07T07:30:13	45.75343	-7.98191	4852.6	ARGOFL	Station start	recovery
PS135/2_10-1	WMO 7900558	2023-04-07T07:52:30	45.74994	-7.98496	4851.8	ARGOFL	Station end	recovery
PS135/2_10-2		2023-04-07T09:49:55	45.75053	-7.98294	4852.2	CTD-RO	max depth	CTD incl. UVP
PS135/2_10-3		2023-04-07T10:26:33	45.75169	-7.98394	4850.6	GSCRS	Station start	
PS135/2_10-3		2023-04-07T11:04:44	45.75223	-7.98329	4851.5	GSCRS	Station end	
PS135/2_10-4		2023-04-07T11:53:51	45.75355	-7.98375	4852.6	MSN	max depth	
PS135/2_10-5	WMO 6904216	2023-04-07T13:10:20	45.75342	-7.97929	4857.0	ARGOFL	max depth	
PS135/2_11-1		2023-04-08T06:22:14	47.80148	-6.14157	154.1	CTD-RO	max depth	CTD incl. UVP
PS135/2_11-2		2023-04-08T06:35:52	47.80113	-6.14416	153.9	GSCRS	Station start	

Event label	Optional label	Date/Time	Latitude	Longitude	Depth [m]	Gear	Action	Comment
PS135/2_11-2		2023-04-08T07:01:24	47.79676	-6.14197	154.6	GSCRS	Station end	
PS135/2_11-3		2023-04-08T06:41:01	47.80084	-6.14526	154.0	MSN	Station start	
PS135/2_11-3		2023-04-08T07:03:47	47.79573	-6.14129	155.0	MSN	Station end	
PS135/2_11-4		2023-04-08T07:08:59	47.79335	-6.13981	155.5	APN	Station start	
PS135/2_11-4		2023-04-08T07:24:38	47.79126	-6.14283	155.1	APN	Station end	

* Comments are limited to 130 characters. See <https://www.pangaea.de/expeditions/events/PS135/2> to show full comments in conjunction with the station (event) list for expedition PS135/2.

Abbreviation	Method/Device
ADCP	Acoustic Doppler Current Profiler
APN	Apstein plankton net
ARGOFL	Argo float
CAME	Camera
CTD-RO	CTD/Rosette
DS3	Swath-mapping system Atlas Hydrosweep DS-3
FBOX	FerryBox
GRAV	Gravimetry
GSCRS	Garrett Screen Sampler
HVAIR	High volume air sampler
MAG	Magnetometer
MICROTOPS-II	Sun photometer, Microtops II
MSN	Multiple opening/closing net
MYON	DESY Myon Detector
NEUMON	Neutron monitor
SNDVELPR	Sound velocity probe
SWEAS	Ship Weather Station
TSG	Thermosalinograph
UWS	Underway water sampling
pCO2	pCO2 sensor



ALFRED-WEGENER-INSTITUT
HELMHOLTZ-ZENTRUM FÜR POLAR-
UND MEERESFORSCHUNG

BREMERHAVEN

Am Handelshafen 12
27570 Bremerhaven
Telefon 0471 4831-0
Telefax 0471 4831-1149
www.awi.de

HELMHOLTZ